

JINANNOUNCED

①

AD-A955 991

VIRTUAL MODE SURFACE DUCT
MODEL FOR FACT

SAI-81-259-WA

by

F. J. Ryan

September 28, 1980

DTIC
ELECTED
JAN 24 1991
S B D

Prepared for:

Code 500

Ocean Programs Office
Naval Ocean Research and Development Activity
Bay St. Louis, Mississippi 39529

Developed Under Contract No. N00014-78-C-0566



SCIENCE APPLICATIONS, LA JOLLA, CALIFORNIA
ALBUQUERQUE • ANN ARBOR • ARLINGTON • ATLANTA • BOSTON • CHICAGO • HUNTSVILLE
LOS ANGELES • MCLEAN • PALO ALTO • SANTA BARBARA • SUNNYVALE • TUCSON

P.O. Box 2361, 1200 Prospect Street, La Jolla, California 92037

DISTRIBUTION STATEMENT A

Approved for public release
Distribution Unlimited

01 7 05 2

TABLE OF CONTENTS

<u>Section</u>		<u>Page</u>
1	INTRODUCTION	1-1
1.1	Background	1-1
1.2	Model Requirements	1-2
1.3	Technical Summary	1-2
1.4	Acknowledgements	1-4
2	TECHNICAL APPROACH	2-1
2.1	Furry Model	2-1
2.2	Virtual Mode Solution	2-1
2.3	Trapped Modes	2-6
2.4	Leaky Modes	2-10
2.5	Eigenfunctions	2-12
2.5a	Trapped Modes	2-13
2.5b	Leaky Modes	2-15
2.5c	Turning Points	2-16
2.5d	Near Surface	2-18
2.6	Rough Surface Effects	2-18
3	MODEL EVALUATION	3-1
3.1	PE Comparisons	3-2
3.2	Normal Mode Comparisons	3-40
3.3	Evaluation Summary	3-42
4	SURFACE DUCT PROGRAM	4-1
5	CONCLUSIONS	5-1
APPENDIX A: EVALUATION OF $T_+ T_-$		A-1
APPENDIX B: SURFACE-DUCT PROGRAM LISTING		B-1
APPENDIX C: SAMPLE EXECUTION		C-1
REFERENCES		R-1

per letter

Distribution/	
Availability Codes	
Dist	Avail and/or
	Special
A-1	

SECTION 1 INTRODUCTION

Since its introduction in April 1973, the FACT Model⁽¹⁾ has proven to be a useful tool for predicting and analyzing long-range low-frequency propagation in range-independent environments. The original development emphasized the incorporation of diffraction and surface-image effects in a fully automated, highly efficient model. For short-range high-frequency surface-ducted propagation, Clay augmented the ray model by an approximate surface-duct model already in use in FACT's predecessor, RP70⁽²⁾. While the Clay Model was recognized to have certain deficiencies, an efficient alternative was not available. This report documents such an alternative which is proposed for incorporation in FACT.

1.1 BACKGROUND

The Clay Model underwent a series of reviews (e.g., Labianca⁽³⁾), and was considered in a comparison by Morris of several models with data from the Surface Duct Sonar (SUDS) experiments⁽⁴⁾. Labianca's analysis showed that the model had an oversimplified depth dependence and the wrong dependence of leakage on environmental parameters. The leakage error resulted from assigning leakage losses to partial reflection from the gradient discontinuity at the bottom of the duct rather than to the correct quantum-mechanical "tunneling" phenomenon. The depth dependence was characterized by a single 10-dB drop in level from that in the duct if one of either the source or receiver were moved below the duct ("cross-layer"). In a number of cases the lack of environmental sensitivity proved critical.

Morris' comparisons showed that the Clay Model, AMOS⁽⁵⁾ and the Bucker surface-duct model⁽⁶⁾ were in fair agreement in a number of cases with none particularly better than the others. Since both the Clay Model and AMOS were largely based on experimental data this result was not altogether surprising. The data set was not a severe test of environmental sensitivity and was apparently contaminated by a range dependence in the sound-speed profile that none of the models were developed to include. Bucker's model clearly had the strongest theoretical basis, however it was

much longer running than the others and based on the comparisons a change was not justified.

In the period following these initial evaluations, considerable progress was made in understanding the basic mechanisms of surface ducted propagation, largely as a result of Labianca's⁽⁷⁾ work on virtual modes. Subsequently, Spofford⁽⁸⁾ identified Labianca's asymptotic expressions for deeply trapped virtual modes with mode bundle ray-equivalents ("smodes") and was able to incorporate rough surface scattering effects. A prototype surface duct propagation code was developed by Spofford, using the smode techniques. While showing improvement over the Clay Model, Spofford's model displayed poor performance for some propagative scenarios.

1.2 MODEL REQUIREMENTS

As FACT saw more and more use, dissatisfaction with the Clay Model increased, and LRAPP authorized the development of a better model subject to the following constraints:

1. increased accuracy for a wide range of environmental parameters;
2. continuity of transmission-loss in depth (including acoustic reciprocity);
3. range-smoothed transmission-loss of the approximate form $A + B \log R + aR$; and
4. sufficient speed to have a minimal impact on overall FACT running time (presently about 4 CPU seconds per 100 nmi).

SAI has developed such a model as reported herein.

1.3 TECHNICAL SUMMARY

The approach used in the new model is a further refinement and extension of Labianca's virtual mode results to include modes near cutoff as well as leaky modes. This permits intensity calculations in ducts below cutoff and/or at short ranges where the leaky modes make important contributions. The WKB work of Spofford was extended to the rough surface losses. A brief description of the model theory is provided here, with detailed discussions postponed till Section 2.

The surface duct model is designed to compute the relative incoherent intensity level from a point source in a canonical bilinear duct. Labianca's formulation of the complex pressure field as a Hankel transform over the continuum eigenspectrum is the theoretical starting point. An approximate, yet highly accurate, evaluation of the transform results in the relative incoherent intensity \tilde{I} being given as a finite sum of virtual modes

$$\tilde{I} \approx \frac{2\pi}{r} \sum_m e^{-\alpha_m r} I_m(z_s) I_m(z_r)$$

where r is the range and $z_s(z_r)$ is the source (receiver) depth. The I_m are modal intensity amplitudes and the α_m are modal attenuation coefficients. Individual terms in the sum arise from resonances in the kernel of the Hankel transform due to the proximity of Regge poles in the complex energy plane. The resonances in the transform occur at locations along the real energy axis corresponding to the real part of the Regge pole E_m .

The intensity amplitudes I_m are related to normalized depth functions and are expressible in terms of Airy functions. Efficient expansions for the Airy functions provide a rapid means for evaluation of the virtual mode sum, while preserving numerical accuracy. For the deeply trapped modes, Labianca's results are obtained as limiting cases.

The modal attenuation coefficient α_m incorporates volume, surface and diffractive losses. Volume losses are obtained from standard absorption loss formulas presently included in FACT. The diffractive portion of α_m is obtained from the imaginary component of the Regge pole and physically arises from leakage of acoustic energy into the region below the duct. The surface loss portion of α_m is computed by using conservation of energy applied to the virtual modes' ray-equivalent reflecting from the rough ocean surface. Each interaction of the ray-equivalent with the surface yields an effective reflection loss which is then accumulated continuously over the ray's cycle distance. The rough surface reflection losses are computed in a separate module as a function of the ray's surface grazing angle, sea state and frequency.

The virtual mode model was compared to a series of benchmarks generated using both the parabolic-equation (PE) code⁽¹⁶⁾ and the NOSC n-layer normal mode (NM) code⁽¹²⁾ for a representative surface duct. The model shows excellent agreement with both PE and NM calculations. Details of the comparisons are described in Section 3.

1.4 ACKNOWLEDGEMENTS

This work was supported by the Ocean Programs office of NORDA (Code 500), under the program management of Mr. Bob Wheatley. The support of technical staff at the Naval Ocean Systems Center (NOSC), particularly Mr. M. A. Pedersen and Dr. D. F. Gordon, in making the normal mode computer runs, is gratefully acknowledged. At SAI, prior work by Dr. H. L. Wilson on modeling surface scattering using the transport equation and by Mr. C. W. Spofford and Ms. R. E. Keenan on rough surface loss was incorporated into the surface duct model. Ms. E. Holmes assisted in making the parabolic equation runs used in the model evaluation. The author is grateful to Mr. C. W. Spofford for initially suggesting this problem and for discussions related to the virtual mode model.

SECTION 2

TECHNICAL APPROACH

This section describes the theoretical basis for a new surface duct model proposed for use in FACT. The model is an extension of previous work by Labianca on virtual mode representations and by Spofford on ray-mode equivalents. The model is designed to compute the incoherent acoustic intensity from a point source in a range independent ocean surface duct as a function of source/receiver geometry. The ocean surface duct is approximated by a canonical bilinear model first analyzed by Furry⁽⁹⁾ in connection with the transmission of electromagnetic waves in the atmosphere.

2.1 FURRY MODEL

Furry's model approximates the square of the refractive index n^2 with the bilinear form [Fig. (2.1)]

$$n^2(z) = \left[c_0 / c(z) \right]^2 = 1 - g_- z , \quad 0 \leq z < d$$

$$= 1 - g_- d + g_+ (z-d) , \quad z \geq d$$

unit: ?
 g_+, g_-
 are gradient
 $\frac{d}{dz}$
 so have m^{-1}

where d is the depth of the surface duct, $g_-(g_+)$ is the gradient within (below) the duct, c_0 is the surface sound speed, and $c(z)$ is the depth dependent sound speed. The Furry model has been employed by a number of authors in the context of ocean acoustics, with the conventional Fourier-Bessel or longitudinal wavenumber (λ) representation being used by Marsh,⁽¹⁰⁾ Hall⁽¹¹⁾ and Pedersen and Gordon,⁽¹²⁾ while the transverse wavenumber (κ) representation was employed by Labianca.⁽⁷⁾ The latter is used in this report.

2.2 VIRTUAL MODE SOLUTION

In polar cylindrical coordinates, the complex pressure field \underline{P} from a unit strength monopole source satisfies the Helmholtz equation

$$\left[\frac{1}{r} \frac{d}{dr} r \frac{d}{dr} + \frac{d^2}{dz^2} + k_0^2 n^2(z) \right] \underline{P}(r, z_r, z_s) = \frac{-1}{2\pi r} \delta(r) \delta(z_r - z_s) .$$

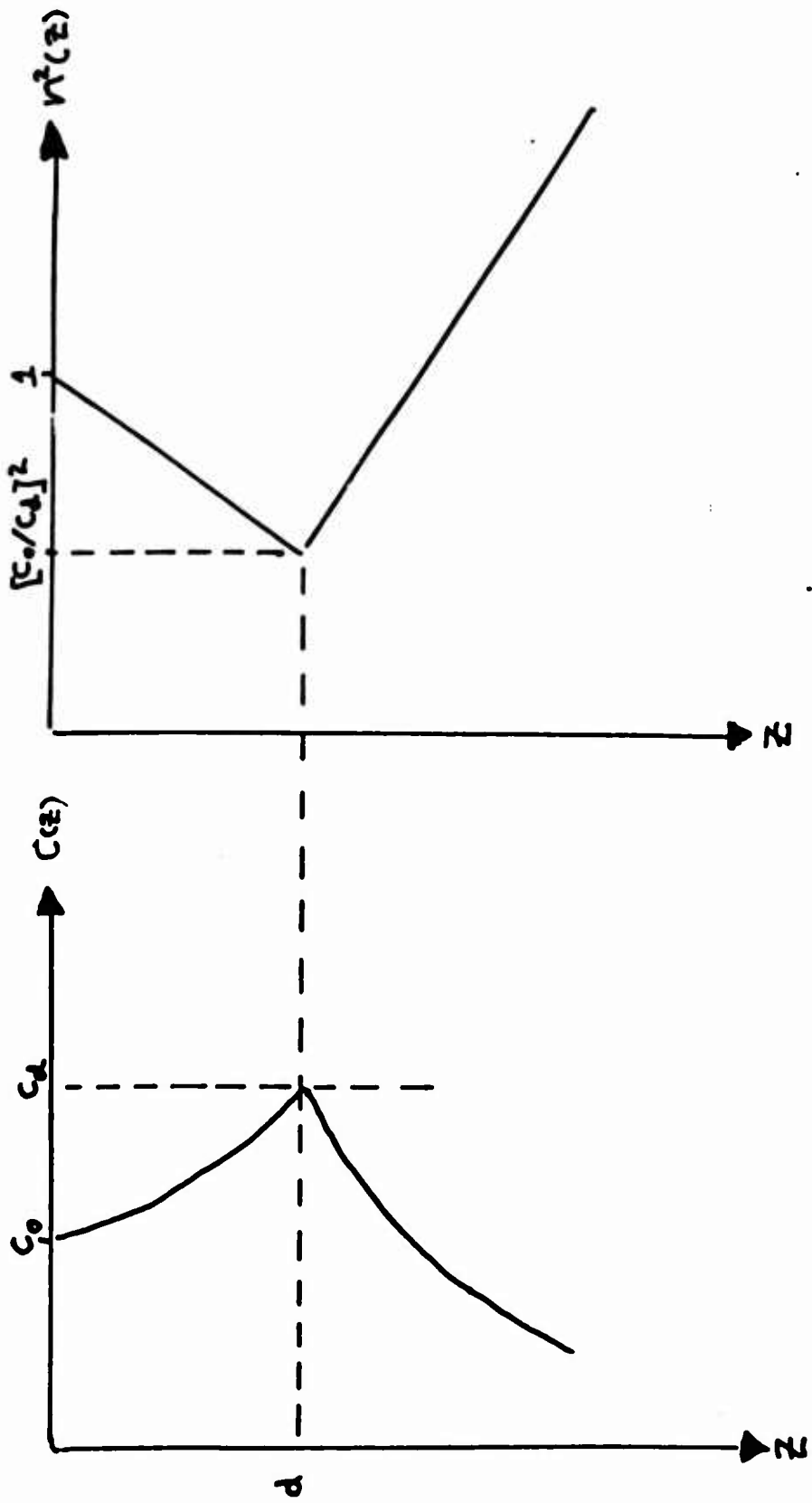


Figure 2-1. Furry Model Profile.

A harmonic time dependence, $\exp(-i\omega t)$, is suppressed with ω the angular frequency and $k_0 = \omega/c_0$. The source is located at $\vec{r} = (0, z_s)$, the receiver at $\vec{r} = (r, z_r)$ and P is to satisfy a pressure release boundary condition ($P=0$) at the surface and a radiation condition at deep depths.

Employing standard separation of variables techniques, the pressure is represented by the convolution

$$P(r, z_r, z_s) = \frac{-1}{8\pi} \int_{\Gamma} H_0^{(1)} \left[r(k_0^2 - \kappa^2)^{\frac{1}{2}} \right] g(\kappa^2, z_r, z_s) d\kappa^2 \quad (2.1)$$

where the depth Green's function g satisfies

$$\left[\frac{d^2}{dz^2} + k_0^2 (n^2 - 1) + \kappa^2 \right] g = -\delta(z_r - z_s)$$

with κ the transverse wavenumber ($k_0^2 = \lambda^2 + \kappa^2$).

The depth Green's function is expanded in a complete set of orthonormal eigenfunctions $\hat{\phi}$ of the homogeneous equation

$$\left[\frac{d^2}{dz^2} + k_0^2 (n^2 - 1) + \kappa^2 \right] \hat{\phi} = 0 \quad , \quad (2.2)$$

subject to the pressure release boundary condition. For the Furry model the eigenfunctions $\hat{\phi}$ form a continuous spectrum and the integral in Eq. (2.1) becomes

$$P(r, z_r, z_s) = \frac{i}{4\pi} \int_{-\infty}^{\infty} H_0^{(1)} \left[r(k_0^2 - \kappa^2)^{\frac{1}{2}} \right] \hat{\phi}(z_r, \kappa^2) \hat{\phi}(z_s, \kappa^2) d\kappa^2 \quad .$$

Analytic solutions for the eigenfunctions are readily obtained by introducing a natural unit of length, $H = (g_+ k_0^2)^{-\frac{1}{2}}$, whereby Eq. (2.2) becomes

$$\left[\frac{d^2}{dx^2} + E - Q(x) \right] \psi(x, E) = 0 \quad . \quad (2.3)$$

The new independent variable is $x = (z - d)/H$, and the "energy" E and "potential" Q are

$$E = H^2 \kappa^2 - s^3 D ,$$

and

$$\begin{aligned} Q(x) &= s^3 x , \quad x \leq 0 \\ &= -x , \quad x > 0 \end{aligned}$$

with $s^3 = g_- / g_+$ and $D = d/H$. Solutions of Eq. (2.3) may be expressed in terms of the Airy functions. Within the duct,

$$\psi(x, E) = \frac{\pi}{s} \left[Ai(-q) Bi(-q_0) - Ai(-q_0) Bi(-q) \right] , \quad x \leq 0 \quad (2.4a)$$

with $q_0 = w + sD$, $q = w - sx$ and $w = E/s^2$, and below the duct

$$\psi(x, E) = \frac{\pi^{1/2}}{2} \left[T_+(E) h_1(p) + T_-(E) h_2(p) \right] , \quad x > 0 \quad (2.4b)$$

with $p = E + x$. The h functions are

$$h_1(p) = Ai(-p) - i Bi(-p)$$

and

$$h_2(p) = Ai(-p) + i Bi(-p) .$$

Continuity of ψ and $d\psi/dx$ at the duct bottom fixes the T coefficients, leading to

$$T_+(E) = -i\pi^{1/2} \left[\psi'(0, E) h_2(E) - \psi(0, E) h_2'(E) \right] , \quad (2.5a)$$

and

$$T_-(E) = i\pi^{1/2} \left[\psi'(0, E) h_1(E) - \psi(0, E) h_1'(E) \right] . \quad (2.5b)$$

The pressure field integral, Eq. (2.1), is then given in terms of the new variables x, ψ as⁽¹³⁾

$$P(r, x_r, x_s) = \frac{i}{4\pi H} \int_{-\infty}^{\infty} H_0^{(1)} \left[r(k_0^2 - \kappa^2)^{\frac{1}{2}} \right] \frac{\psi(x_r, E)\psi(x_s, E)}{T_+(E)T_-(E)} dE , \quad (2.6)$$

with $\kappa^2 = (E + s^3 D)/H^2$.

The kernel of the Hankel transform in Eq. (2.6) has resonances along the real E axis from Regge poles in the lower half E plane. The Regge poles are the complex roots of $T_-(E_m) = 0$, with the real part of E_m corresponding to the resonance position and the imaginary part of E_m proportional to the resonance width. An approximate, yet highly accurate, evaluation of the integral in Eq. (2.6) is obtained by evaluating the integrand in the region of the resonances. The incoherent intensity, $\tilde{I} = |P|^2$, is then given in the far field $\left[r(k_0^2 - \kappa^2)^{\frac{1}{2}} \gg 1 \right]$ as⁽¹⁴⁾

$$\tilde{I} \simeq \frac{2\pi}{r} \sum_m e^{-ra_m^L} \frac{I_m(x_s)I_m(x_r)}{|k_0^2 - \kappa_m^2|^{\frac{1}{2}}} \quad (2.7)$$

with $\kappa_m^2 = (E_m + s^3 D)/H^2$,

$$\alpha_m^L = 2 \operatorname{Im} \left[(k_0^2 - \kappa_m^2)^{\frac{1}{2}} \right] ,$$

$$I_m(x) = |\psi_m^2(x, E_m)/N_m|$$

and

$$N_m = H \int_{-D}^{\infty} \psi_m^2(x) dx . \quad (2.8)$$

The ψ_m have been termed virtual modes by Labianca.

When the imaginary part of E_m is small (low attenuation) the depth function $\psi_m(x)$ is contained or "trapped" within the duct. The trapped modes

are capable of propagating acoustic energy to long ranges. Conversely, modes with large imaginary part are not localized in the duct and are termed "leaky".

Trapped modes have $E_r = \text{Re}(E_m)$ negative, and there are two zeroes (turning points) of $E_r - Q(x)$ denoted by x_1 and x_2 (Figure 2.2). When $x < x_1$, or $x > x_2$ ψ_m is oscillatory; when $x_1 < x < x_2$ ψ_m is exponential. The region between the turning points acts as a barrier, confining the depth function to the duct. ψ_m has an imaginary component that is essentially zero until below the barrier ($x > x_2$) and then spirals about the origin of the complex plane in a counter-clockwise sense with increasing magnitude as x increases.

Leaky modes have positive E_r and complex turning points. ψ_m is oscillatory and complex everywhere with no enhancement in the duct. While of lesser importance at long ranges, the leaky modes may make significant contributions at short ranges and need to be included in the residue series.

A ray-equivalent may be associated with ψ_m by defining a surface grazing angle θ_m through

$$\sin\theta_m = \left[g_+ H(E_r + s^3 D) \right]^{1/2} = \left[g_+ + s^2 - g_- d \right]^{1/2}$$

now the leaky modes
grazing angle

The trapped modes are thus seen to have ray-equivalents which turn within the duct, while the leaky modes correspond to ray-equivalents with large grazing angle.

The major effort in using the virtual mode series is in finding the Regge poles E_m . The roots of $T_-(E_m) = 0$ are generally obtained using complicated numerical methods as was done by Pedersen and Gordon.⁽¹²⁾ A different approach will now be discussed which provides accurate approximate expressions for the E_m , yet is very efficient.

2.3 TRAPPED MODES

The Regge pole E_m satisfies $T_-(E_m) = 0$, which upon using Eq. (2.5b) becomes the transcendental equation

$$\psi'(0, E_m) h_1(E_m) = \psi(0, E_m) h'_1(E_m) .$$

Pedersen use
numerical solution
Newton-Raphson
technique

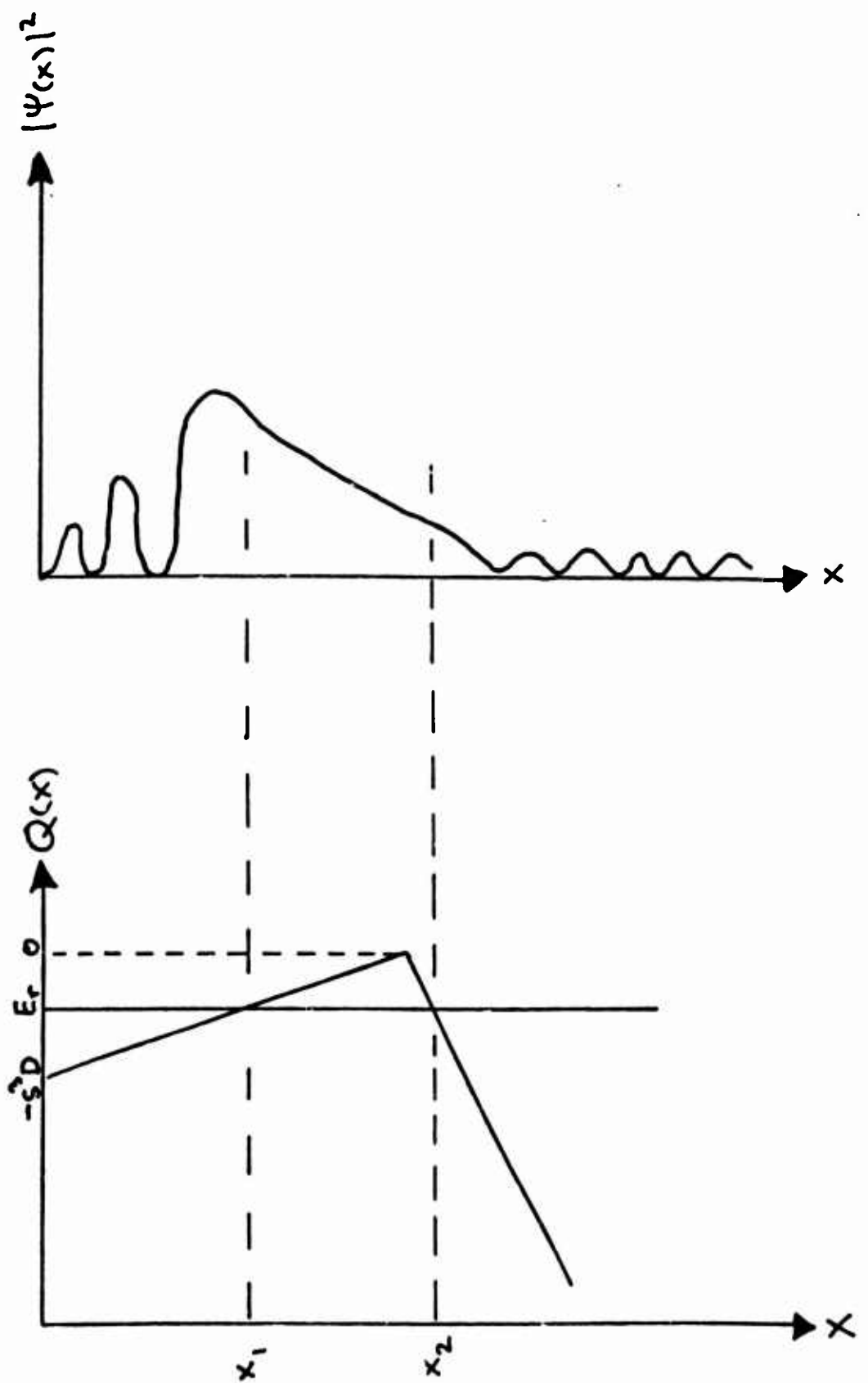


Figure 2-2. Potential $Q(x)$ and Schematic of Trapped Eigenfunction.

Using ψ from Eq. (2.4a), the above eigenvalue equation can be recast as (the mode subscript will be suppressed on E)

$$\frac{Ai(-q_0)}{Bi(-q_0)} = \frac{Ai'(-w) - Z(E)Ai(-w)s}{Bi'(-w) - Z(E)Bi(-w)s} . \quad (2.9)$$

with the effective "impedance" Z of the duct bottom expressed as

$$Z(E) = h_1'(E)/h_1(E) \quad (2.10)$$

and where $w = E/s^2$ and $q_0 = w + sD$.

If phase integral (WKB) methods were used to solve for the trapped eigenvalues, the m-th mode quantization condition would be

$$\int_{-D}^{x_1} (E - s^3 x)^{\frac{1}{2}} dx = \frac{2}{3} q_0^{\frac{3}{2}} = (m - \frac{1}{4})\pi \quad (2.11)$$

where x_1 (complex) is the upper turning point. Since the imaginary part of E is small for the trapped modes, a good approximation for x_1 is to assume it to be real. This corresponds to q_0 in Eq. (2.11) being an approximate root of $Ai(-q_0) = 0$, and suggests a zeroth order approximation to E as $E \sim E_0 = (q_0^* - sD)s^2$ where q_0^* is a real zero of Ai. Zeroes of Ai lie along the negative real axis and are tabulated in Abramowitz and Stegun.⁽¹⁵⁾

Next, expand the left side of Eq.(2.9) around q_0^* with $q_0 = q_0^* + \Delta q$ and use the Wronskian relation of the Ai and Bi to give

$$\left. \frac{Ai}{Bi} \right|_{-q_0} \simeq \Delta q \pi Ai'(-q_0^*)^2 + O(\Delta q^2) \quad \begin{array}{l} \text{automatically} \\ \text{get imaginary} \\ \text{term} \\ E_0 + iEi \end{array} \quad (2.12)$$

$$= \Delta q q_0 , q_0 = \pi Ai'(-q_0^*)^2 .$$

Finally, expanding the right side of Eq. (2.9) around E_0 yields the linearized form

$$a_0 \Delta q = \left| \begin{array}{c} \text{Ai}' - Z_0 \text{Ai} \\ \text{Bi}' - Z_0 \text{Bi} \end{array} \right|, \quad Z_0 = Z(E_0) \quad (2.13)$$

$-E_0/s^2$

from which the perturbed eigenvalue is $E = E_0 + \Delta q s^2$. This perturbation solution for E , using Δq from Eq. (2.13), is fast and direct unlike the complicated iterative solution of the original equation (2.9). Furthermore, since E_0 is real, the Airy functions have real arguments greatly simplifying numerical calculations.

For well trapped modes ($E_0 \ll 0$), asymptotic expansion of the Airy functions gives

$$a_0 \Delta q = - \left[\frac{(1+s^3)e^{-\zeta}}{16(-E_0)^{\frac{3}{2}}} + \frac{i}{4} e^{-\zeta(1+s^3)} \right] \quad (2.14)$$

$$\text{with } \zeta = 4(-E_0)^{\frac{3}{2}}/3s^3.$$

The expression for Δq in Eq. (2.14) is based on large argument asymptotic expansions of Ai and Bi . Careful analysis of these expansions indicate that this form is not valid if $w, E \gtrsim -3.5$. Instead, when E_0 is not large and negative (or s^3 not small), Z_0 is evaluated from Eq. (2.10) and Δq computed by direct methods from Eq. (2.13). Compared with the numerical calculations of Pedersen and Gordon, this procedure yields excellent agreement for the trapped modes [$\text{Re}(E) < 0$].

The perturbation expression for Δq [Eq. (2.13)] is only valid if q_0 is near a zero of Ai . Thus a "cutoff" condition is $sD > 2.338$, the first zero of Ai . Ducts with smaller values of sD cannot support trapped modes. Using the asymptotic formulas for zeroes of Ai , an approximate expression for the number of trapped modes N_{vm} is

$$N_{vm} \simeq .25 + (sD)^{\frac{3}{2}}/1.5\pi.$$

2.4 LEAKY MODES

The leaky wave [$\text{Re}(E_m) > 0$] Regge poles are difficult to calculate by solving for roots of $T_-(E)$ as was done for the trapped modes. The imaginary part of the pole is comparable to the real part and recourse is usually made to iterative numerical solutions of Eq. (2.9). Instead a different approach will be used for the leaky modes, which gives an approximate, yet accurate, solution.

As discussed previously, the integrand in Eq. (2.6) resonates for real values of E corresponding to the real part of E_m . Expanding the product $T_+(E)T_-(E)$ using modulus and phase representations for the Airy functions (Appendix A) yields

$$T_+(E)T_-(E) = C(E)G^2(E)$$

where

$$G^2(E) = \beta^2 \sin^2 x_+ + \sin^2 x_- + 2\beta \sin x_+ \sin x_- \cos \Delta . \quad (2.15)$$

The envelope $C(E)$ is a slowly varying function of the energy while G^2 has resonances. The various terms in Eq. (2.15) are

$$\beta = M(w)N(E)/sN(w)M(E) ,$$

$$\Delta = \phi(E) - \theta(E) , \quad \delta = \phi(w) - \theta(w) ,$$

$$x_{\pm} = (x \pm \delta)/2 ,$$

and

$$x = 2\theta(q_0) - \phi(w) - \theta(w) .$$

The M , N , θ , and ϕ functions are the moduli and phases of the various Airy functions and their derivatives.

All the terms in Eq. (2.15) are slowly varying functions of E with the exception of the angle x . Analysis shows that minima in G^2 occur at those energy values E_r where x is a negative multiple of 2π

$$x(E_r) = -2m\pi , \quad m = 1, 2, \dots \quad (2.16)$$

When $E_r \gg 0$, the asymptotic expansions for the phase functions θ and ϕ yield

$$\chi(E_r) \sim \pi/2 - \frac{4}{3} q_0^{3/2} - \pi + \frac{4}{3} w^{3/2} = -\frac{\pi}{2} - \frac{4}{3} (q_0^{3/2} - w^{3/2}) \quad (2.17)$$

and thus the eigenvalue condition is

$$\left. \frac{4}{3} (q_0^{3/2} - w^{3/2}) \right|_{E_r} = \frac{4}{3s} 3 \left[(E_r + s^3 D)^{3/2} - E_r^{3/2} \right] = 2\pi(m - 1/4) \quad (2.18)$$

But, the phase integral between the surface and duct bottom is just

$$J(E_r) = \int_{-D}^0 (E_r - s^3 x)^{1/2} dx = \frac{2}{3} (q_0^{3/2} - w^{3/2}) \quad , \quad \text{phase integral action integral} \quad (2.19)$$

so the eigenvalue condition for highly leaky modes is just $J(E_r) = \pi(m - 1/4)$, or the usual WKB quantization condition. Equation (2.17) in practice proves to be a good approximation even for small values of E_r , and is used to solve Eq. (2.16) numerically.

Once the real part E_r of the Regge pole is obtained from the extremum in G^2 , the imaginary portion E_I is found from conservation of energy. From the form Eq. (2.7), E_I gives rise to an attenuation coefficient a^L :

$$a^L = 2 I_m \left\{ \left[k_0^2 - (E_r - iE_I + s^3 D)/H^2 \right]^{1/2} \right\} \quad .$$

Using the ray-equivalent to the leaky mode, a^L is

$$a^L = - \ln [R(\theta_m)] / D(\theta_m) \quad (2.20)$$

where θ_m is the surface grazing angle of the ray-equivalent defined by

$$\sin^2 \theta_m = g_+ H(E_r + s^3 D) \quad ,$$

$R(\theta_m)$ is the reflection coefficient of the ray equivalent by the gradient discontinuity in refractive index at the duct bottom, and where $D(\theta_m)$ is the ray's cycle distance. The cycle distance $D(\theta_m)$ is given by

$$D(\theta_m) = -2k_0 H^2 \frac{\partial}{\partial E} X(E_r) \sim 4k_0 H (q_0^{1/2} - w^{1/2})$$

where X from Eq. (2.17) has been used.

The reflection coefficient $R(\theta_m)$ is found to be

$$R(\theta_m) = R(E_r) = \frac{\beta^2 + 1 + 2\beta \cos(\delta + \Delta)}{\beta^2 + 1 + 2\beta \cos(\delta - \Delta)},$$

with limiting values

$$R = (1 + s^3)/(1 + s)^3, \quad E_r \rightarrow 0$$

$$R = \frac{(1 + s^3)^2}{64 E_r^3}, \quad E_r \rightarrow \infty$$

The results [Eqs. (2.18) and (2.20)] obtained for the leaky modes are suggestive of WKB formulas. As pointed out by Furry, however, (Ref. 9) phase integral solutions for the bilinear profile are not strictly valid due to the non-analytic nature of the refractive index profile. In particular the phase integral methods do not give the proper above barrier ($E_r > 0$) reflection coefficient Eq. (2.22) arising from gradient discontinuities in n at the duct bottom.

2.5 EIGENFUNCTIONS

Once the eigenvalues E_m are known, the virtual mode depth functions $\psi_m = \psi(x, E_m)$ are obtained from Eq. (2.4a) or Eq. (2.4b). The latter can be simplified, by making use of continuity across the duct bottom, to

$$\psi_m(x) = \psi_m(0) h_1(p)/h_1(E_m) \quad , \quad x > 0 \quad (2.23)$$

with $p = E_m + x$. The normalization N_m is easily obtained from properties of the Airy functions and Eqs. (2.4a) and (2.23) as

$$N_m = H \int_{-D}^{\infty} \psi_m^2(x) dx = \frac{H}{s^3} \left[1 + (1 + s^3) \psi_m^2(0) \frac{d}{dE_m} \left(h_1'/h_1 \right) \right] . \quad (2.24)$$

The calculation of ψ_m and N_m involves computing Airy functions of complex arguments (due to the complex nature of the Regge pole E_m), which tends to be time consuming. Instead various approximations are used to significantly reduce the numerical calculations.

2.5a TRAPPED MODES

Trapped modes have imaginary components E_I of the Regge pole that are small. Since the virtual mode depth functions are analytic with respect to the energy, this suggests a Taylor series expansion about $E_r = \text{Re } E_m$:

$$\psi(x, E) \simeq \psi(x, E_r) + i E_I \frac{\partial \psi(x, E_r)}{\partial E} .$$

For positions within the duct, this yields

$$\psi(x) \sim \frac{\pi}{s} B_1(-q_0^*) \left[(A_1 - \alpha_0 \Delta q_r B_1) + i \Delta q_i (A_1' - \alpha_0 \Delta q_r B_1') \right] \Big|_{-q_r}$$

where $\alpha_0 = \pi A_1'(-q_0^*)^2$, $\Delta q = \Delta q_r + i \Delta q_i$, and $q_r = E_r/s^2 - sx$. The squared amplitude is thus

$$|\psi(x)|^2 \sim \frac{\pi}{\alpha_0 s^2} \left[(A_1 - \alpha_0 \Delta q_r B_1)^2 + \Delta q_i^2 (A_1' - \alpha_0 \Delta q_r B_1')^2 \right] . \quad (2.25)$$

Strongly trapped modes have $|\Delta q| \ll 1$ and therefore

$$|\psi(x)|^2 \sim \frac{\pi}{\alpha_0 s^2} A_i^2 (1 - \alpha_0 \Delta q_r B_i/A_i)^2 , \quad (2.26)$$

where the A_i, B_i are evaluated at $q_r = E_0/s^2 - sx$.

Similar considerations for the below duct region ($x > 0$) lead to

$$h_1(p) \sim h_1(p_r) + i E_i h_1'(p_r) , \quad p_r = x + E_r , \quad E_i = \text{Im}(E)$$

and thus

$$\psi(x) \sim \psi(0) \frac{h_1(p_r) + i E_i h_1'(p_r)}{h_1(E_r) + i E_i h_1'(E_r)} .$$

The squared amplitude of u then is

$$|\psi(x)|^2 \sim |\psi(0)|^2 \cdot \frac{M^2(p_r) + N^2(p_r)E_i^2 - 2E_i/\pi}{M^2(E_r) + N^2(E_r)E_i^2 - 2E_i/\pi}$$

where $M^2(x) = A_i^2(-x) + B_i^2(-x)$, and $N^2(x) = A_i'(-x)^2 + B_i'(-x)^2$. For those modes with $|\Delta q| \ll 1$, this becomes

$$|\psi(x)|^2 \sim |\psi(0)|^2 \frac{M^2(E_0 + x)}{M^2(E_0)} . \quad (2.27)$$

The normalization N_m is

$$N_m = \frac{H}{s^3} \left[1 + (1+s^3) \psi^2(0) \left. \frac{d}{dE} \left(\frac{h_1'}{h_1} \right) \right|_{E_0} \right] ,$$

and for well trapped modes becomes

$$N_m \sim \frac{H}{s^3} \left[1 + \frac{(1+s^3)e^{-\zeta}}{4w_0^2 s^2} \right] \rightarrow \frac{H}{s^3} \quad (2.28)$$

where $w_0 = |E_0|/s^2$ and $\zeta = 4/3 w_0^{3/2}$.

2.5b LEAKY MODES

Leaky virtual modes have positive E_r with E_i not small. Asymptotic expansion of the Airy functions with arguments in the sector $|\arg z| < 2/3 \pi$ yield for the in duct form (Eq. 2.4a) of ψ

$$\psi(x, E) \sim s^{-1} (q q_0)^{-1/2} [\sin(\zeta - \zeta_0) - \cos(\zeta - \zeta_0) 5/72 \zeta]$$

where $\zeta = 2/3 q^{3/2}$, $\zeta_0 = 2/3 q_0^{3/2}$ ($|\arg(q, q_0)| < 2/3 \pi$). The squared amplitude of ψ is then

$$\begin{aligned} |\psi(x, E)|^2 &= s^{-2} |q q_0|^{-1/2} |\sin(\zeta - \zeta_0) - \cos(\zeta - \zeta_0) 5/72 \zeta|^2 \\ &= s^{-2} |q q_0|^{-1/2} |\sin(\zeta - \zeta_0)|^2 , \quad |\zeta| \gg 1 \end{aligned}$$

or

$$|\psi(x)|^2 = \frac{1}{2} s^{-2} |q q_0|^{-1/2} (\cosh 2\Delta\zeta_r - \cos 2\Delta\zeta_i) , \quad x < 0 \quad (2.29)$$

with $\Delta\zeta = \Delta\zeta_r + i \Delta\zeta_i = \zeta - \zeta_0$.

Below the duct, similar expansions are made for $h_1(p)$ in Eq. (2.23) to give

$$\begin{aligned} h_1(p) &= A_1(-p) - i B_1(-p) \\ &\simeq \sqrt{\pi} p^{-1/2} e^{i(t-\pi/4)} (1 - i 5/72 t) , \quad |p| \gg 1 \end{aligned}$$

with $p = E + x$, and $t = t_r + i t_i = 2/3 p^{3/2}$.

The squared modulus of h_1 is

$$|h_1(p)|^2 \simeq \pi p^{-\frac{1}{2}} e^{-2t_f} |1 - 15/72t|^2 , \\ \rightarrow \pi p^{-\frac{1}{2}} e^{-2t_f} , \quad (2.30)$$

which leads to ψ having the form

$$|\psi(x)|^2 \sim \frac{|\psi(0)|^2}{|h_1(E_m)|^2} \pi p^{-\frac{1}{2}} e^{-2t_f} \quad (2.31)$$

below the duct. Note that since $E_f < 0$, Eq. (2.31) predicts an exponential increase in the virtual mode amplitude with increasing depth below the duct. This behavior is in precise agreement with the numerical results of Pedersen and Gordon.

2.5c TURNING POINTS

The expressions for the virtual mode depth function ψ_m developed thus far are based on large argument expansions of the Airy functions which fail near turning points (i.e., regions where q or p are zero). However, ψ_m is an analytic function of its arguments and thus can be expanded in a Taylor series about the turning point.

Concentrating on the in-duct form [Eq. (2.4a)] of ψ , a series expansion about the turning point is ($q = E_m/s^2 - sx$)

$$\psi_m(x) = \psi(q) = \psi_0 + q \psi'_0 + \frac{q^2}{2} \psi''_0 + \frac{q^3}{6} \psi'''_0 + \dots \quad (2.32)$$

where $\psi_0 = \psi(q=0)$, $\psi'_0 = \partial\psi(q=0)/\partial q$, etc. The series can be greatly simplified by using the differential equation satisfied by ψ

$$\partial^2 \psi / \partial q^2 = -q\psi$$

to yield

$$\begin{aligned}\psi(q) &= \psi_0 \left(1 - q^3/3! + 4q^4/6! - \dots \right) \\ &\quad + q\psi'_0 \left(1 - 2q^3/4! + 10q^6/7! - \dots \right) .\end{aligned}\quad (2.33)$$

The depth function and its derivative at the turning point are .

$$\psi = c_1 \frac{\pi}{s} \left[Bi(-q_0) - \sqrt{3} Ai(-q_0) \right] , \quad (2.34)$$

$$\psi'_0 = c_2 \frac{\pi}{s} \left[Bi(-q_0) + \sqrt{3} Ai(-q_0) \right] , \quad (2.35)$$

where $c_1 = Ai(0)$ and $c_2 = -Ai'(0)$. Separate asymptotic expressions for ψ_0 , ψ'_0 are obtained depending on whether the mode is trapped or leaky (i.e., depending on q_0).

Trapped modes have q_0 near a zero of Ai , and the perturbation expansion of Eq. (2.12) leads to

$$|\psi_0|^2 \sim \frac{\pi c_1^2}{a_0 s^2} \left[(1 - a_0 \sqrt{3} \Delta q_r)^2 + 3a_0^2 \Delta q_i^2 \right] \quad (2.36)$$

and

$$\psi'_0/\psi_0 \sim \frac{c_2 (1 + a_0 \sqrt{3} \Delta q)}{c_1 (1 - a_0 \sqrt{3} \Delta q)} , \quad \Delta q = \Delta q_r + i\Delta q_i . \quad (2.37)$$

Similar results for leaky modes are obtained by using the complex asymptotic forms of $Ai(-q_0)$ and $Bi(-q_0)$:

$$\psi'_0/\psi_0 \sim -\frac{c_2 \cos(\zeta_0 - \pi/12)}{c_1 \sin(\zeta_0 + \pi/12)} , \quad \zeta_0 = \frac{2}{3} q_0^{\frac{3}{2}} \quad (2.38)$$

and

$$|\psi_0|^2 \sim \frac{4\pi c_1^2}{s^2} |q_0|^{-\frac{1}{2}} |\sin(\zeta_0 + \pi/12)|^2 . \quad (2.39)$$

For both trapped and leaky modes, the amplitude of $|\psi|^2$ is obtained from Eq. (2.33) as

$$|\psi(q)|^2 \sim |\psi_0|^2 \left| \left(1 - \frac{q^3}{3!} + \frac{4q^4}{6!} \right) + q \frac{\psi'_0}{\psi_0} \left(1 - \frac{2q^3}{4!} + \frac{10q^6}{7!} \right) \right|^2 . \quad (2.40)$$

2.5d NEAR SURFACE

Near the surface ($x \sim -D$) the virtual mode depth function can be expanded in a Taylor series as was done for the turning point region

$$\psi(q) = \psi(q_0) + \Delta q \psi'(q_0) + \frac{\Delta q^2}{2} \psi''(q_0) + \dots \quad (2.41)$$

with $\Delta q = q - q_0$ and $q_0 = E/s^2 + sD$ the surface value for q . At the surface $\psi(q_0) = 0$ and $\psi'(q_0) = 1/s$ so Eq. (2.41) becomes

$$\psi(q) = \frac{\Delta q}{s} \left(1 - q_0 \frac{\Delta q^2}{s^3 3!} - 2 \frac{\Delta q^3}{s^4 4!} + \dots \right) \quad (2.42)$$

where $\Delta q = q - q_0 = -s(x+D)$. The amplitude of ψ is then

$$|\psi|^2 \sim (x+D)^2 \left| 1 - q_0 s(x+D)^2 / 6 - s^3 (x+D)^3 / 12 + \dots \right|^2 \quad (2.43)$$

which displays the proper quadratic depth dependence and pressure-release condition at $x = -D$.

2.6 ROUGH SURFACE EFFECTS

The presence of a non-planar ocean surface will modify the Regge poles E_m leading to a larger imaginary component. The virtual mode intensity decays with range at an increased rate due to an additional attenuation term arising from rough surface scattering. The resultant attenuation is the sum

of the previously computed leakage term α^L and the surface scattering term α^S

$$\alpha = \alpha^L + \alpha^S .$$

The surface scattering term is found by applying energy conservation to the modal ray-equivalent interacting with the ocean surface.

A ray-equivalent may be identified with each virtual mode through a surface grazing angle θ_m defined by

$$\sin^2 \theta_m = (E_r + s^3 D) / (k_0 H)^2$$

previously $\sin^2 \theta_m = g_r / t (E_r + s^3 D)$
the "correct" \nearrow

and a corresponding cycle distance $D(\theta_m)$

$$D(\theta_m) = 2H \cos \theta_m \int_{-D}^{x_1} [E_r - Q(x)]^{-\frac{1}{2}} dx .$$

x_1 is the upper turning point (real) of the mode and for leaky modes is taken as the duct bottom ($x = 0$). Each interaction of the ray-equivalent with the rough surface is treated as a specular reflection with corresponding reflection coefficient $R^S(\theta_m)$. The intensity decay with range is then modeled as a "loss per bounce" applied continuously over the ray's cycle distance, leading to

$$\alpha^S = - \ln [R^S(\theta_m)] / D(\theta_m) .$$

The rough surface specular reflection coefficient R^S is computed as a function of frequency, grazing angle and sea-state from previous work by Spofford and Keenan.⁽¹⁷⁾ Strictly speaking, the rough surface effects should be included as a modification of the surface impedance condition and the Regge poles found in a self consistent manner. The error made in adopting the present approach is, however, consistent with present understanding of surface scattering phenomena and within the approximation of replacing the true index of refraction profile by the Furry model.

SECTION 3 MODEL EVALUATION

The virtual mode surface duct model described earlier was evaluated by comparisons with output from the parabolic equation (PE) code⁽¹⁶⁾ and the NOSC n-layer normal mode (NM) code. The test environment was a bilinear n^2 profile for a deep (1,000 foot) surface duct with a corresponding sound speed profile having a pressure gradient ($\sim .018 \text{ sec}^{-1}$) within the duct and a moderate ($\sim - .1 \text{ sec}^{-1}$) gradient below the duct. The ocean was assumed infinitely deep with a smooth, pressure-release surface and no surface loss. Incoherent transmission loss, for a monochromatic point source, was computed for a variety of source/receiver geometries.

Source frequencies of 25, 50, 100, 250, 500, and 1,000 Hz were considered which yielded propagation conditions corresponding to zero and 21 trapped modes respectively. This effectively simulated results for thinner ducts at higher frequencies. Source-receiver combinations for all depth pairs between 250 and 1,500 feet in 250-foot increments (21 distinct pairs) were chosen to cover a wide range of in-layer, cross-layer and below-layer geometries for the various source frequencies. In total, 126 different frequency/geometry propagation scenarios were examined in the comparisons.

Two types of surface duct model evaluations were made: (1) incoherent transmission-loss for all 126 scenarios, and (2) individual comparisons of modal attenuation coefficients and intensity amplitudes.

The transmission-loss evaluations were made by direct comparison of the virtual mode surface duct model results with those of the PE and NM codes. The PE code actually outputs coherent transmission-loss values, displaying characteristic interference features. These oscillations were removed by intensity averaging the PE output with an eight (8) nautical mile moving window to simulate incoherent levels.

The NM code, in addition to providing TL output, also output the individual modes used in the TL calculation. Modal attenuation coefficients and eigenfunction intensity amplitudes were available for direct comparison with the surface duct model.

3.1 PE COMPARISONS

The AESD PE code was run at six source frequencies (25, 50, 100, 250, 500, and 1,000 Hz) and for six receiver depths (250, 500, 750, 1000, 1250, and 1500 feet). The PE code is a finite depth ocean model, requiring an absorbing bottom to effectively simulate an infinitely deep ocean. The bottom was placed at 8,000 feet for the 25 Hz run and at 2,000 feet for all other frequencies. The FFT transform size used by the PE code was 2^8 for 25, 500, and 1,000 Hz runs, and 2^7 for the 50, 100, and 250 Hz runs. Due to the use of a running intensity average, PE results at ranges closer than 8 nautical miles are not reliable and are ignored. The PE code implicitly includes the leaky as well as the trapped waves and thus provides a check on the validity of truncating the virtual mode spectrum after three leaky modes.

Comparisons between the virtual mode surface duct model and PE are shown in Figures (3.1) to (3.36) for the various propagation scenarios. Good agreement with the PE code is indicated for within-, cross-, and below-layer geometries.

The 25 Hz run had no trapped modes and the three lowest leaky virtual modes were included in the virtual mode sum. Good agreement with the PE results are seen for ranges exceeding 10-15 nautical miles. Deviation between PE and model results for shorter ranges are possibly an artifact of the PE smoother and/or due to insufficient terms in the modal sum.

The 50 Hz run case corresponds to one trapped mode. The PE code predicts a higher intensity (by ~1-2 dB) at 50 nautical miles. This is probably an artifact of the PE run due to the bottom being too shallow. Such an effect occurred on earlier 25 Hz runs with shallower bottoms and arises from the non-radiation boundary condition used in the PE code. The PE code boundary condition effectively forces an increase in the pressure field within the water column, leading to higher intensities, hence less TL. Additional deviation between the PE code and the surface duct model occur at intermediate ranges (10 - 20 nm) where PE shows more loss. This trend persists for other frequencies. A plausible explanation for this, is phase cancellation leading to a deep null in this region. Since the surface duct model is not designed

to compute phased TL, such differences are to be expected. In any case, the maximum deviation is ~ 2 dB.

The 100 Hz runs exhibit the same general trends as the 50 Hz data, with the exception of much smaller offset at 50 nm. This is due to the decreasing effect of the finite depth bottom used by the PE code, and a corresponding decrease in intensity from "ghost" reflections off the bottom.

The 250, 500, and 1,000 Hz runs can be grouped as a whole for comparisons. Generally the agreement between PE and the virtual mode code is good at longer ranges. For short ranges ($r \lesssim 10$ nm) possible spectrum truncation and/or PE smoother effects are noticed. Medium ($10 \lesssim r \lesssim 25$ nm) ranges exhibit a weak null in the PE results which is not seen in the virtual mode data. This is most probably caused by phase cancellation which the virtual mode model is not treating. For sources within the duct, the PE results display a characteristic interference with range that the smoother has not completely removed. This effect is more pronounced with increasing frequency.

A volume absorption loss term α_v , of the form $\alpha_v = .125 (f/1000)^2$ dB/nm (f the frequency in Hertz), has been added to the virtual mode model results shown in Figures (3.1) to (3.36) to comply with the PE predictions.

SOURCE: FREQUENCY- 25 (HZ) , DEPTH- 250 (FT)

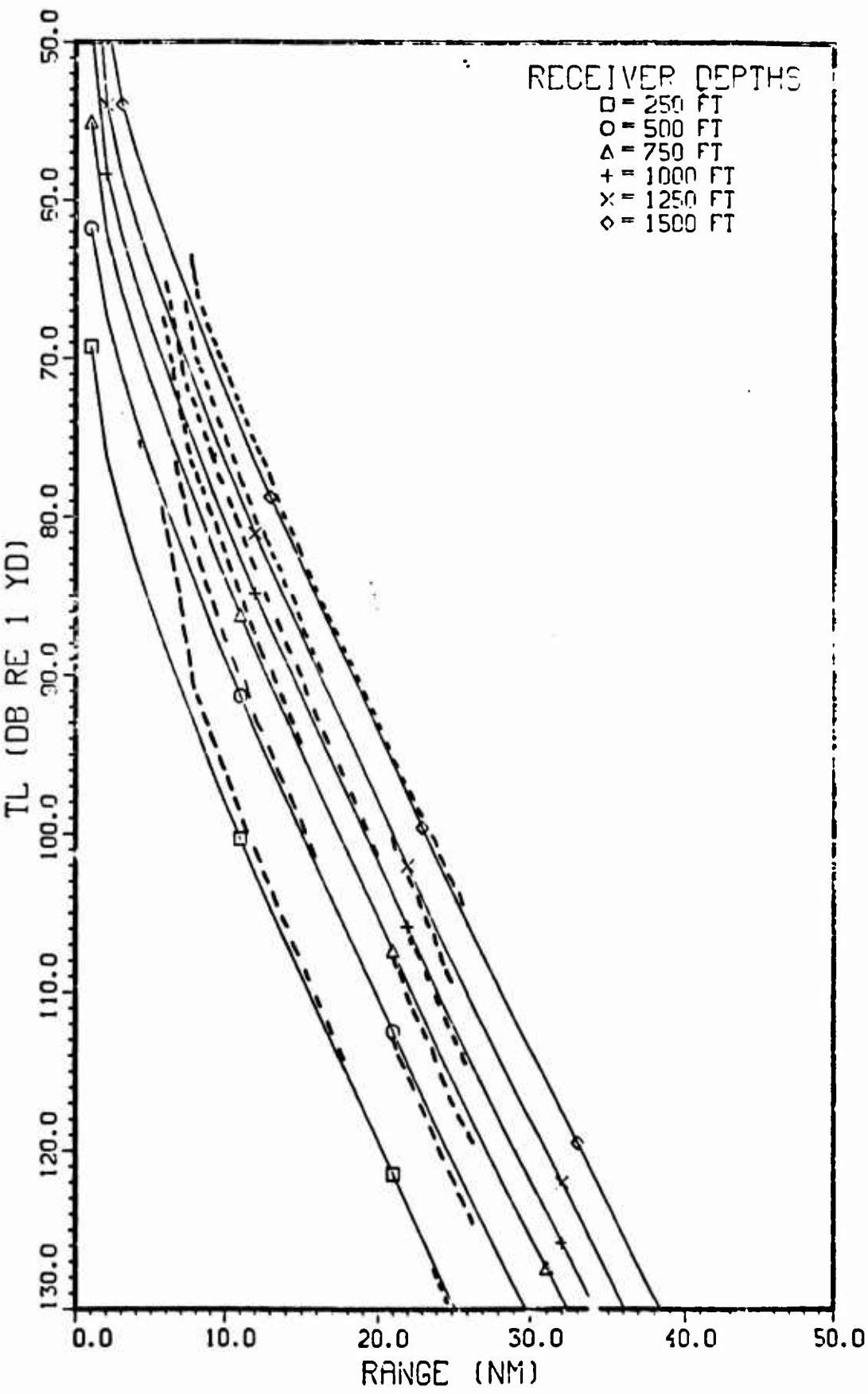


Figure 3-1 . Comparison of Surface-Duct Model (solid) with PE (dash).
Consecutive curves displaced 5 db up .

PNT 2 20.00 MED 1 OCT, 1980 , SAI DISPLA VER 8.2

SOURCE: FREQUENCY- 25 (HZ) , DEPTH- 500 (FT)

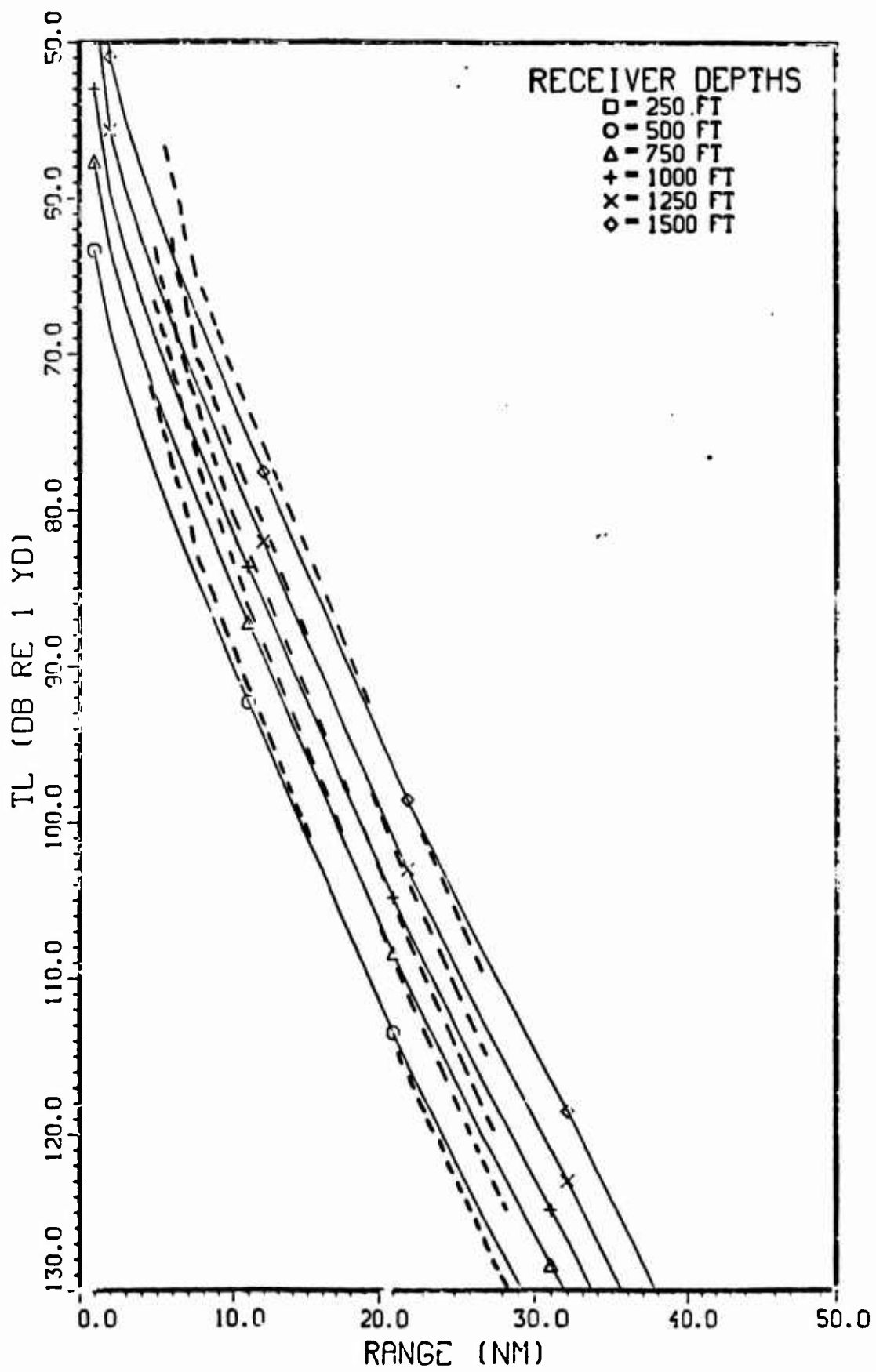


Figure 3-2 . Comparison of Surface-Duct Model (solid) with PE (dashed). Consecutive curves displaced 5 db up .

SOURCE: FREQUENCY= 25 (HZ) , DEPTH= 750 (FT)

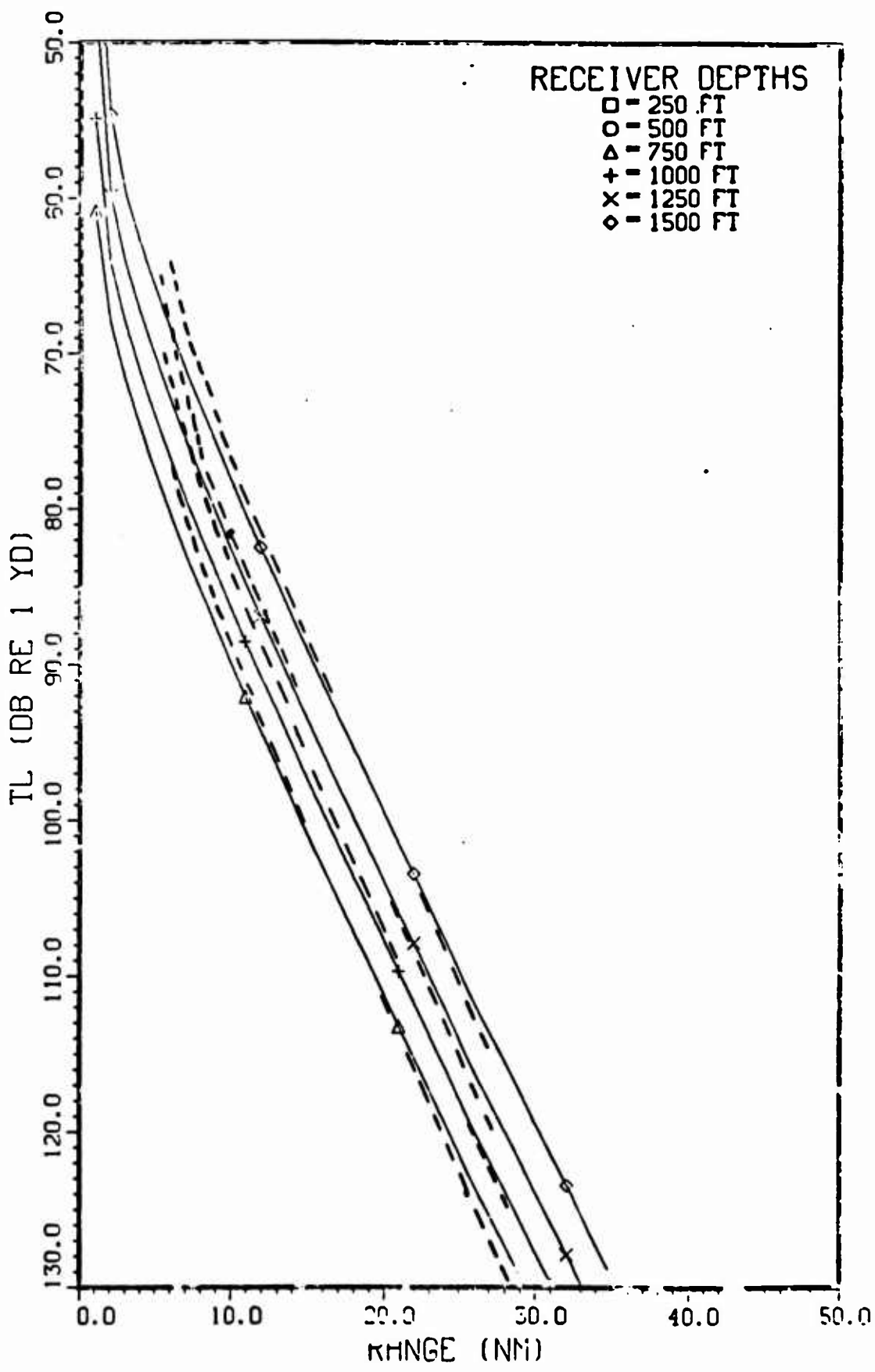


Figure 3-3 . Comparison of Surface-Duct Model (solid) with FE (dash). Consecutive curves displaced 5 db up .

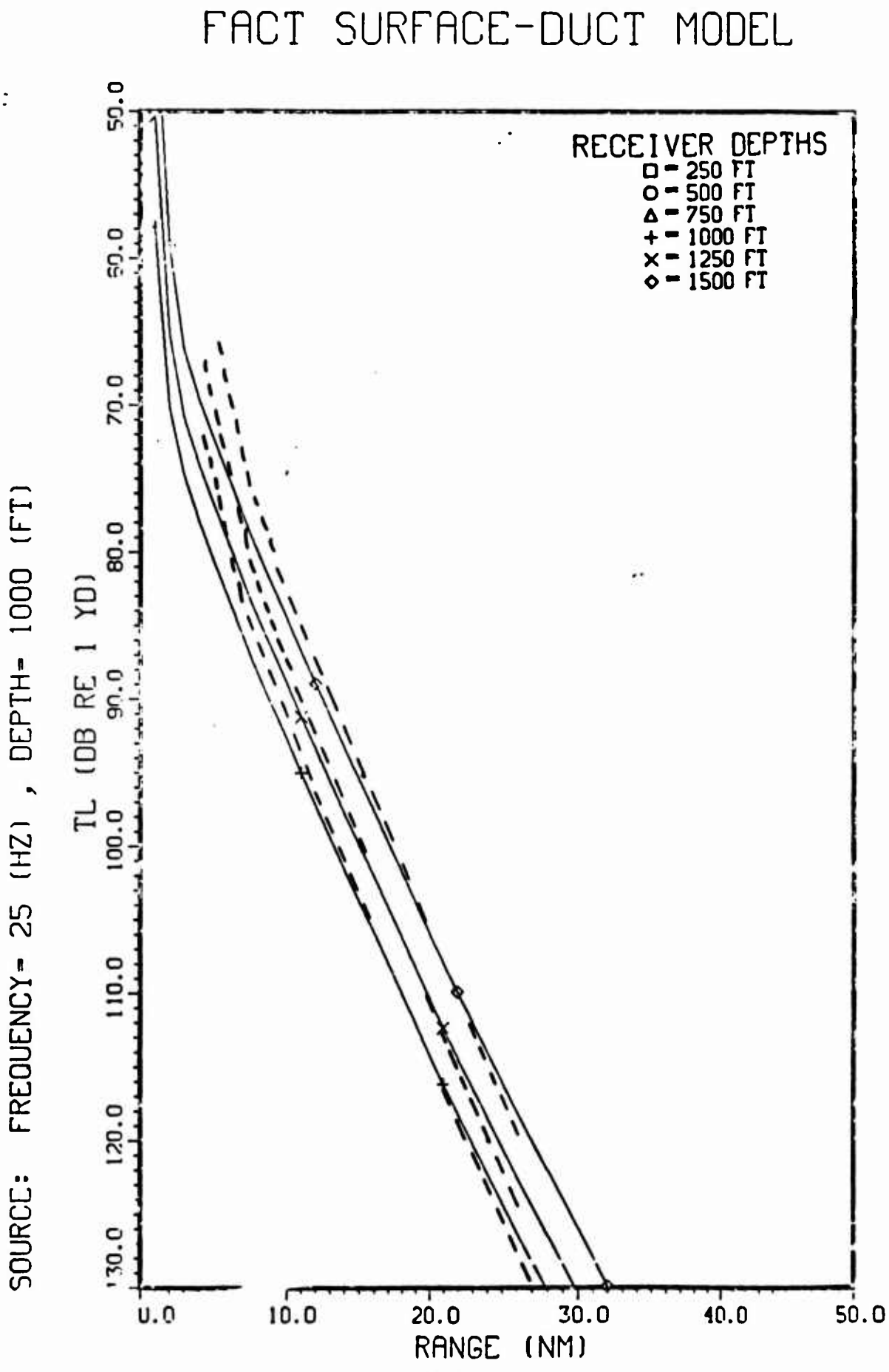


Figure 3-4 . Comparison of Surface-Duct Model (solid) with PE (dash). Consecutive curves displaced 5 db up .

SOURCE: FREQUENCY- 25 (HZ) , DEPTH- 1250 (FT)

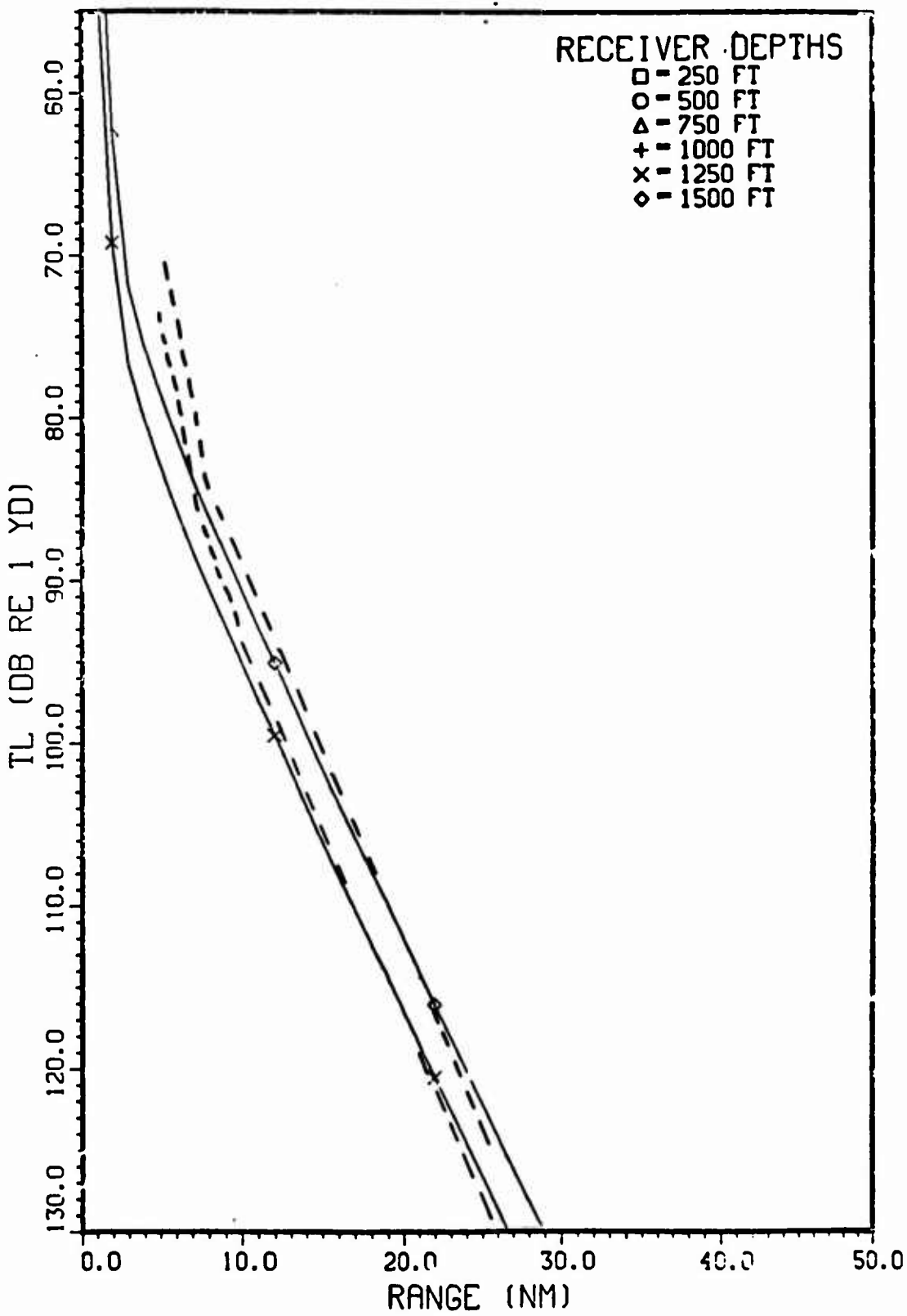


Figure 3-5 . . . Comparison of Surface-Duct Model (solid) with PE (dash).
Consecutive curves displaced 5 db up .

SOURCE: FREQUENCY= 25 (HZ) , DEPTH= 1500 (FT)

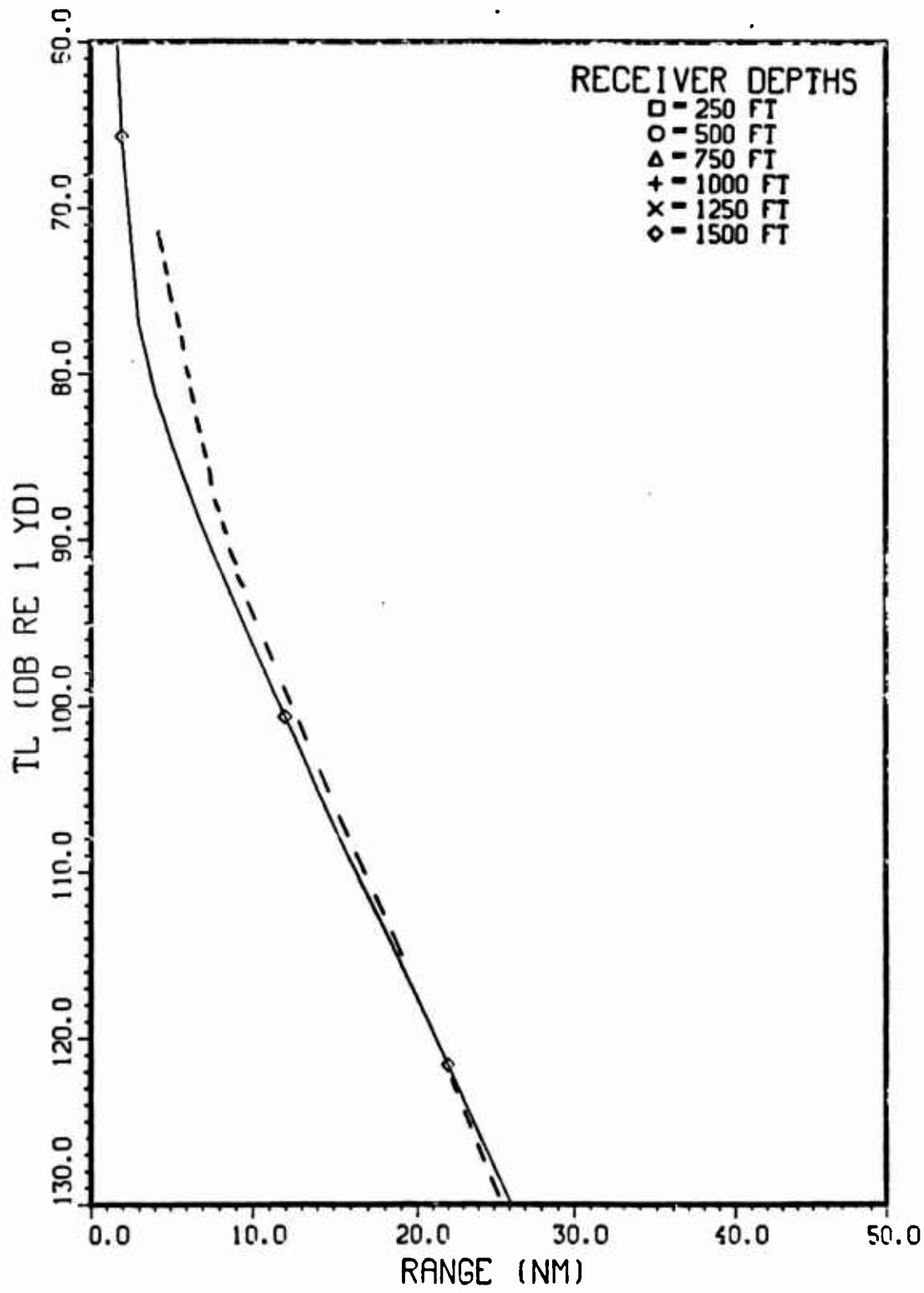


Figure 3-6. Comparison of Surface-Duct Model (solid) with PE (dash).

SOURCE: FREQUENCY- 50 (HZ) , DEPTH- 250 (FT)

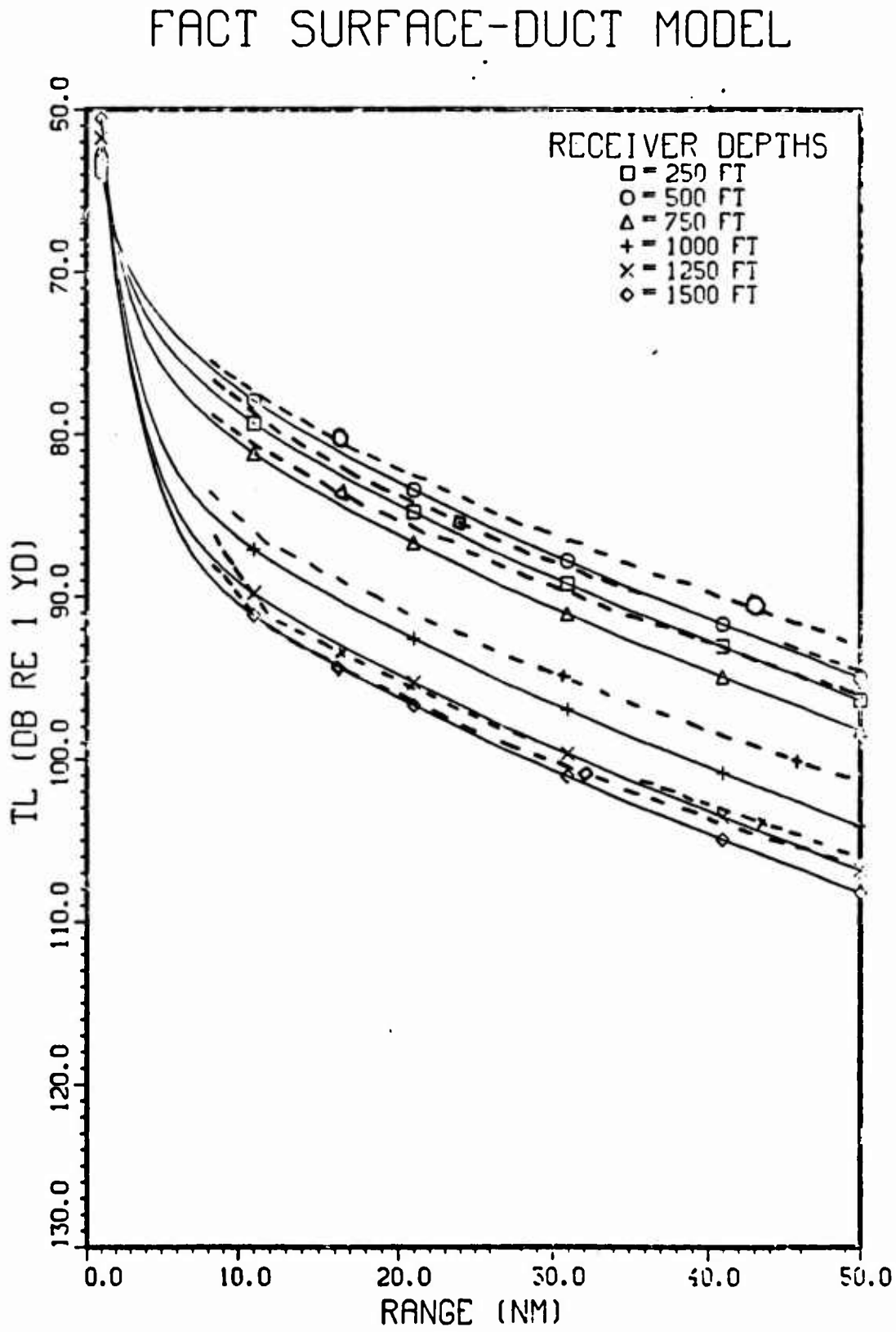


Figure 3-7 . Comparison of Surface-Duct Model (solid) with PC (dashed).

SOURCE: FREQUENCY- 50 (HZ) , DEPTH- 500 (FT)

FACT SURFACE-DUCT MODEL

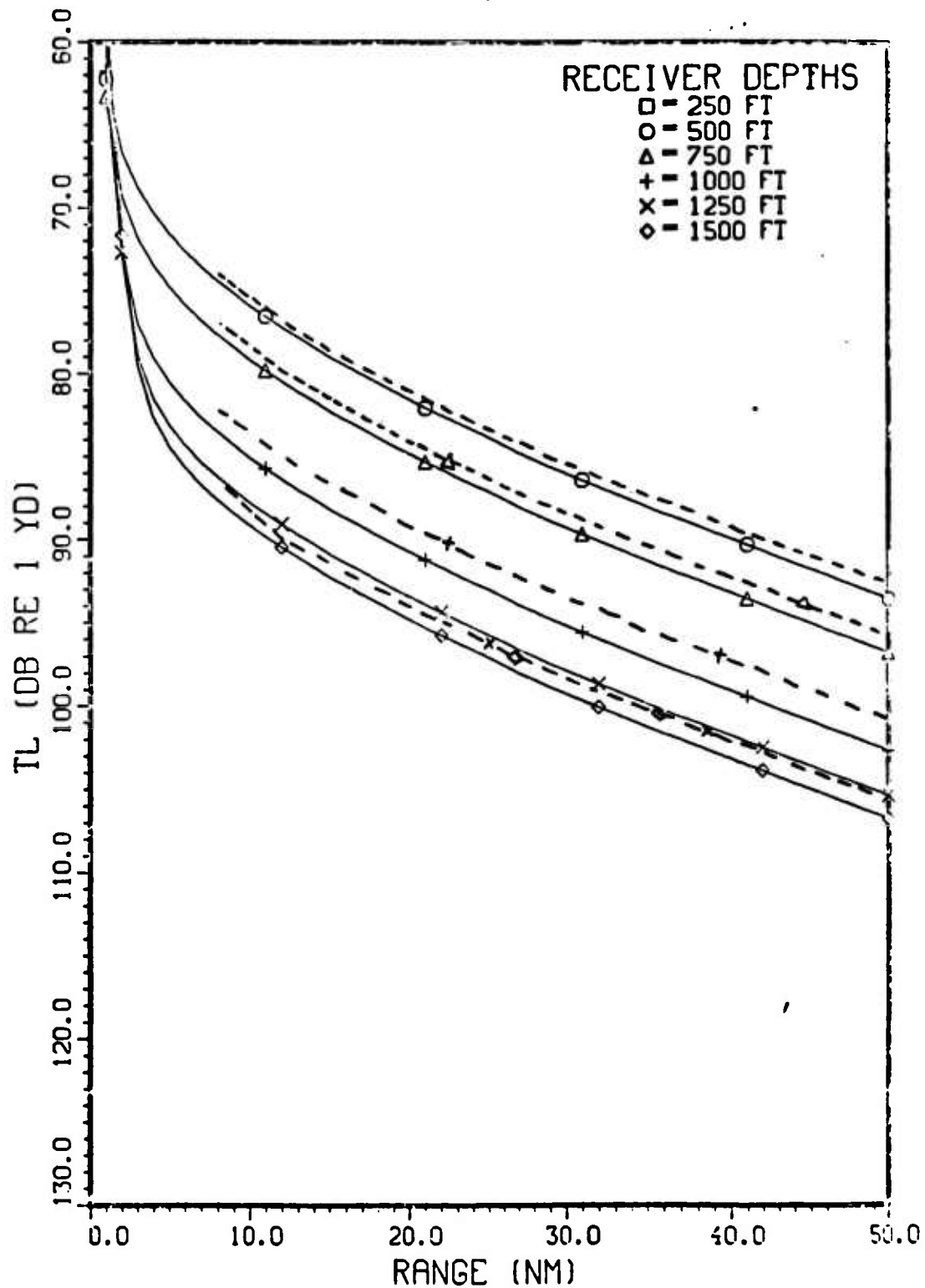


Figure 3-8 . Comparison of Surface-Duct Model (solid) with PC (dashed).

SOURCE: FREQUENCY- 50 (HZ) , DEPTH- 750 (FT)

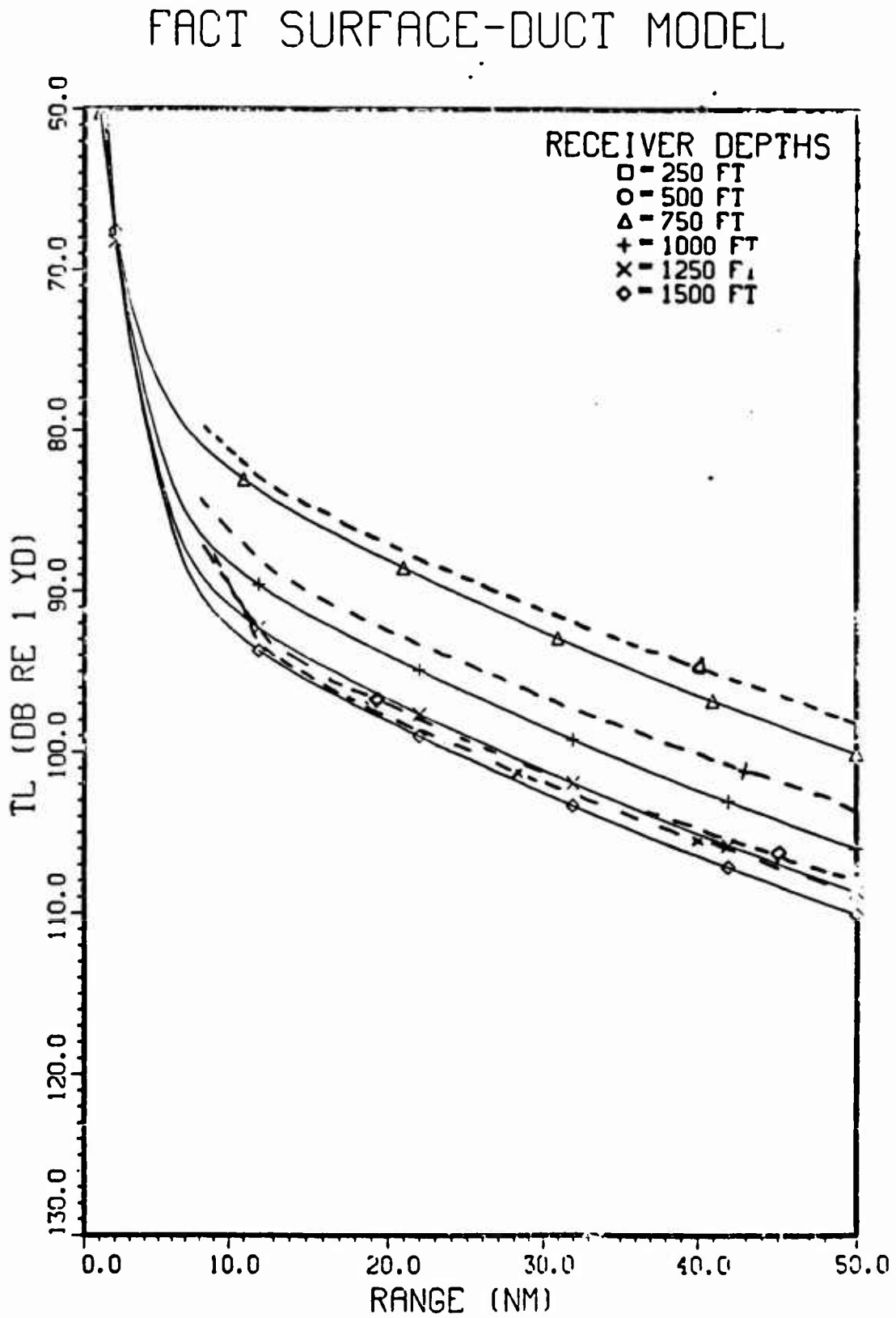


Figure 3-9 . Comparison of Surface-Duct Model (solid) with PE (dash-dot).

FACT SURFACE-DUCT MODEL

SOURCE: FREQUENCY - 50 (HZ) , DEPTH- 1000 (FT)

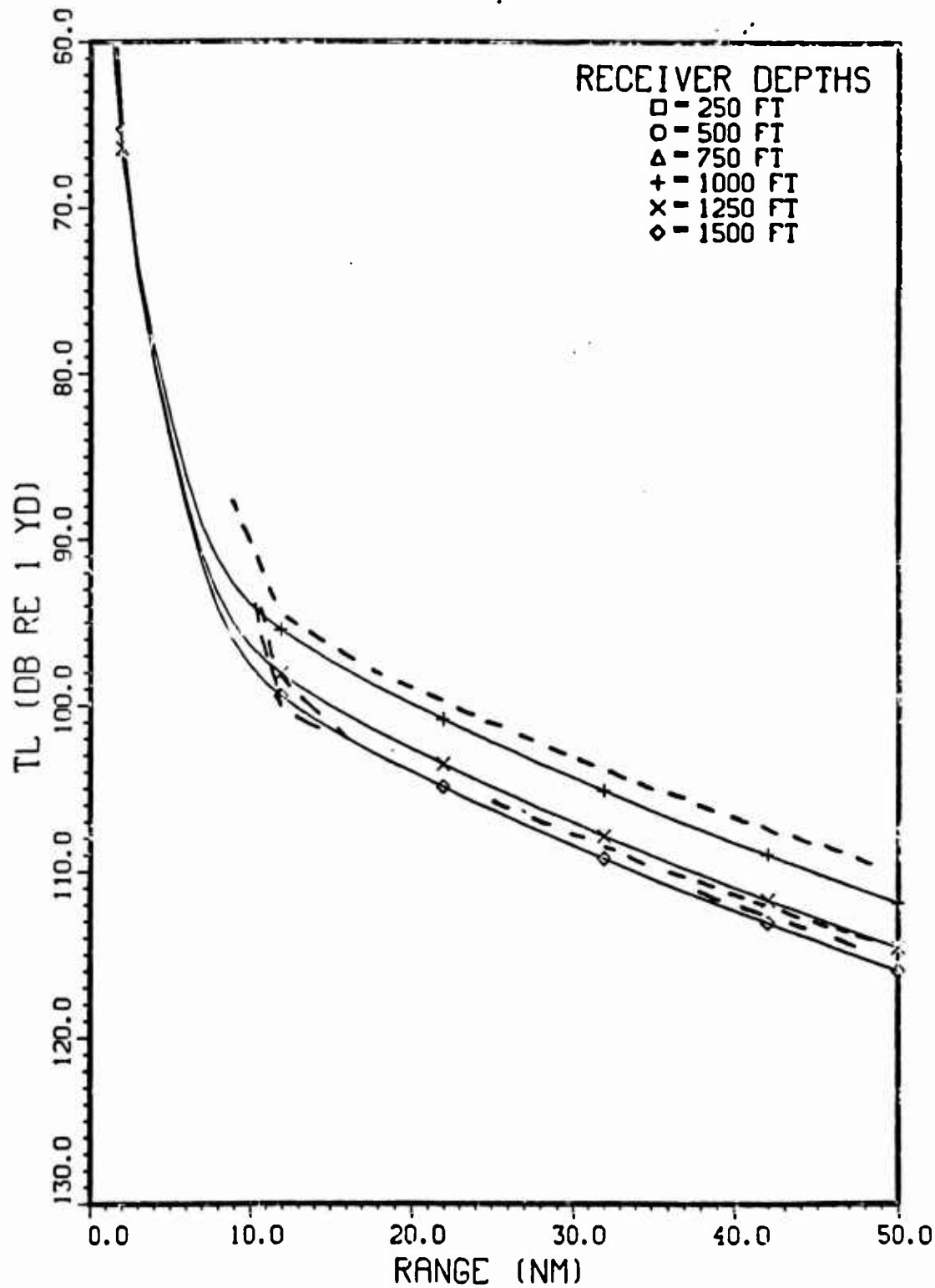


Figure 3-10 .

Comparison of Surface-Duct Model (solid) with PE (dash).

SOURCE: FREQUENCY- 50 (HZ) , DEPTH- 1250 (FT)

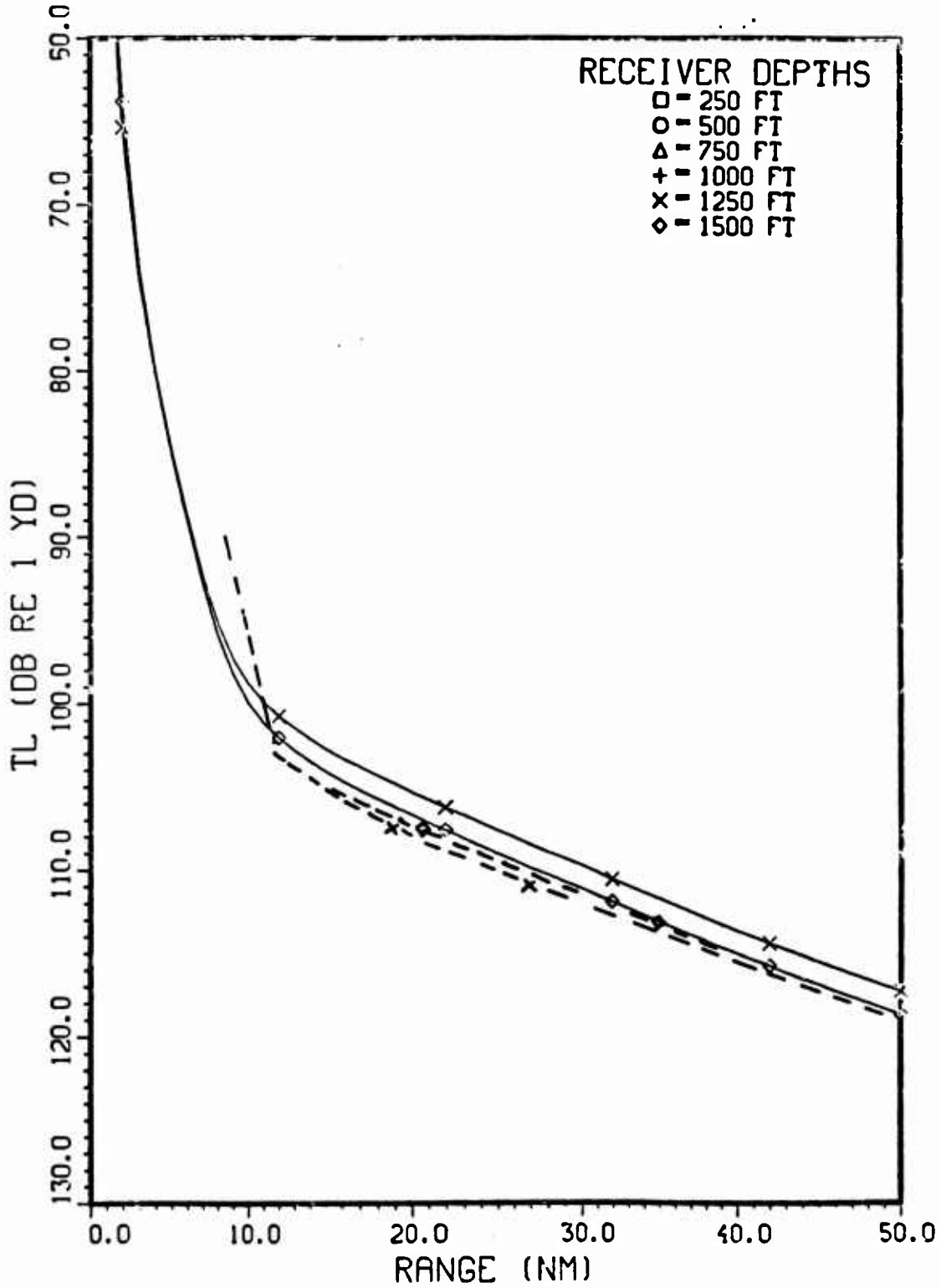


Figure 3-11 .

Comparison of Surface-Duct Model (solid) with PE (dash).

SOURCE: FREQUENCY- 50 (HZ) , DEPTH- 1500 (FT)

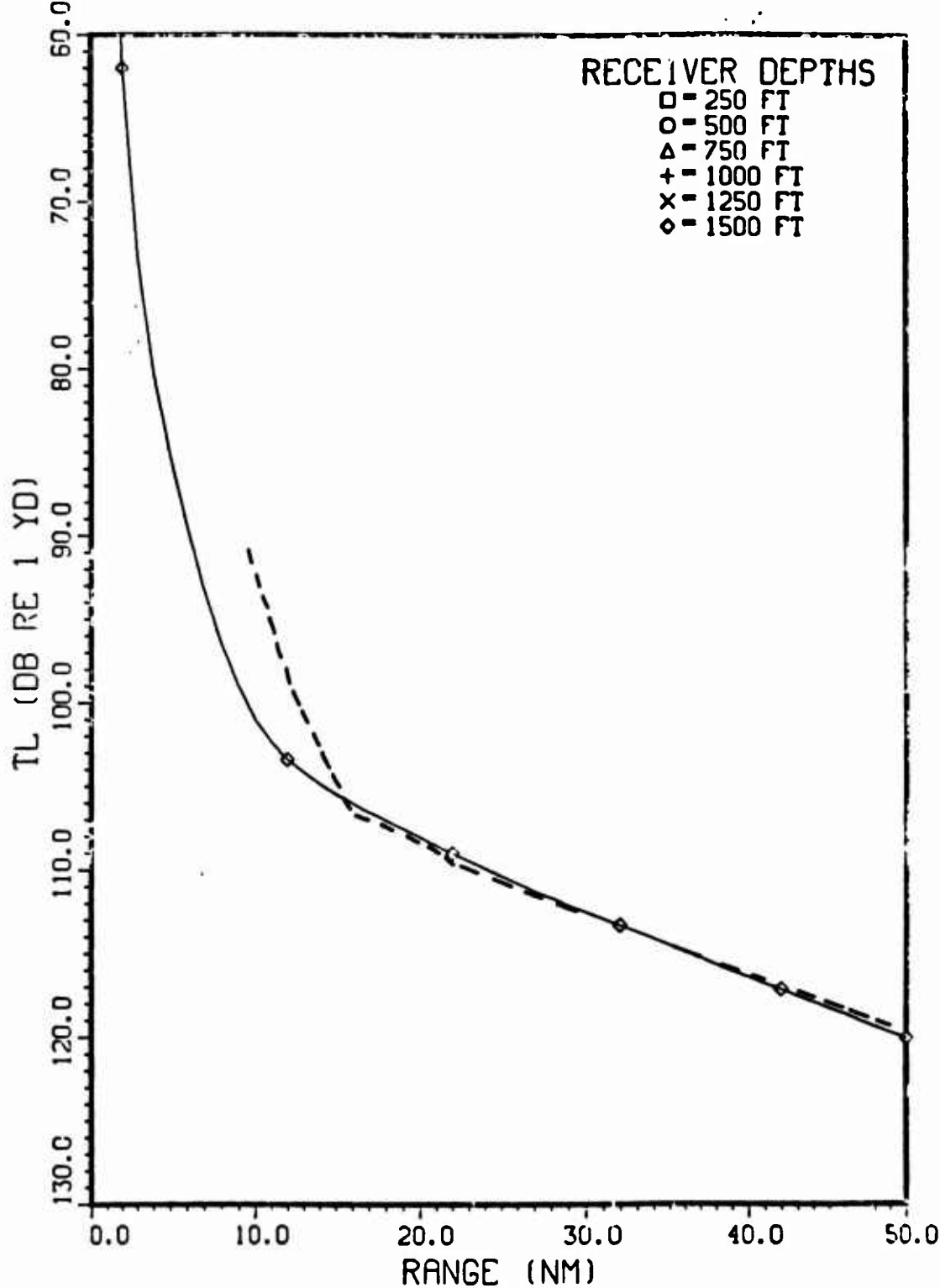


Figure 3-12 .

Comparison of Surface-Duct Model (solid) with PE (dash).

SOURCE: FREQUENCY- 100 (HZ) , DEPTH- 250 (FT)

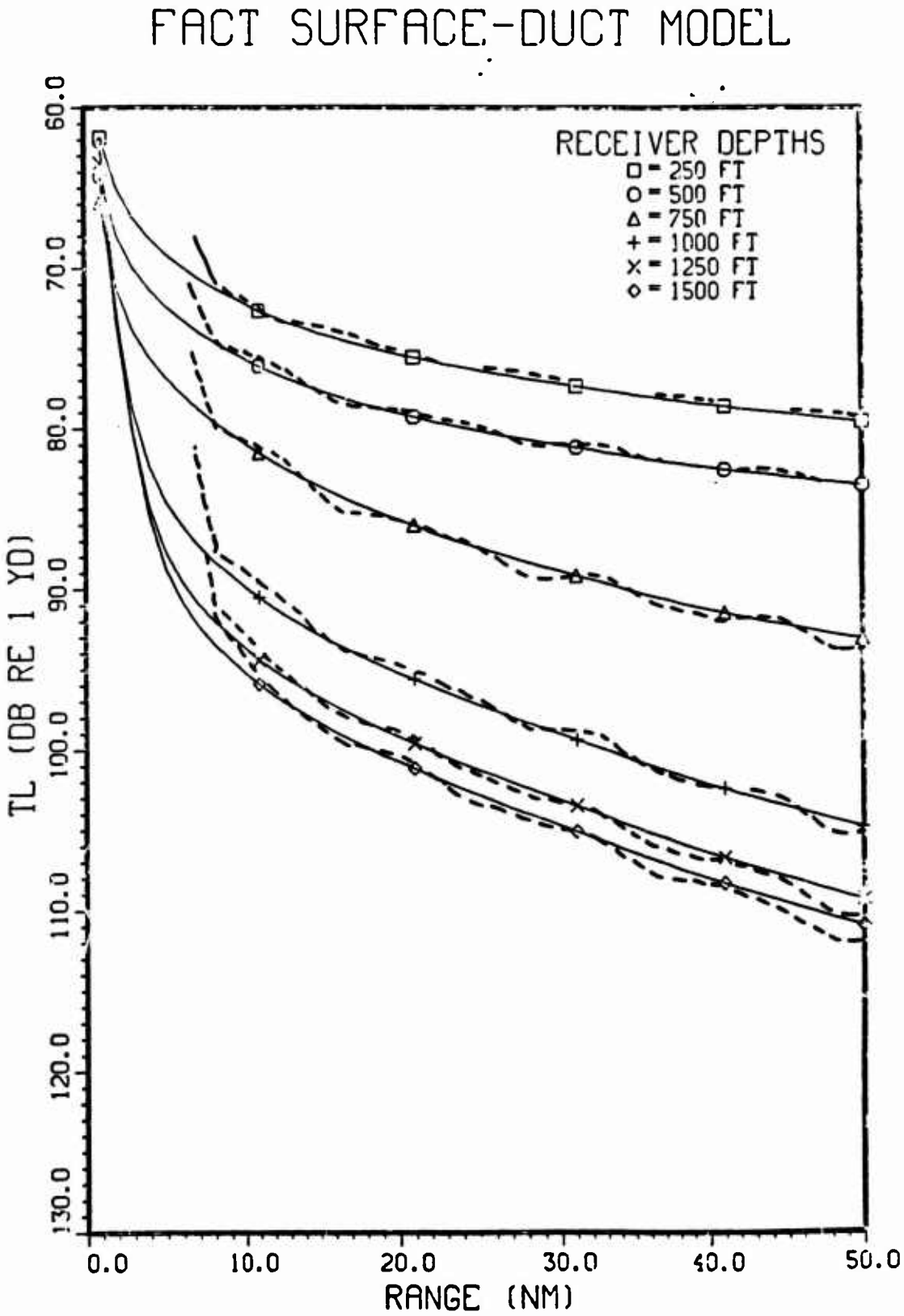


Figure 3-13 . Comparison of Surface-Duct Model (solid) with PE (dash).

FACT SURFACE-DUCT MODEL

SOURCE: FREQUENCY- 100 (HZ) , DEPTH- 500 (FT)

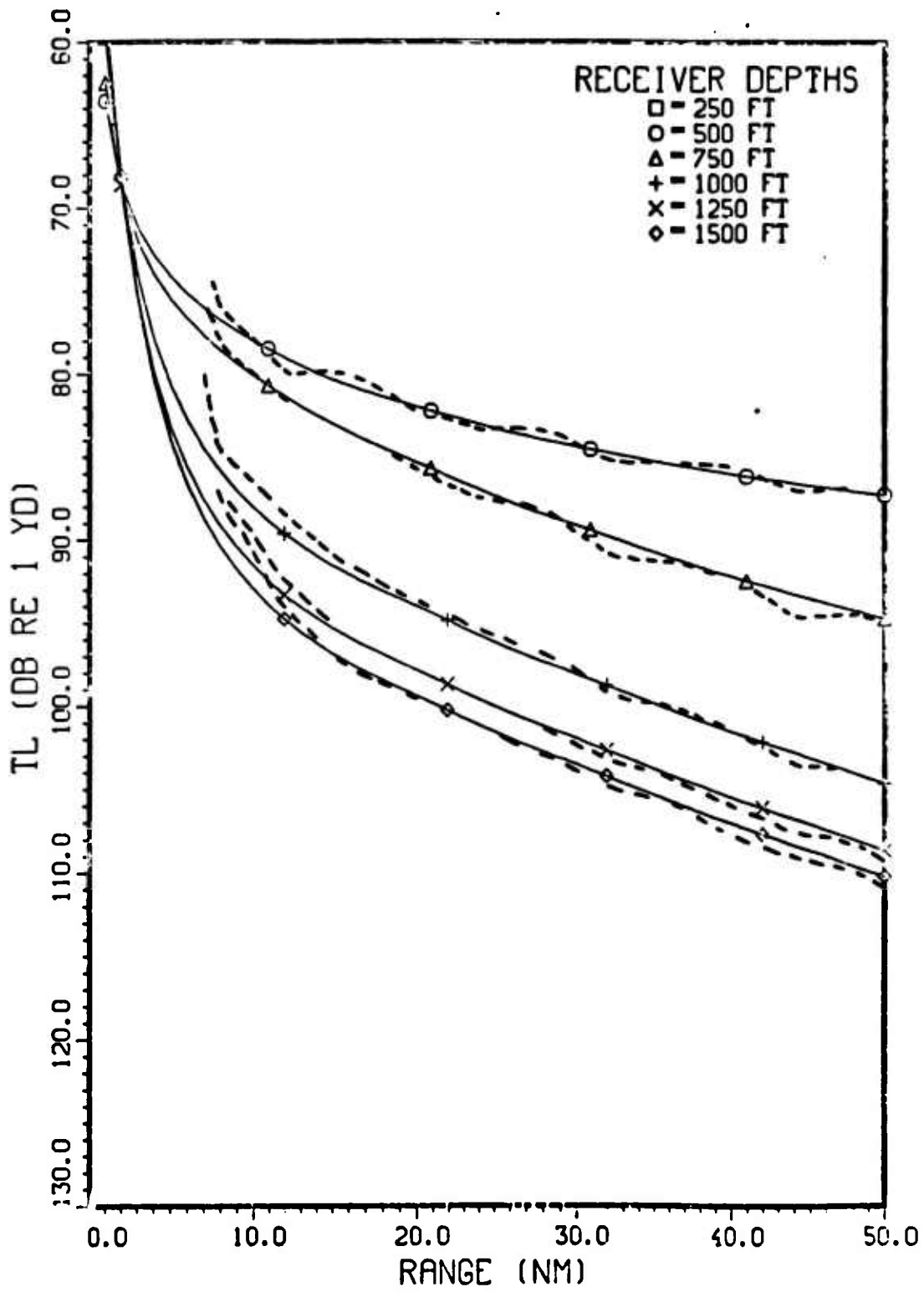


Figure 3-14 . Comparison of Surface-Duct Model (solid) with PC (dorn).

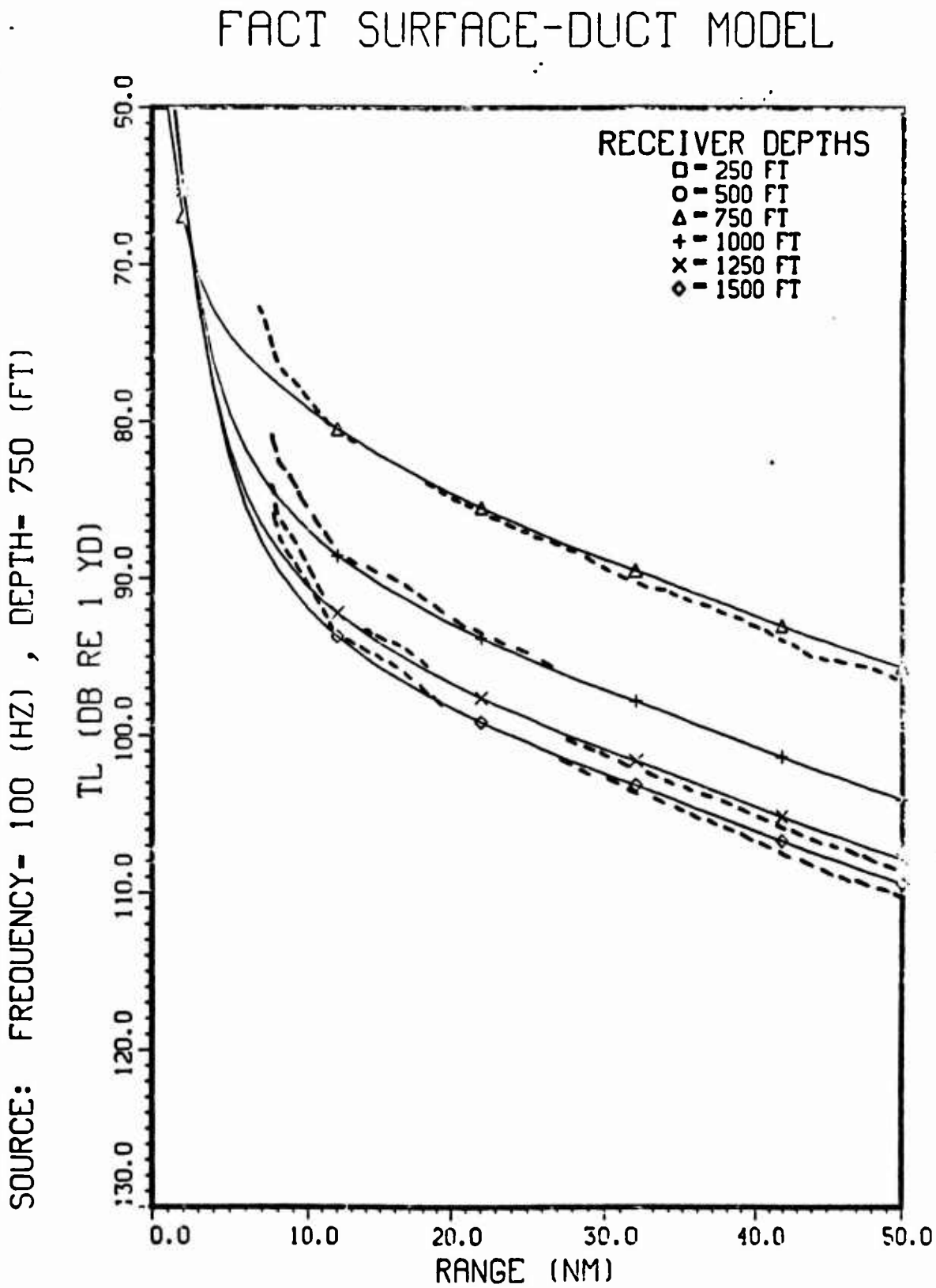


Figure 3-15 . Comparison of Surface-Duct Model (solid) with PE (dash).

SOURCE: FREQUENCY= 100 (HZ) , DEPTH= 1000 (FT)

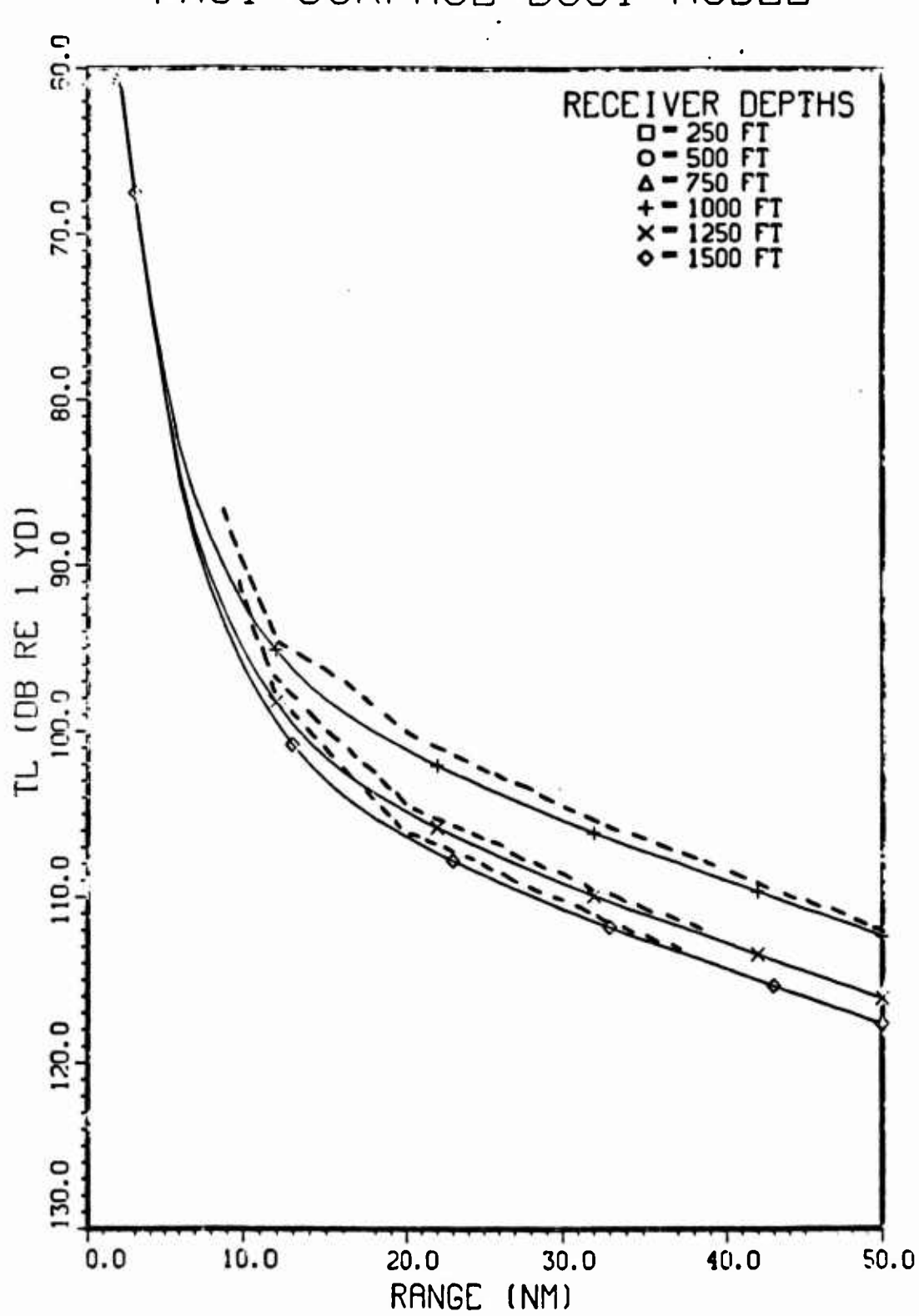


Figure 3-16 . Comparison of Surface-Duct Model (solid) with PE (dash).

SOURCE: FREQUENCY- 100 Hz DEPTH- 1250 (FT)

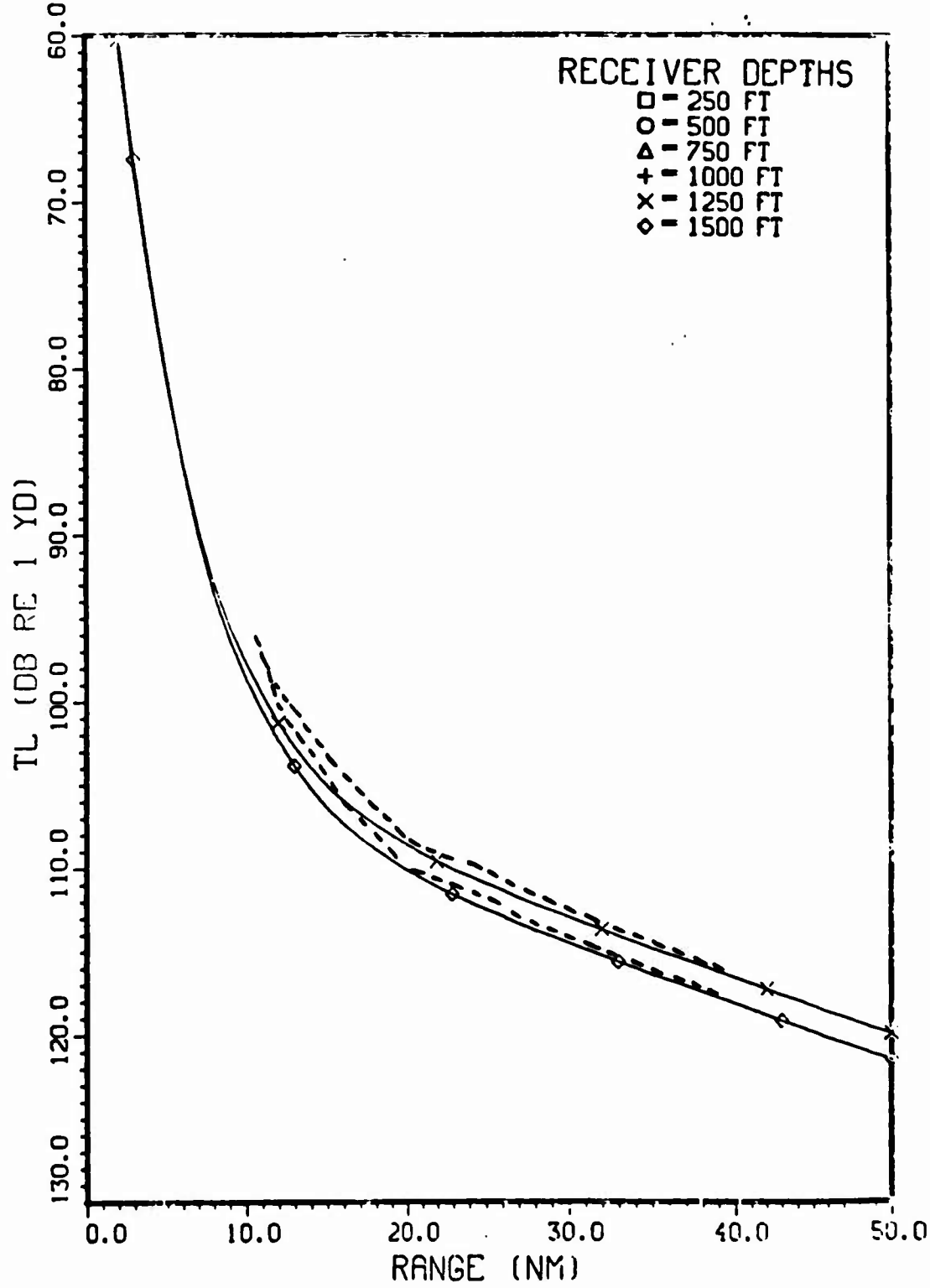


Figure 3-17 . Comparison of Surface-Duct Model (solid) with PE (dash).

SOURCE: FREQUENCY= 100 (HZ) , DEPTH= 1500 (FT)

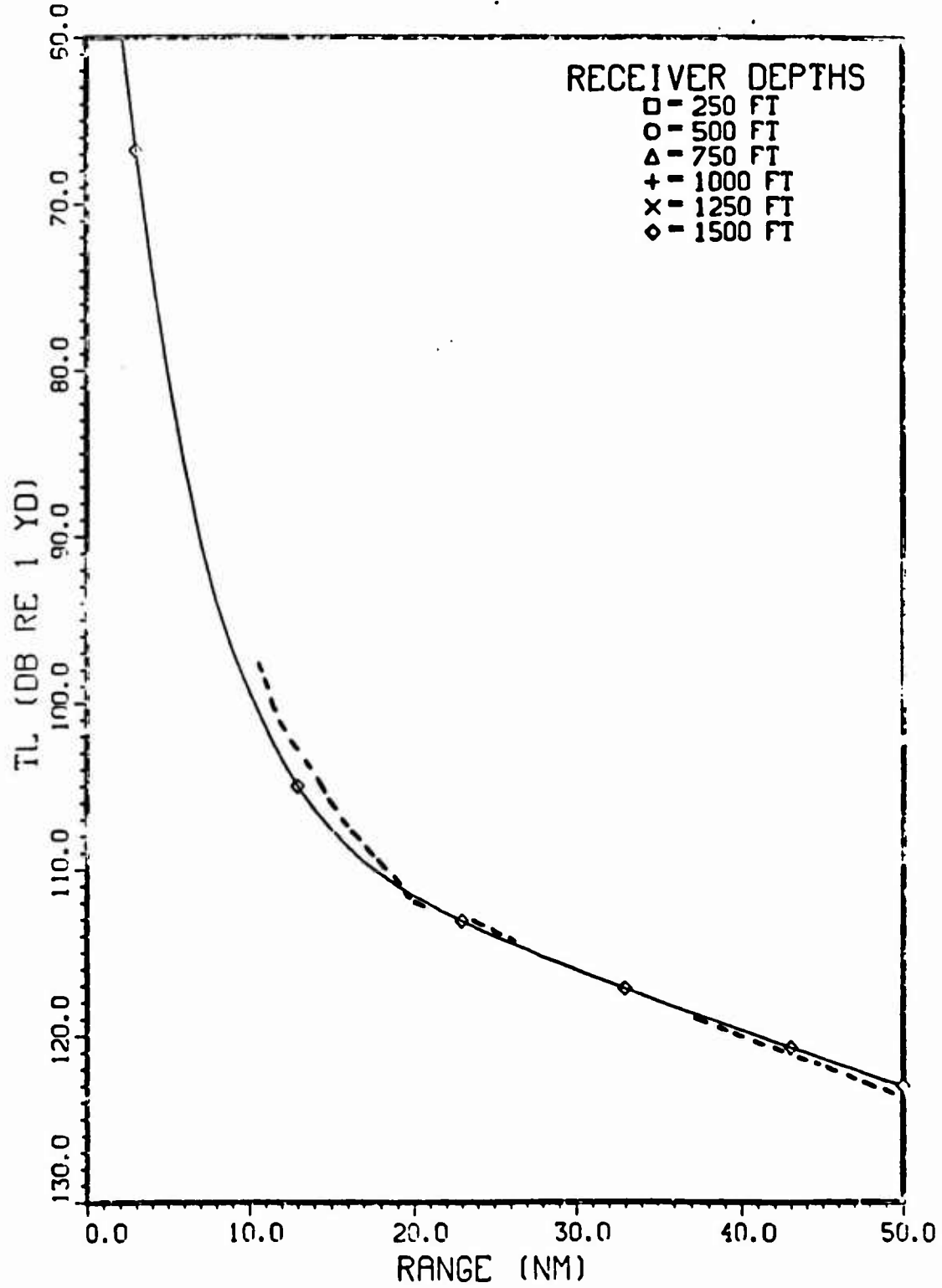


Figure 3-18 .

Comparison of Surface-Duct Model (solid) with PE (dashed).

SOURCE: FREQUENCY - 250 (HZ) , DEPTH- 250 (FT)

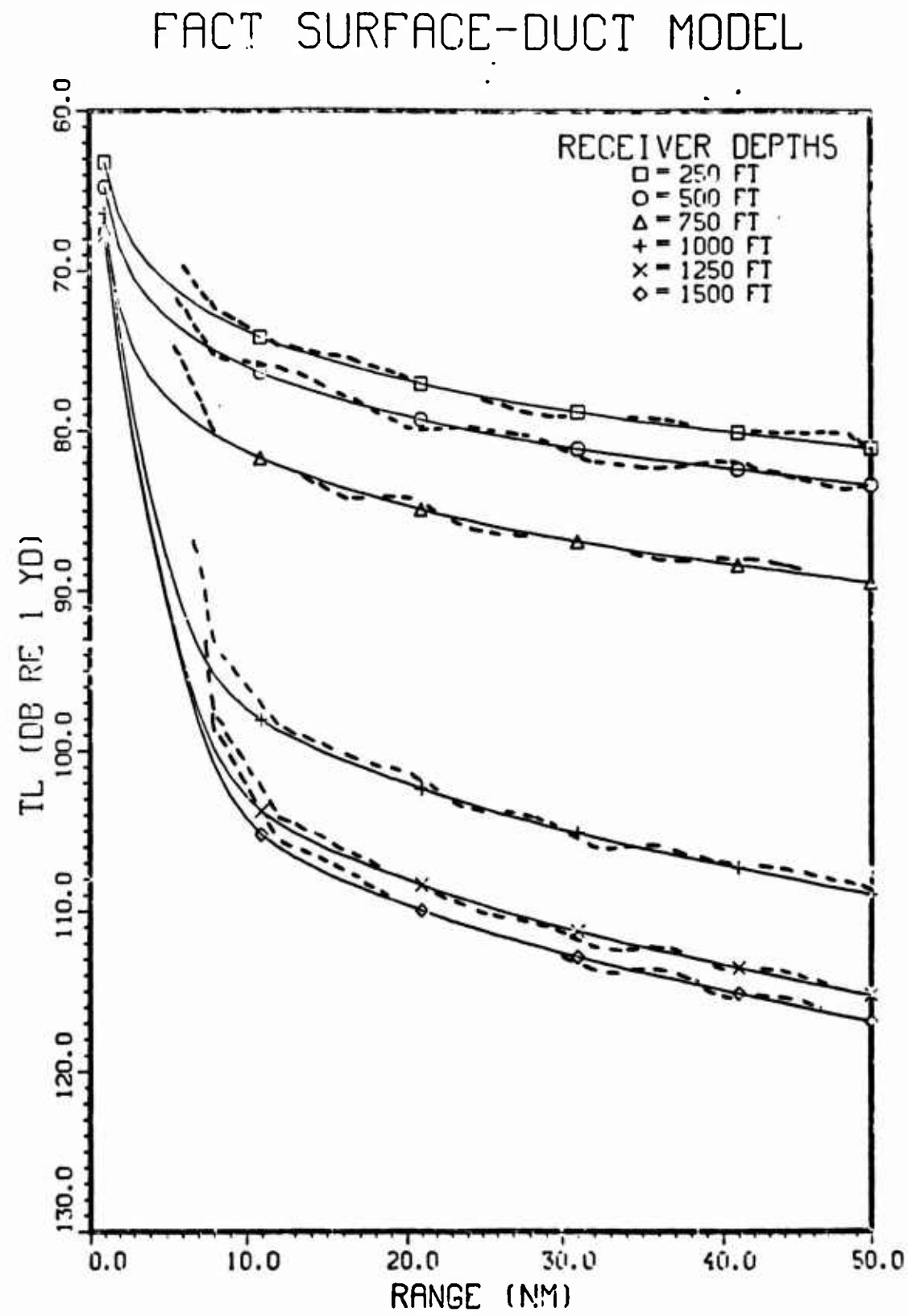


Figure 3-19 . Comparison of Surface-Duct Model (solid) with PE (dashed).

FACT SURFACE-DUCT MODEL

SOURCE: FREQUENCY = 250 (HZ) , DEPTH= 500 (FT)

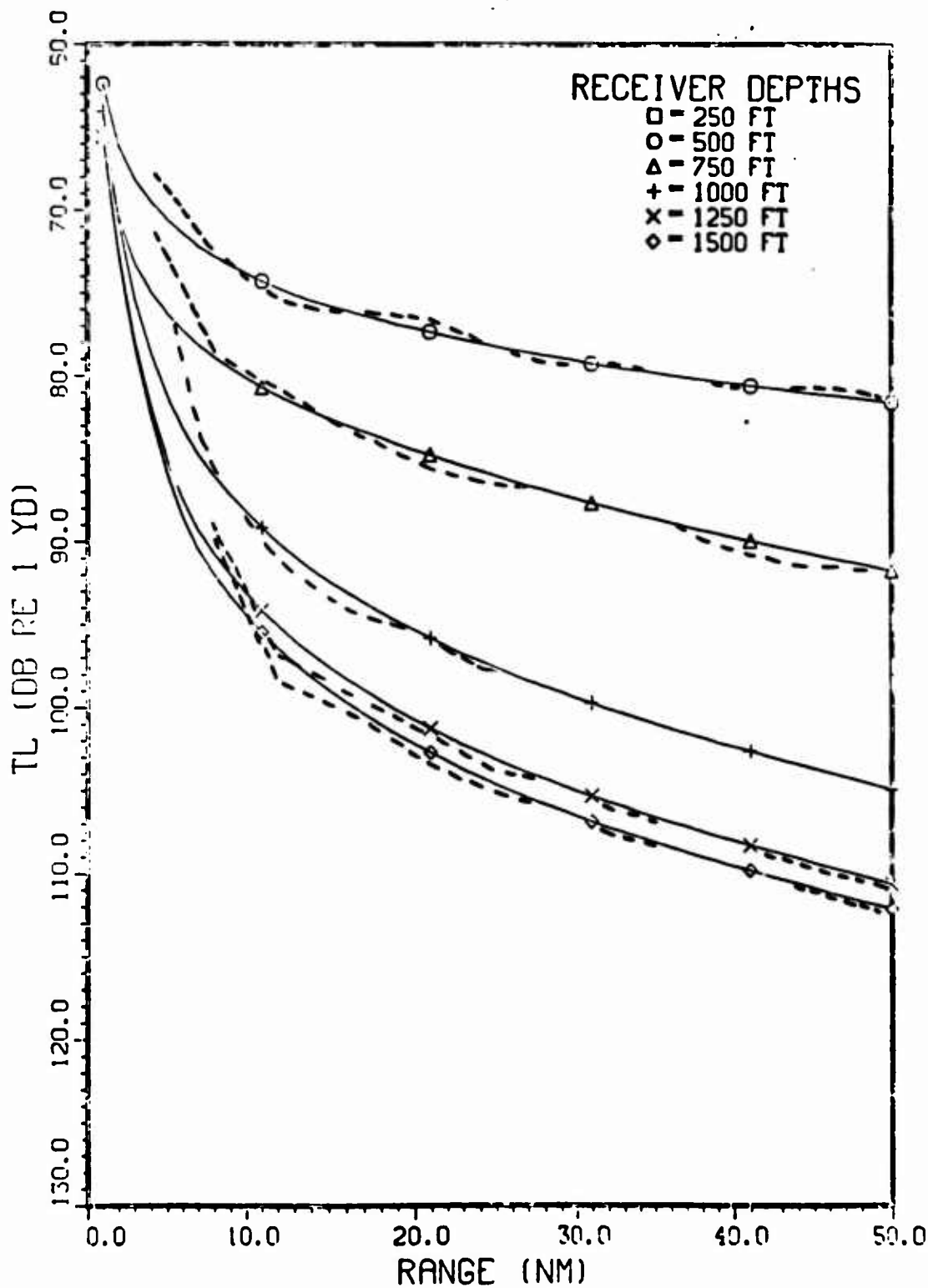


Figure 3-20 . Comparison of Surface-Duct Model (solid) with PC (dash).

SOURCE: FREQUENCY= 250 (HZ) , DEPTH= 750 (FT)

FACT SURFACE-DUCT MODEL

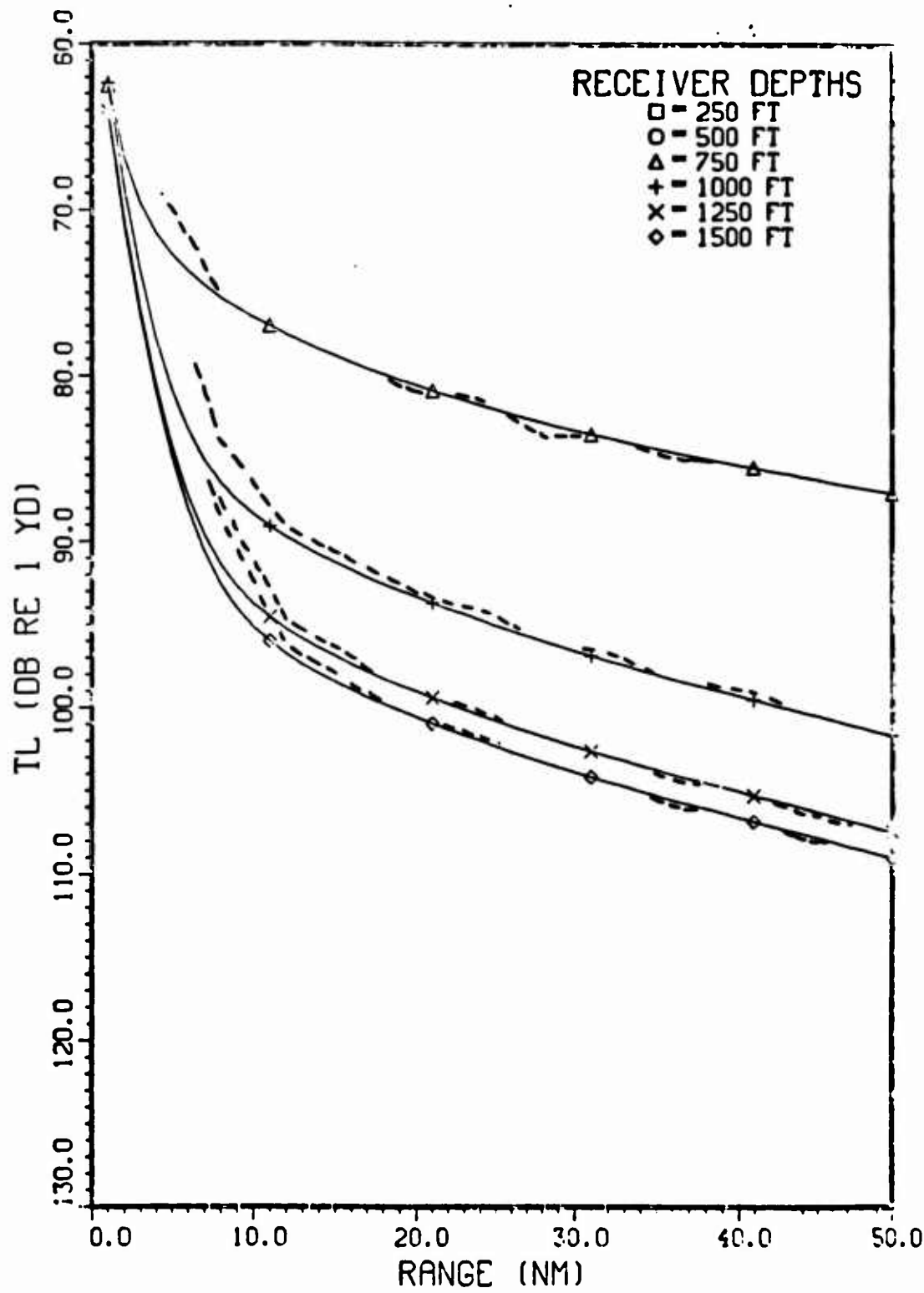


Figure 3-21 . Comparison of Surface-Duct Model (solid) with PE (dashed).

SOURCE: FREQUENCY = 250 (HZ) , DEPTH= 1000 (FT)

FACT SURFACE-DUCT MODEL

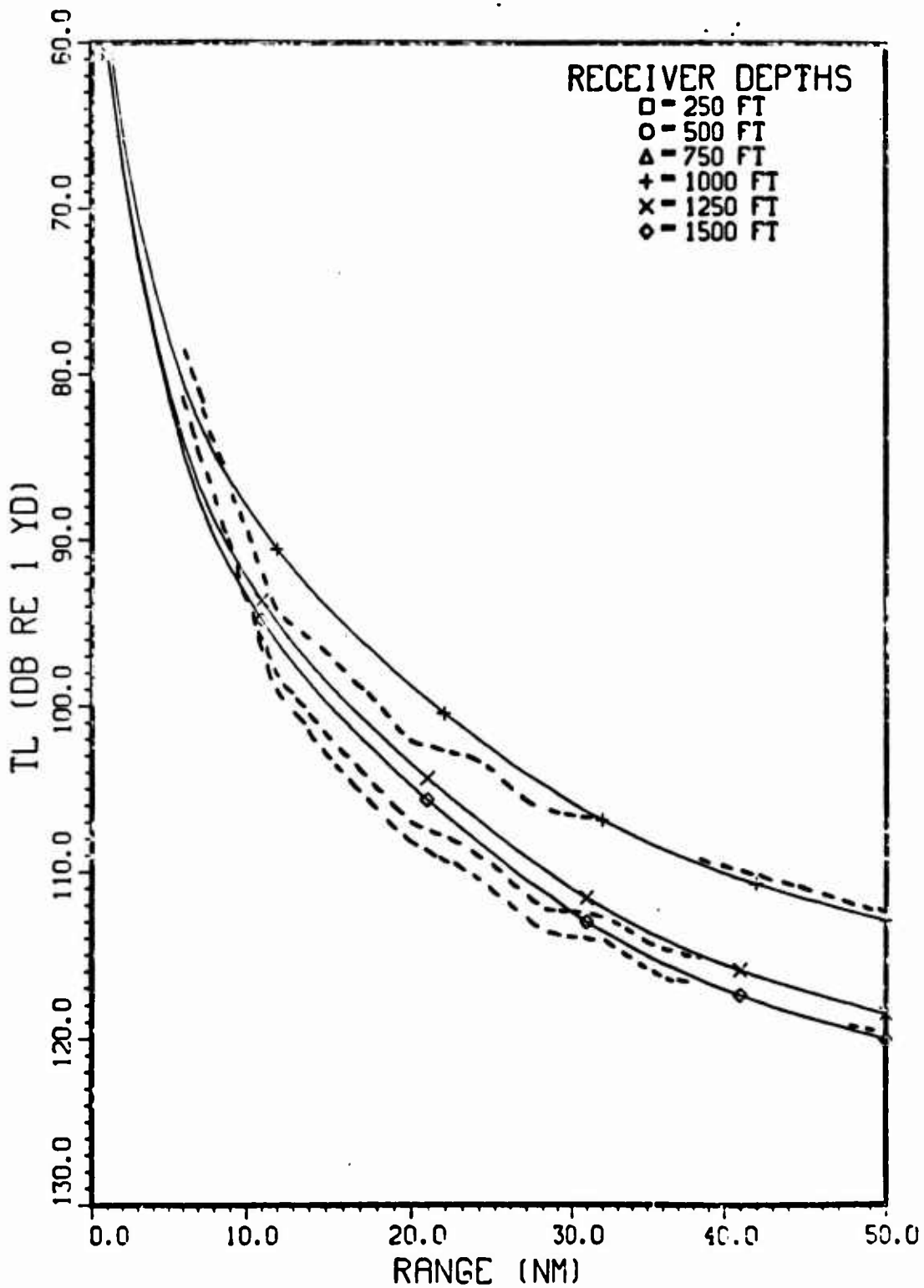


Figure 3-22 . Comparison of Surface-Duct Model (solid) with PE (dash).

SOURCE: FREQUENCY = 250 (HZ) , DEPTH= 1250 (FT)

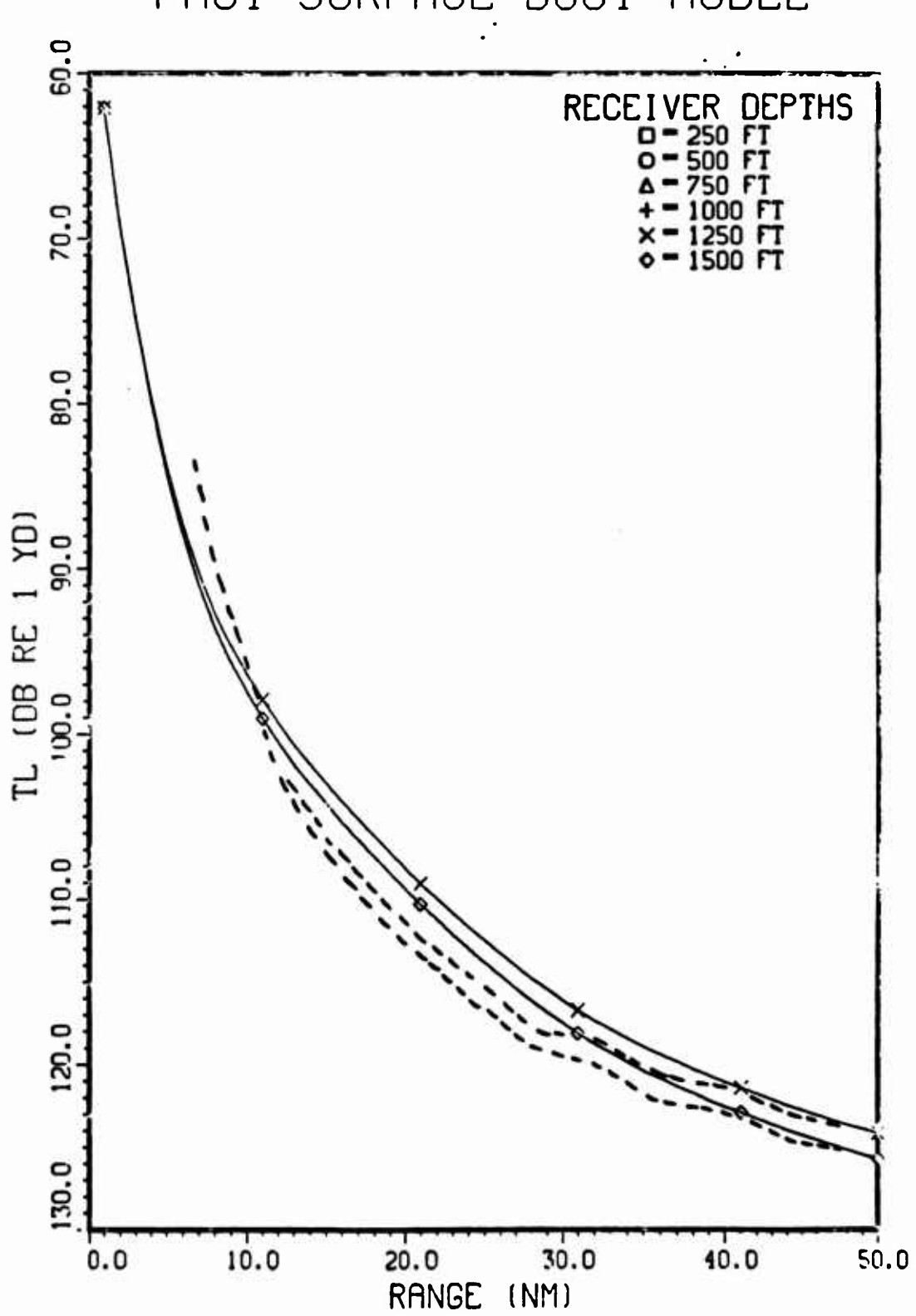


Figure 3-23 . Comparison of Surface-Duct Model (solid) with PE (dash).

FACT SURFACE-DUCT MODEL

SOURCE: FREQUENCY= 250 (HZ) , DEPTH= 1500 (FT)

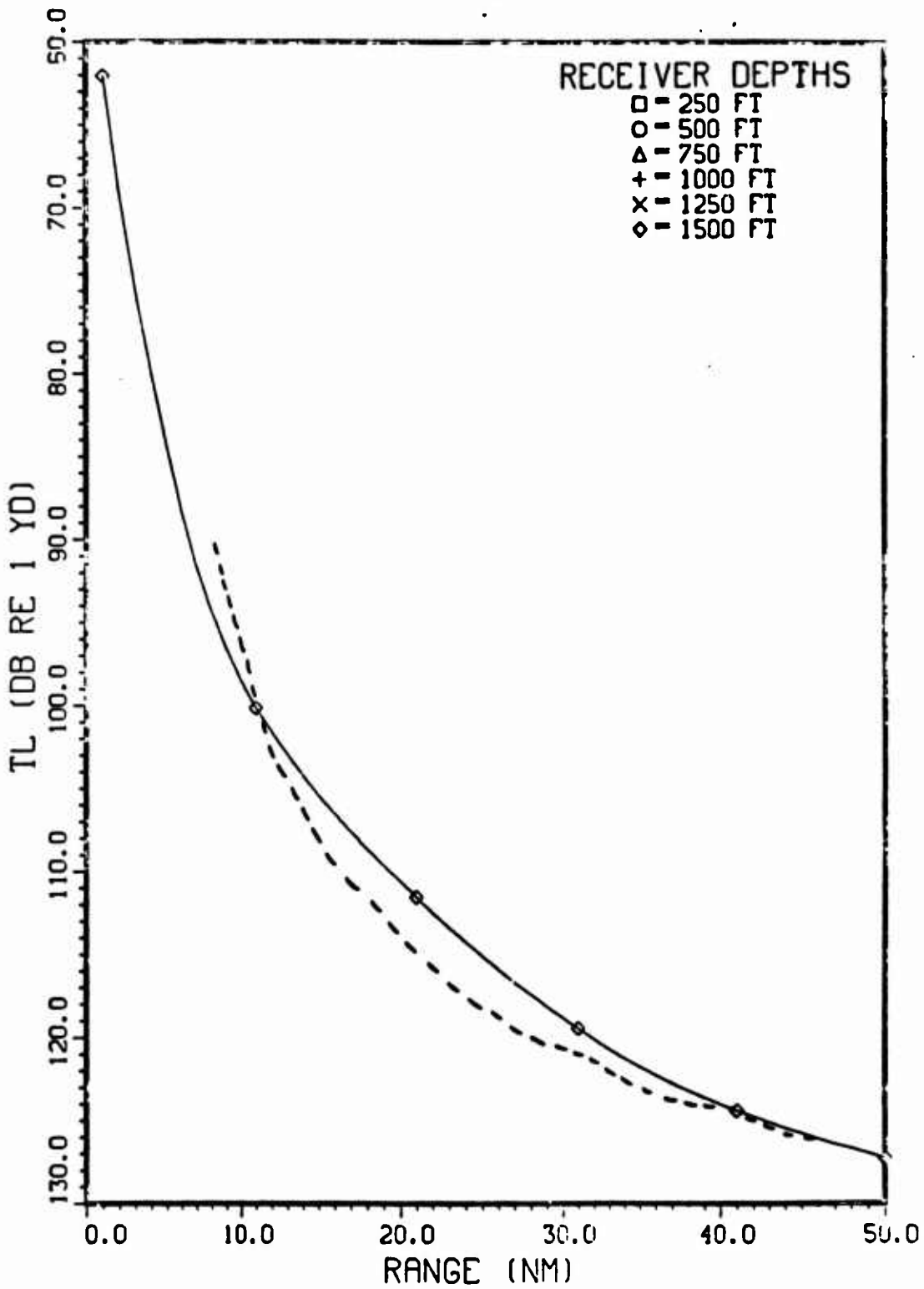


Figure 3-24 . Comparison of Surface-Duct Model (solid) with FE (dash).

SOURCE: FREQUENCY = 500 (HZ) , DEPTH= 250 (FT)

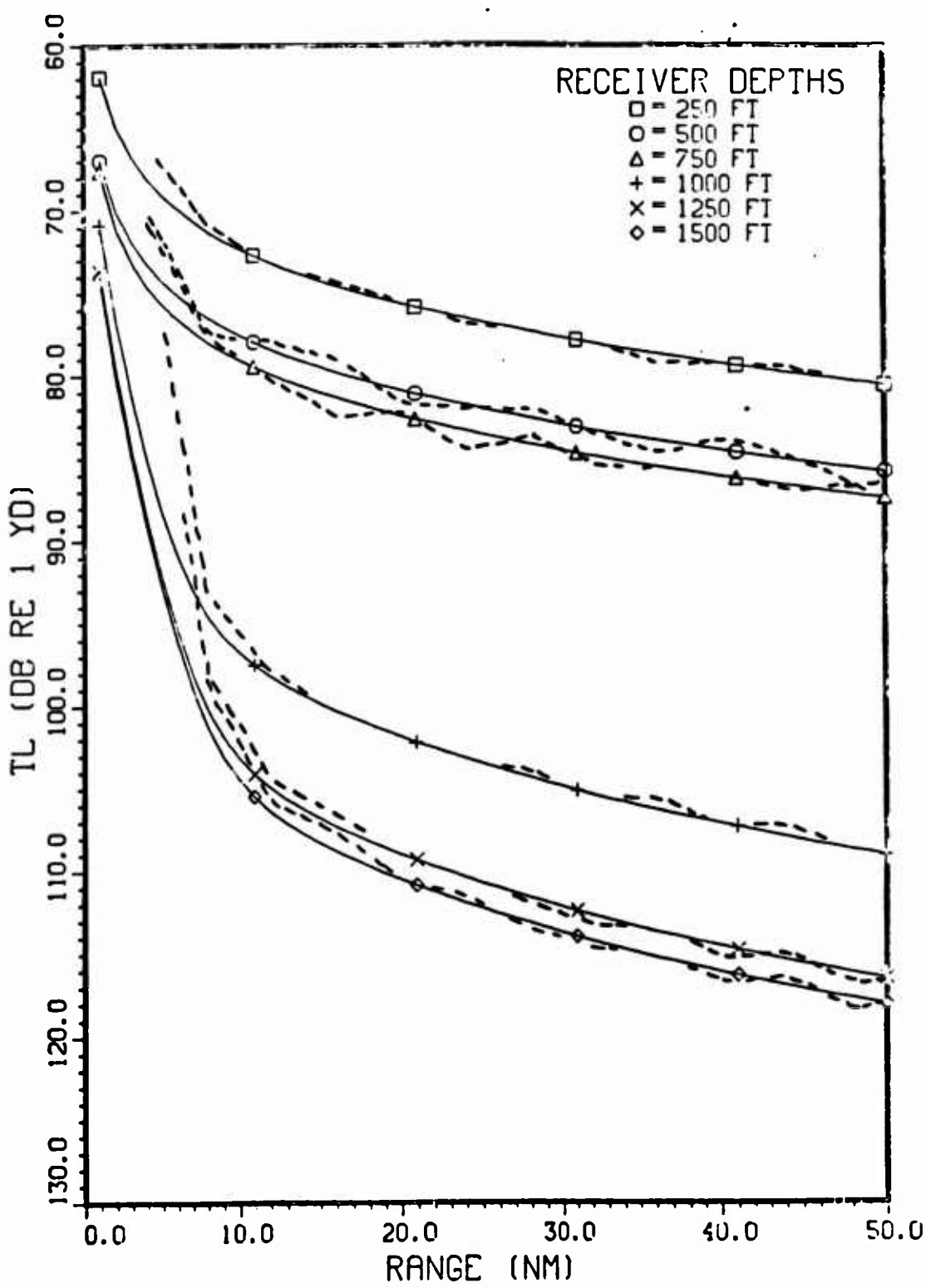


Figure 3-25 . Comparison of Surface-Duct Model (solid) with PC (dash).

SOURCE: FREQUENCY- 500 (HZ) , DEPTH- 500 (FT)

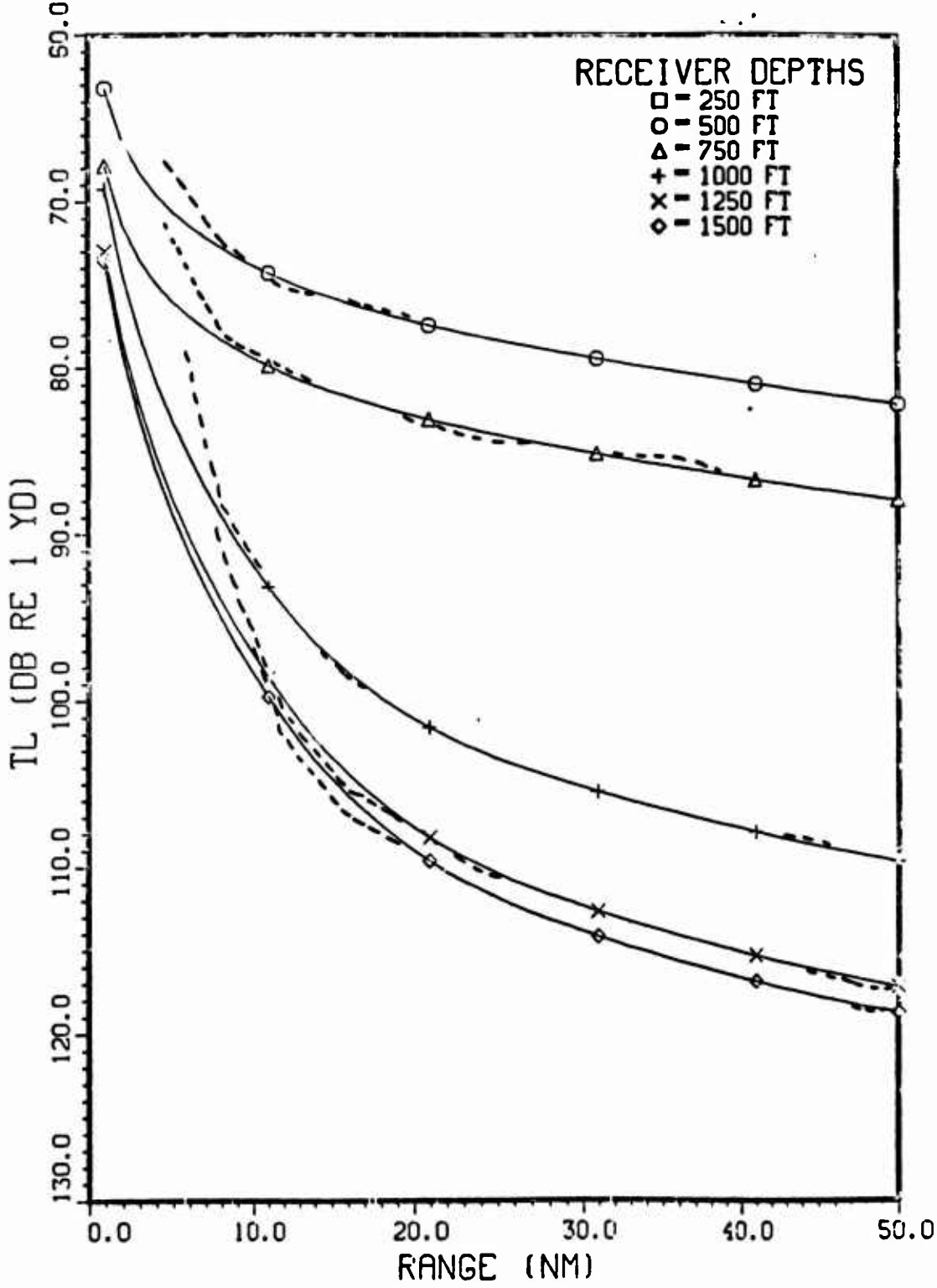


Figure 3-26 . Comparison of Surface-Duct Model (solid) with PE (dash).

SOURCE: FREQUENCY= 500 (HZ) , DEPTH= 750 (FT)

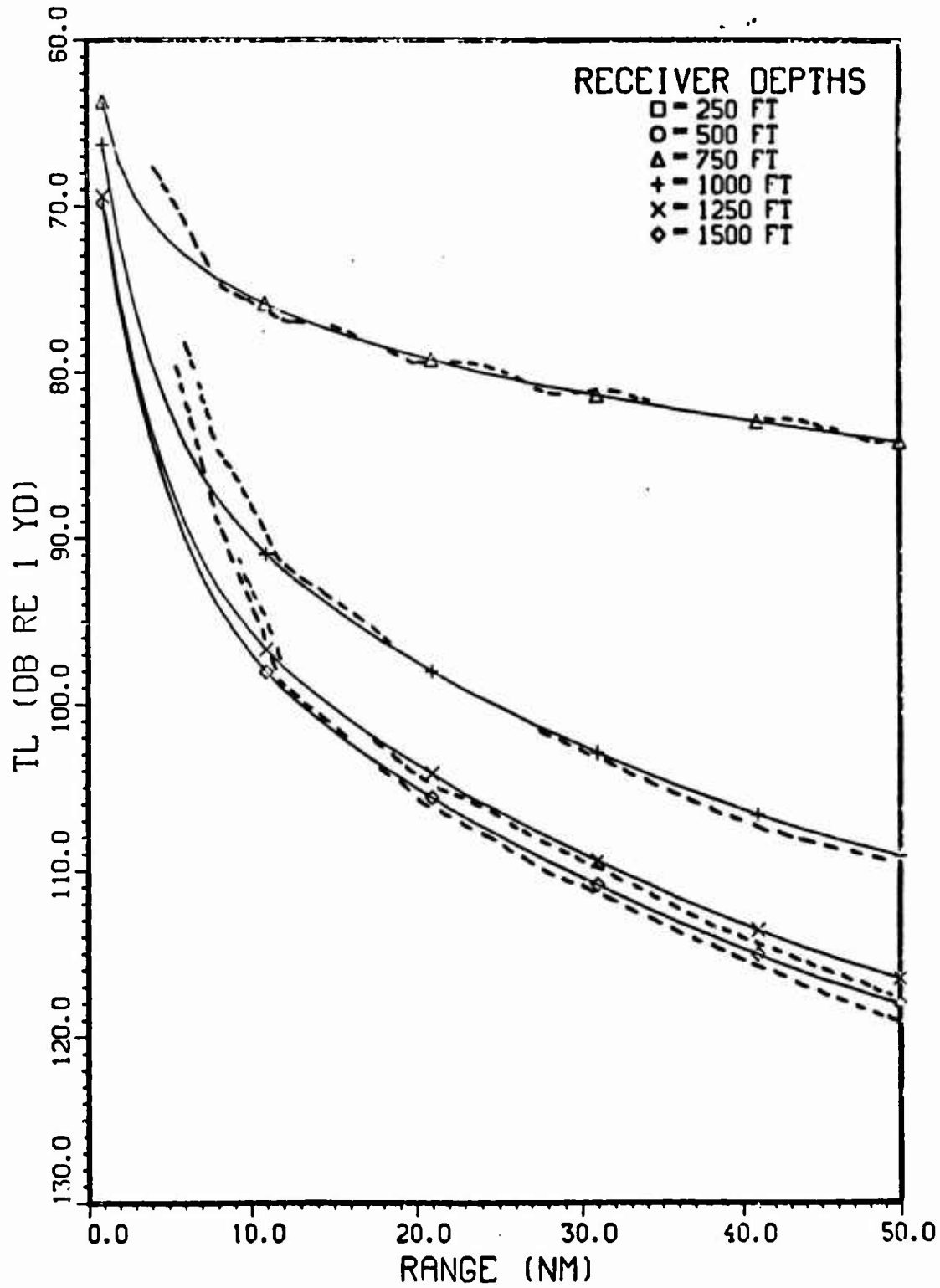


Figure 3-27 . Comparison of Surface-Duct Model (solid) with PE (dash).

PLOT 28 20.10.00 MDO 1 OCT, 1980 , SRI DISSEM VER 8.2

SOURCE: FREQUENCY- 500 (HZ) , DEPTH- 1000 (FT)

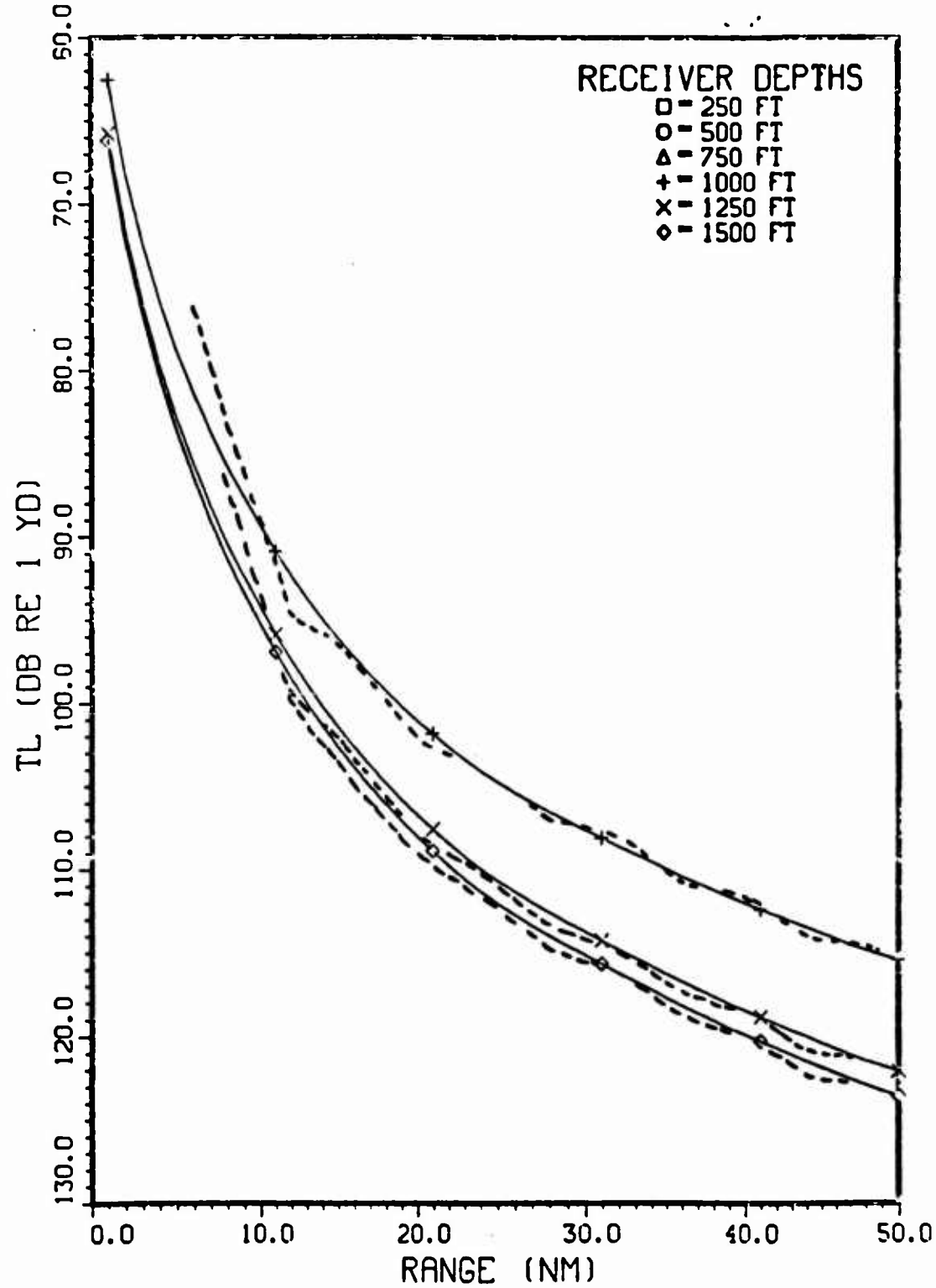


Figure 3-28 .

Comparison of Surface-Duct Model (solid) with FE (dash).

SOURCE: FREQUENCY= 500 (HZ) , DEPTH- 1250 (FT)

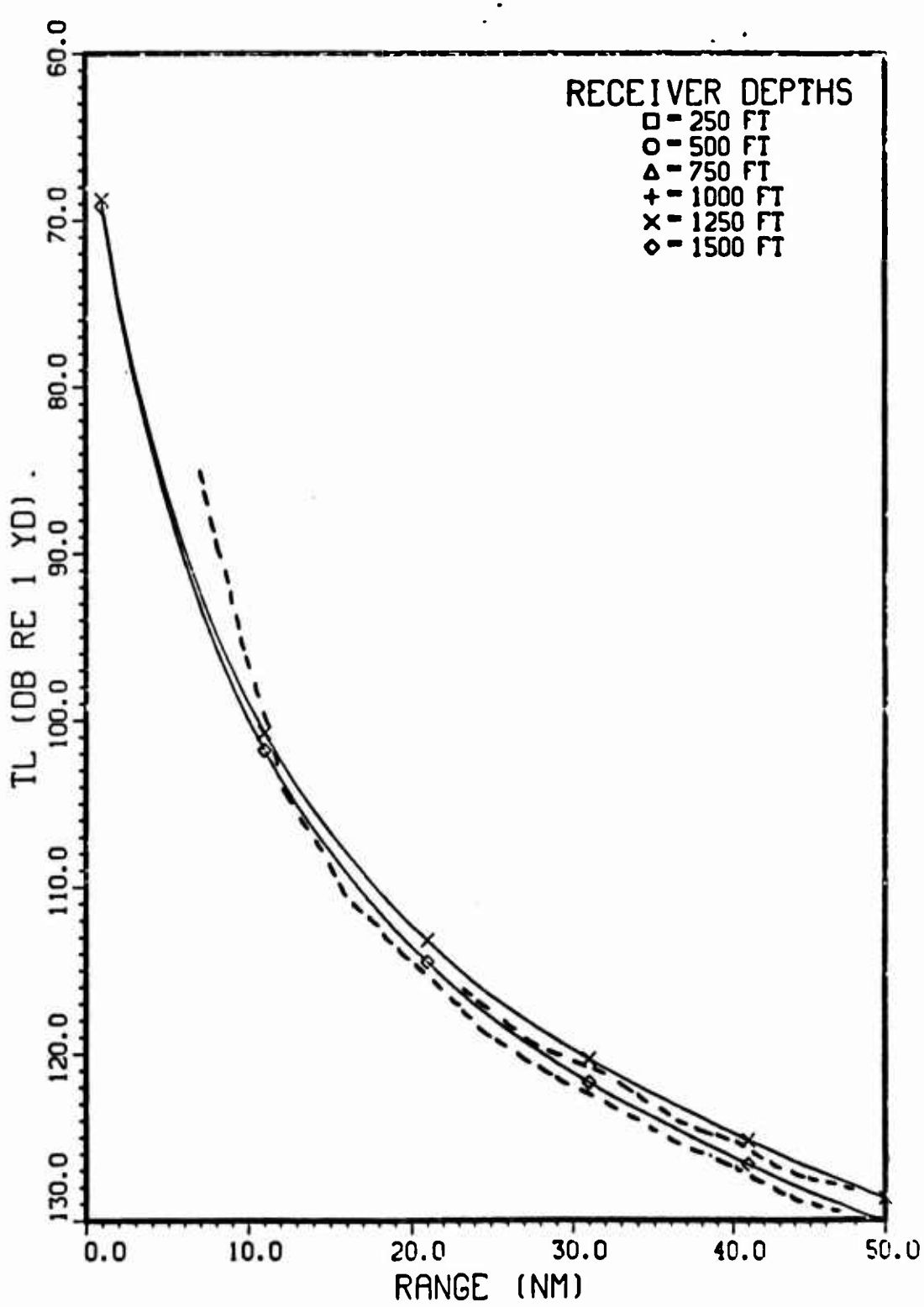


Figure 3-29 . Comparison of Surface-Duct Model (solid) with FE (dash).

SOURCE: FREQUENCY= 500 (HZ) , DEPTH- 1500 (FT)

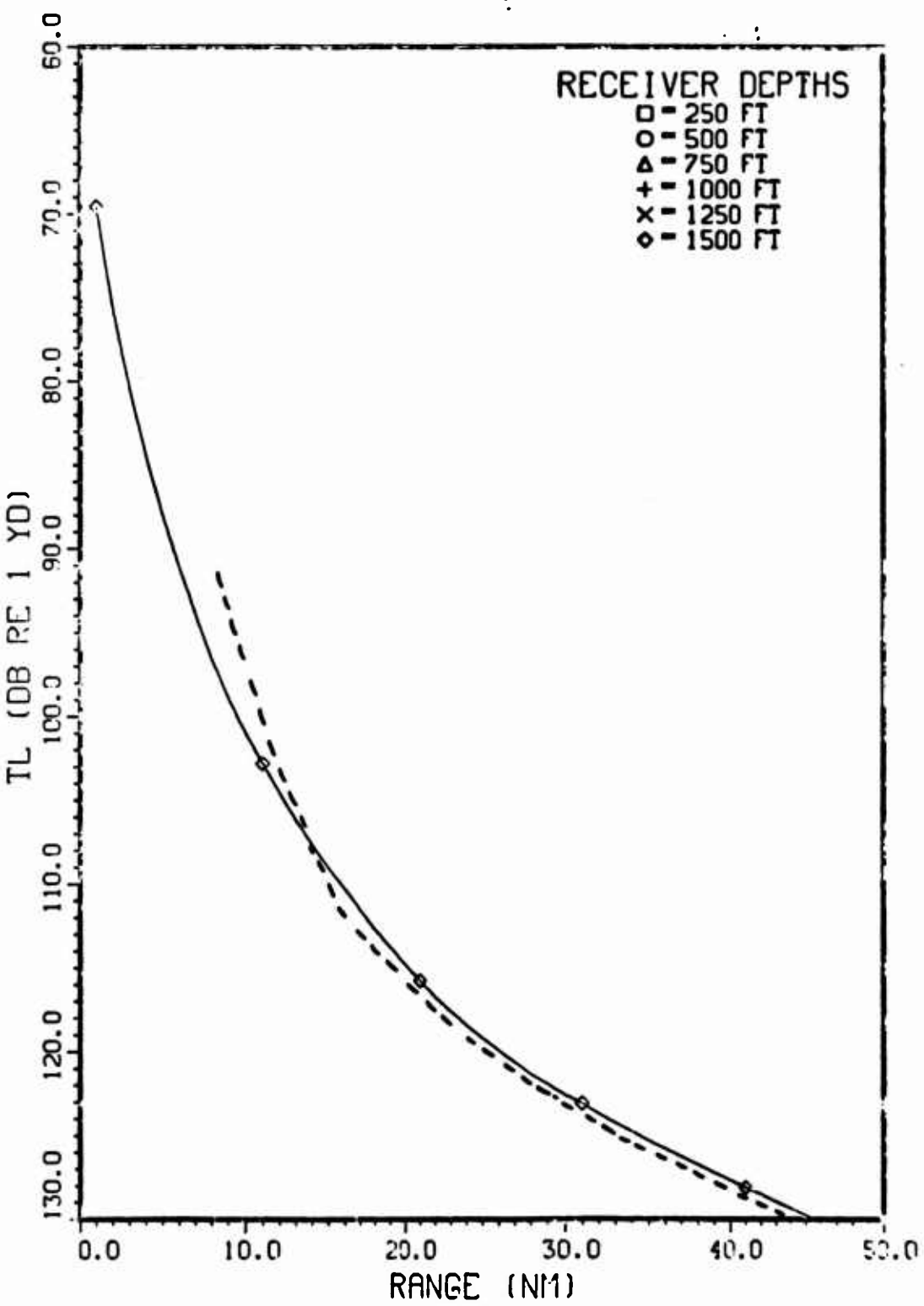


Figure 3-20 . Comparison of Surface-Duct Model (solid) with FE (dash).

SOURCE: FREQUENCY= 1000 (HZ) , DEPTH= 250 (FT)

FACT SURFACE-DUCT MODEL

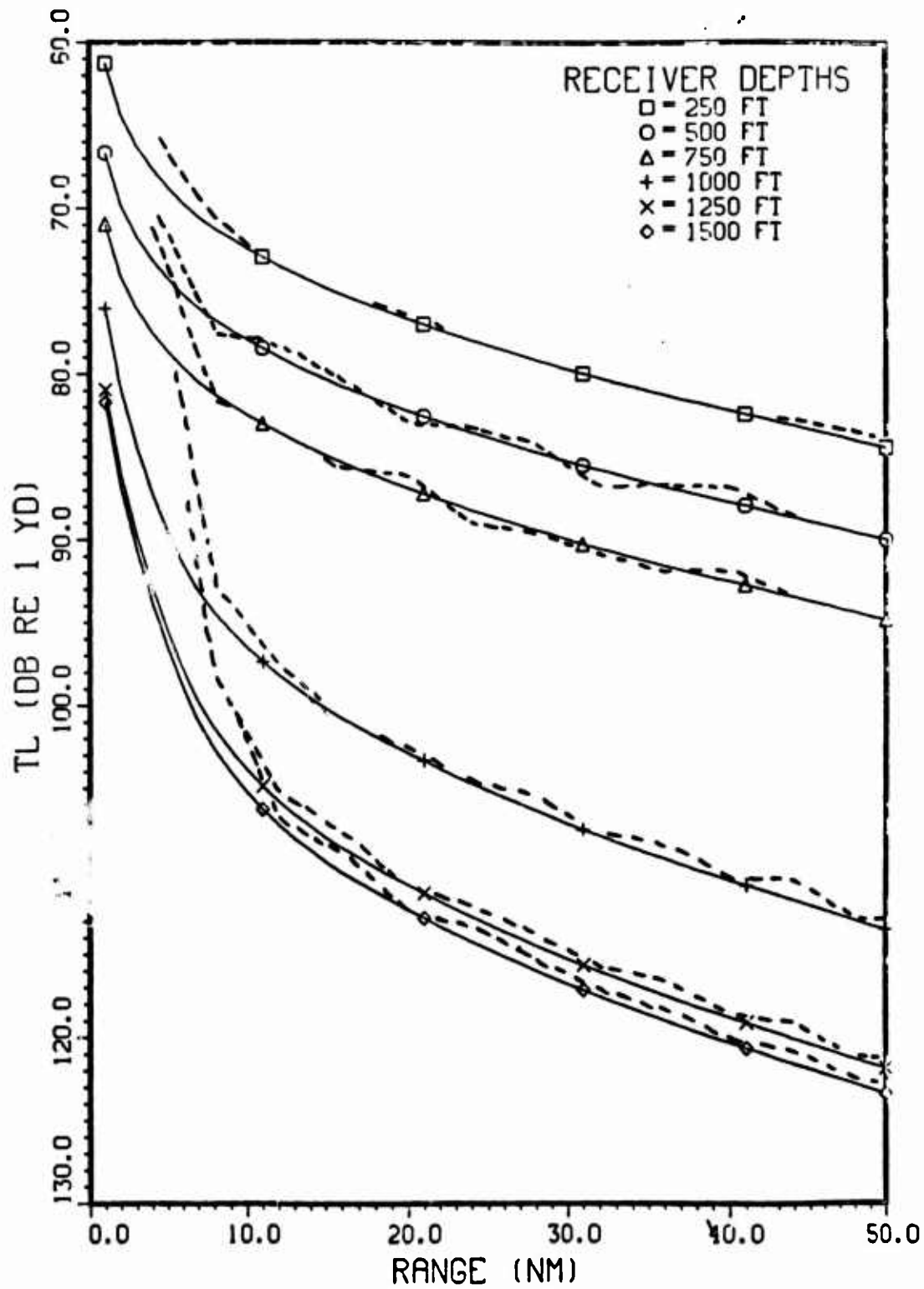


Figure 3-31 . Comparison of Surface-Duct Model (solid) with PE (dash).

FACT SURFACE-DUCT MODEL

SOURCE: FREQUENCY - 1000 (HZ) , DEPTH- 500 (FT)

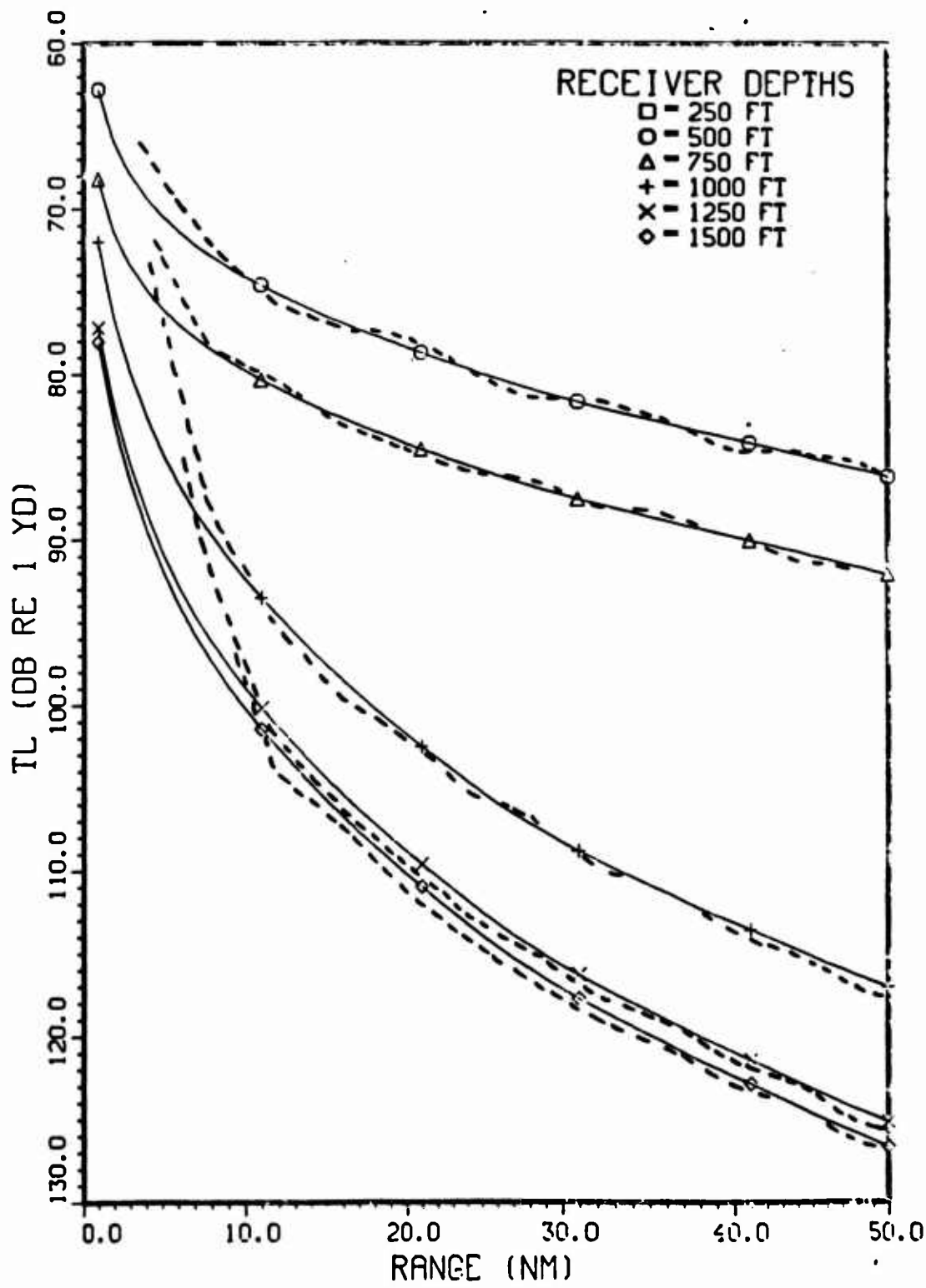


Figure 3-32 . Comparison of Surface-Duct Model (solid) with PC (dash).

FACT SURFACE-DUCT MODEL

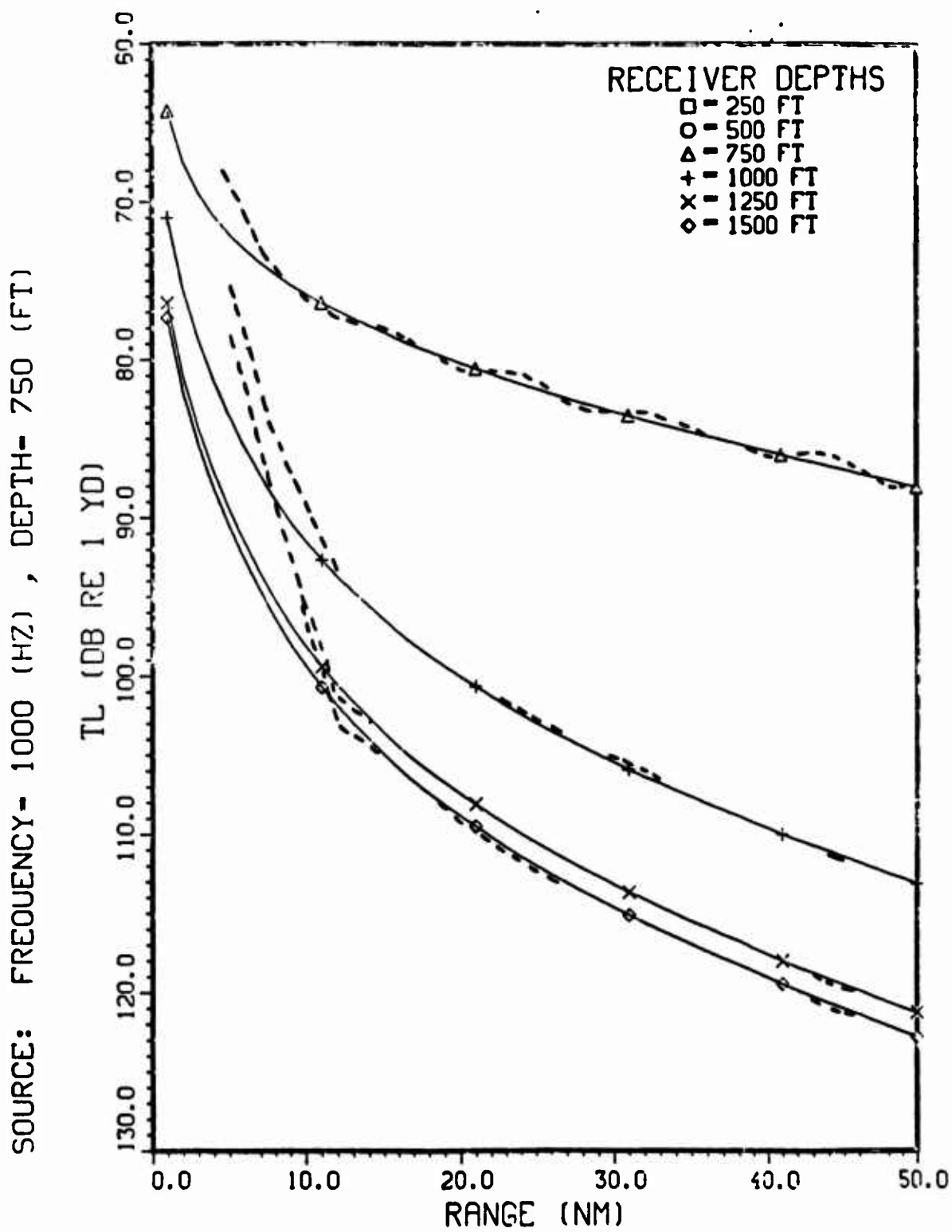


Figure 3-33 . Comparison of Surface-Duct Model (solid) with PC (dashi).

SOURCE: FREQUENCY- 1000 (HZ) , DEPTH- 1000 (FT)

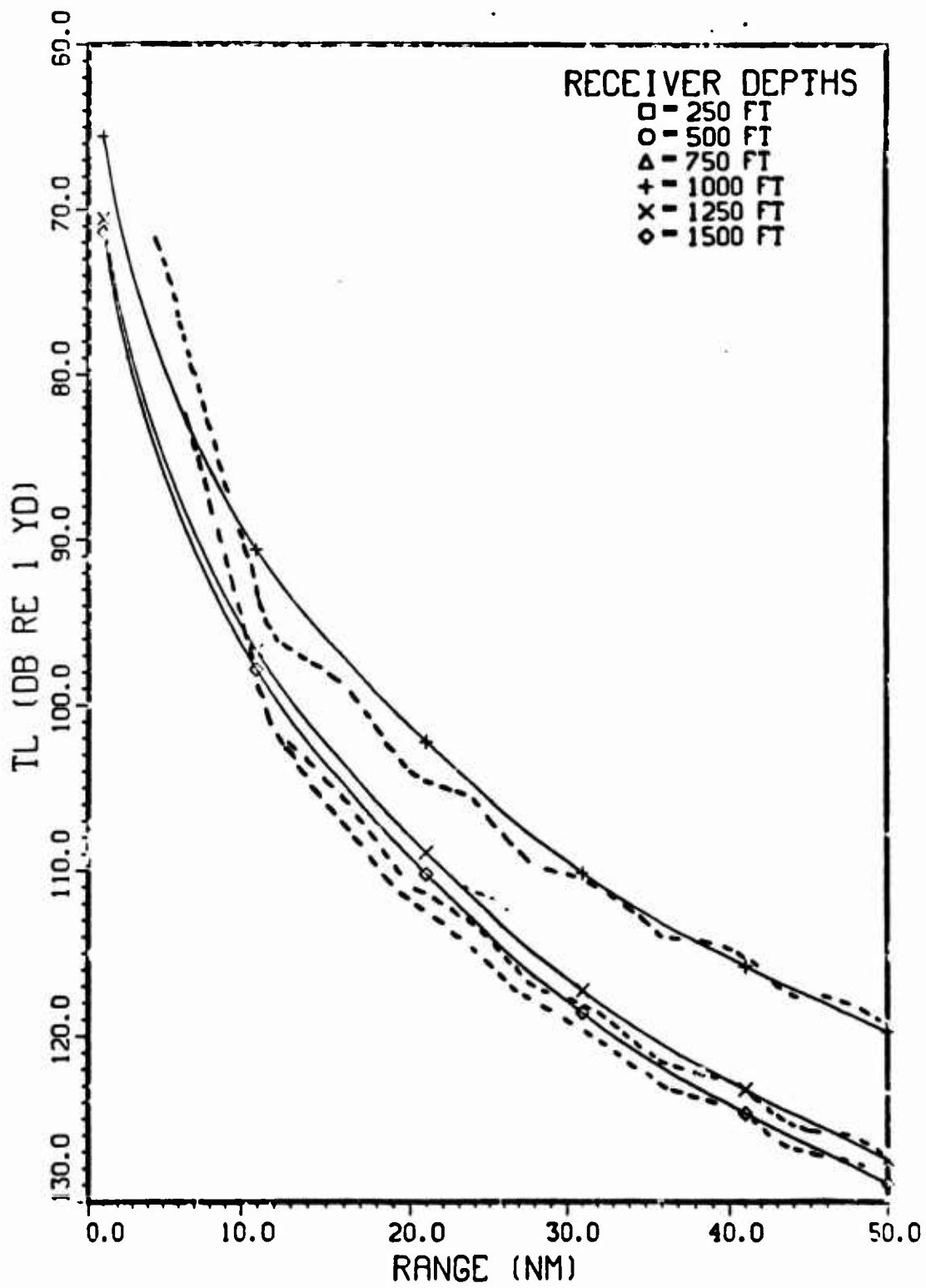


Figure 3-34 . Comparison of Surface-Duct Model (solid) with PE (dash).

SOURCE: FREQUENCY= 1000 (HZ) , DEPTH= 1250 (FT)

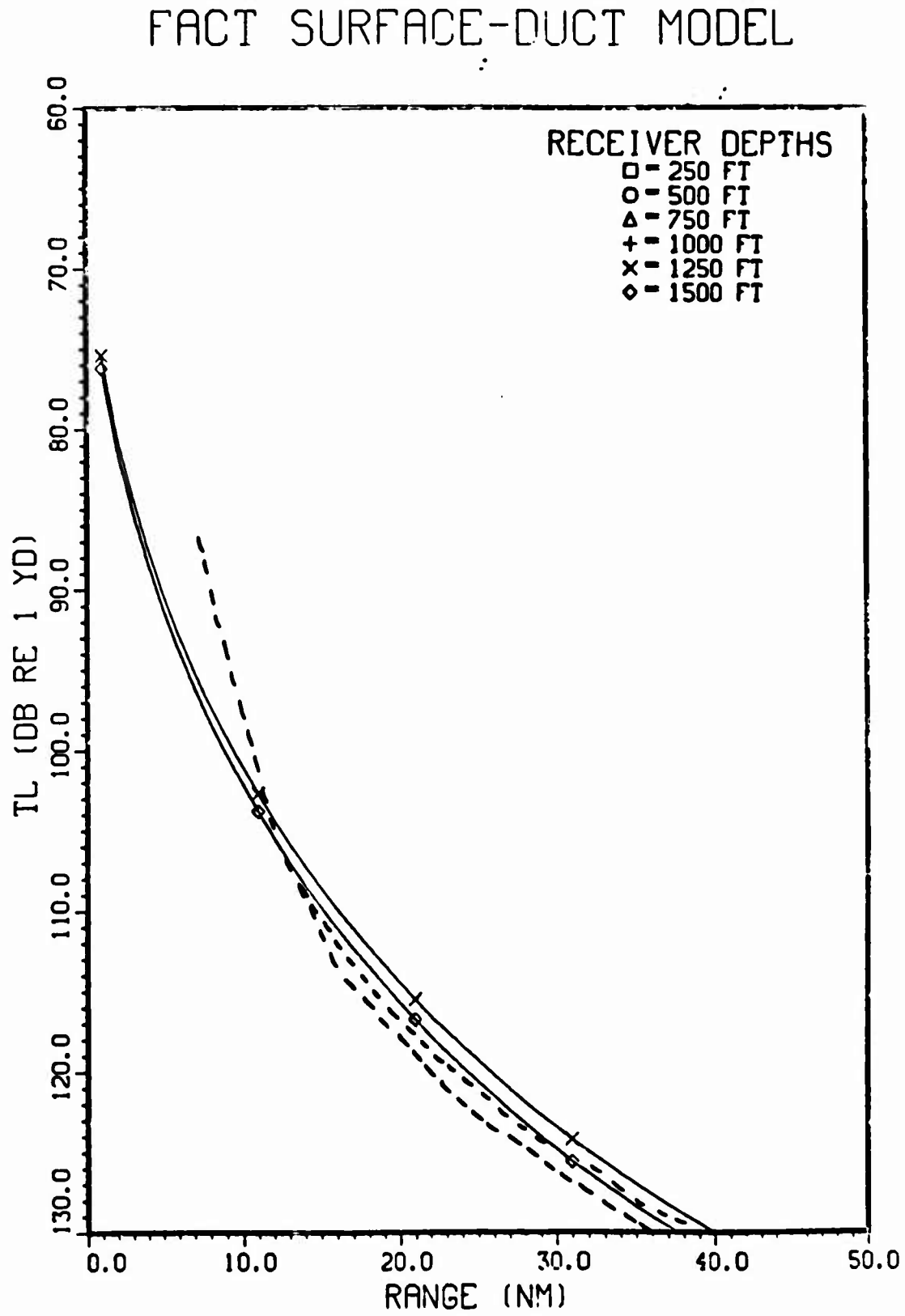


Figure 3-35 . Comparison of Surface-Duct Model (solid) with PE (dash).

SOURCE: FREQUENCY= 1000 (HZ) , DEPTH= 1500 (FT)

FACT SURFACE-DUCT MODEL

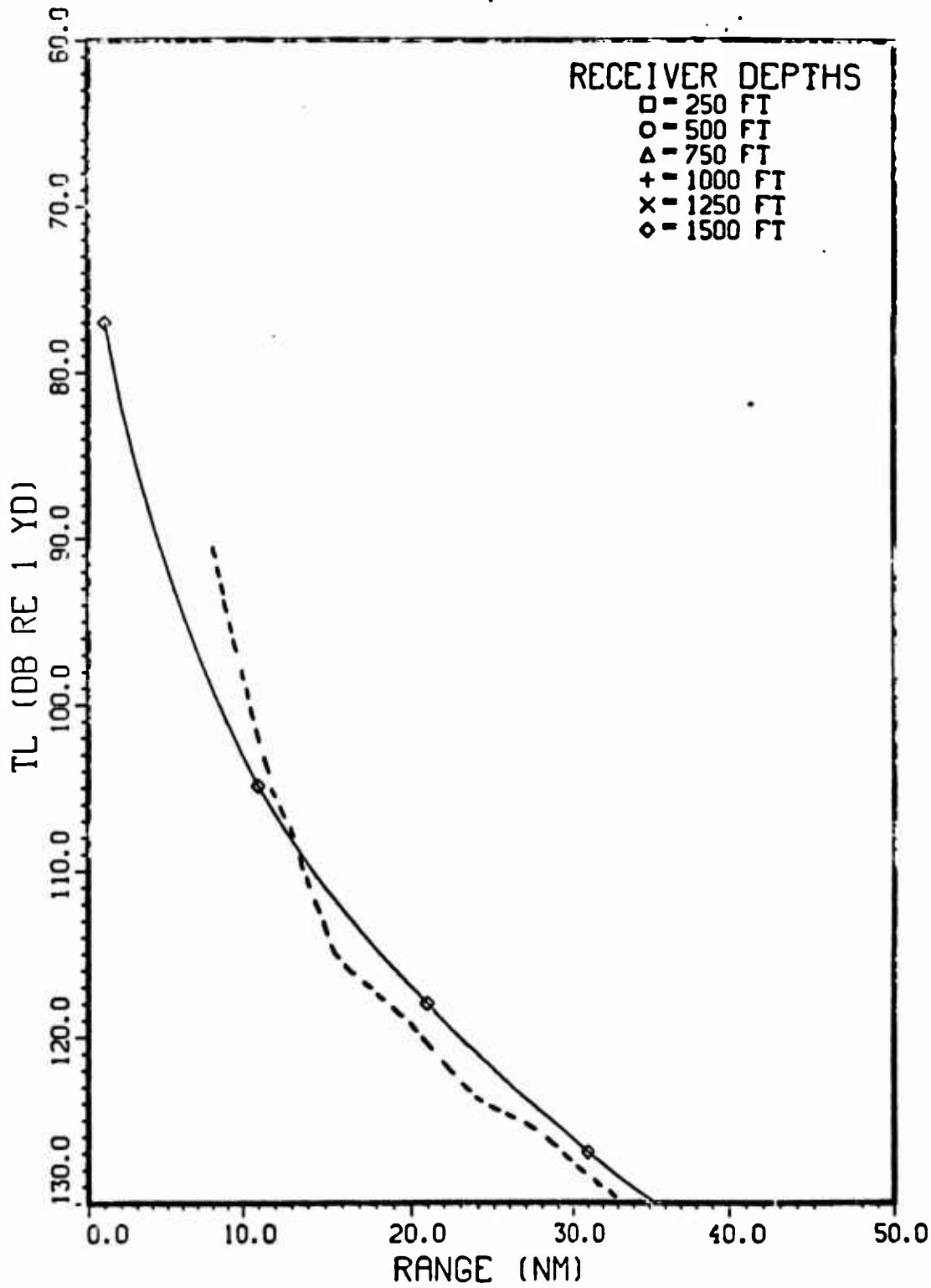


Figure 3-36 . Comparison of Surface-Duct Model (solid) with PE (dash).

3.2 NORMAL MODE COMPARISONS

A more detailed evaluation of the virtual mode surface duct model was made by comparing the predicted modal longitudinal wavenumbers λ_m and intensity amplitudes ψ_m with corresponding values computed using the NOSC n-layer normal mode code. The NM code was run with the same bilinear profile used by the surface duct model and the ocean modeled as infinitely deep. Both models (surface duct and NM) truncated the modal spectrum, hence near field TL values may be in error due to an insufficient number of modes. The imaginary part of λ_m is related to the attenuation coefficient a_m by $a_m = 2 I_m(\lambda_m)$.

The λ_m computed by the virtual mode surface duct model agree quite well with the NM results: relative error in $|I_m(\lambda_m)| \lesssim 10^{-1}$ and $|\text{Re}(\lambda_m)| \lesssim 10^{-4}$. Agreement is better for the trapped modes and gets worse for the strongly leaky waves. However, the strongly leaky modes have large attenuation coefficients and contribute little to the intensity at ranges greater than a few nautical miles.

Intensity amplitudes ψ_m are close to the NM predictions with two exceptions. First, the true ψ_m may exhibit deep nulls which are clipped in the surface duct model. The second exception involves deeply trapped modes where ψ_m is computed within or below the barrier. In the NOSC NM code, numerical difficulties in computing Hankel functions lead to a modification of the bilinear profile. The virtual mode model uses a different formulation of the ψ 's and avoids this problem. Thus computed intensity amplitudes are expected to be lower than those predicted by the NM code. This is in fact observed.

Detailed comparison of λ_m for the surface duct model predictions and the NM code results are provided for 25, 100, and 500 Hz. This corresponds to cases with zero, two, and eleven trapped modes, respectively. The λ_m are shown in Tables (3-1) with values in parenthesis being the NM results.

Table 3-1. Comparison of λ_m (NM results in parenthesis).

<u>Mode</u>	<u>$\text{Re}(\lambda_m)$</u>	<u>$I_m(\lambda_m)$</u>
	<u>$\approx 25 \text{ Hz}$</u>	
1	3.126790 E-2 (3.126250)	3.492409 E-5 (3.778848)
2	3.087473 E-2 (3.097519)	2.877695 E-4 (2.453416)
3	3.015320 E-2 (3.035346)	6.646130 E-4 (6.215050)
	<u>$\approx 100 \text{ Hz}$</u>	
1	.1254460 (.1254452)	3.310623 E-8 (3.177127)
2	.1252816 (.1252807)	4.514341 E-6 (4.761233)
3	.1251256 (.1251152)	3.782473 E-5 (3.949632)
4	.1248763 (.1248825)	1.075746 E-4 (1.041099)
5	.1245431 (.1245658)	1.917165 E-4 (1.856100)
	<u>$\approx 500 \text{ Hz}$</u>	
1	.6279464 (.6279451)	5.030603 E-33 (0.)
2	.6276678 (.6276654)	3.230407 E-27 (0.)
3	.6274396 (.6274364)	8.766610 E-23 (0.)
4	.6272378 (.6272339)	3.685180 E-16 (0.)
5	.6270533 (.6270487)	4.186859 E-14 (3.466829)
6	.6268813 (.6268761)	1.684570 E-13 (1.430650)
7	.6267190 (.6267133)	2.801780 E-11 (2.433916)
8	.6265645 (.6265582)	2.104337 E-9 (1.868979)
9	.6264166 (.6264097)	7.414939 E-8 (6.730201)
10	.6262741 (.6262668)	1.181578 E-6 (1.103277)
11	.6261333 (.6261259)	7.110299 E-6 (7.500457)
12	.6259948 (.6259753)	2.183201 E-5 (2.295352)
13	.6258225 (.6258053)	4.323009 E-5 (4.329292)
14	.6256280 (N/A)	6.543505 E-5 (N/A)

3.3 EVALUATION SUMMARY

The surface-duct model transmission-loss (TL) results were found to be in good agreement with PE and NM computations for a bilinear test case. The virtual mode model predicted the proper frequency dependence of the TL and exhibited excellent performance in predicting the depth dependence of the TL for within-, cross-, and below-layer propagation geometries. Comparison with the NM results shows good agreement for mode attenuation coefficients, giving the proper range decay of intensity.

The execution time of the surface duct model for the 126 scenarios was about 12 CPU seconds on a Digital DEC-10, including loading and I/O. For comparison, a CDC CYBER-76/175, or UNIVAC 1110 are approximately eight (8) times faster than the DEC-10, leading to projected execution times of ~2 seconds - well within the time constraint of the FACT model.

Deviations between model computed TL's and PE results are small (2 - 3 dB max) and generally occur at short ranges. These ranges are within the direct-path regime and can be adequately modeled using ray theory as is presently being done in FACT. Systematic deviations, not related to the surface duct model, are probably present in the PE data arising from the smoother and/or "ghost" bottom reflections. In any event, larger variations in the computed TL are more apt to arise from use of the bilinear approximation to the environmental index of refraction.

SECTION 4

SURFACE DUCT PROGRAM

The virtual mode surface duct model described earlier has been implemented into a FORTRAN program suitable for inclusion into the FACT model. The surface duct program is written in ANSI standard FORTRAN-77, compatible with compilers on CDC, UNIVAC and DEC computers. The surface duct model is designed to operate as a self-contained module needing only environmental specifications and desired propagation scenarios. The virtual mode calculations are automatic and require no initial conditions from the user.

The surface duct code is configured as a main control sub-program, SDUCT, and six ancillary subroutines: TRAPED, LEAKY, SMODE, AIRY, H1SQ, and REFLKT. To facilitate use as a stand-alone module, a separate driver program DRIVER is supplied which automatically calls SDUCT. A FORTRAN source listing of the surface duct model and the stand-alone driver are provided in Appendix B.

User inputs to DRIVER are provided via free-format NAMELIST inputs. The surface duct model is configured to handle up to six frequencies and six distinct source/receiver depths for a total of $6 \times 21 = 126$ distinct transmission-loss scenarios. The surface duct program is capable of using either metric or english units and automatically adjusts outputs accordingly. Transmission-loss (TL) is computed as a function of range, and optional debug flags allow individual modal values of attenuation coefficient α_m and intensity amplitude ψ_m to be printed. A sample execution, corresponding to the deep duct test case used in Section 3, is shown in Appendix C.

SECTION 5

CONCLUSIONS

The virtual mode surface duct model described in this report is proposed as a replacement to the current FACT surface duct model. The virtual mode model was compared with parabolic equations and normal mode calculations for a bilinear duct over a wide range of propagation scenarios and found to be in good agreement with each. The virtual mode model exhibited the proper frequency and depth dependence displayed by the PE code results. Model execution times are well within FACT constraints and no user interaction is required other than environmental inputs and specification of frequency/depth scenarios.

The major limitation of the surface duct model is in approximating the environmental refractive index profile by the Furry model, and future efforts should be directed toward removing this limitation. Additional work in the area of surface loss mechanisms is also warranted.

APPENDIX A

EVALUATION OF $T_+ T_-$

For real arguments, the Airy functions are real valued hence the expressions for T_+ and T_- [Eqs. (2.5)] are complex conjugates of one another and

$$T_+(E)T_-(E) = |T(E)|^2 = \pi |\psi(0, E)h_1(E) - \psi'(0, E)h_1'(E)|^2 .$$

Now $\psi(0, E)$ and $\psi'(0, E)$ are found from Eq. (2.4a) to be

$$\psi(0, E) = \frac{\pi}{s} [Ai(-w)Bi(-q_0) - Ai(-q_0)Bi(-w)] .$$

and

$$\psi'(0, E) = \frac{d\psi(0, E)}{dx} = \pi [Ai'(-w)Bi(-q_0) - Ai(-q_0)Bi'(-w)] .$$

Since w and q_0 are positive for leaky modes, the Airy functions and their derivatives can be expressed in terms of modulus and phase as

$$Ai(-w) = M(w)\cos\theta(w) , \quad Bi(-w) = M(w)\sin\theta(w) ,$$

and

$$Ai'(-w) = N(w)\cos\phi(w) , \quad Bi'(-w) = N(w)\sin\phi(w) ,$$

with similar expressions for $Ai(-q_0)$, $Bi(-q_0)$. Thus

$$\psi(0, E) = \frac{\pi}{s} M(w)M(q_0) \sin[\theta(q_0) - \theta(w)] .$$

and

$$\psi'(0, E) = \pi M(q_0)N(w) \sin[\theta(q_0) - \phi(w)] .$$

The function $h_1(E)$ and its derivative $h'_1(E)$ are

$$h_1(E) = A\phi(-E) - iB\psi(-E) = M(E)e^{-i\theta(E)}$$

and

$$h'_1(E) = -[A\phi'(-E) - iB\psi'(-E)] = -N(E)e^{-i\phi(E)}.$$

Thus the expression for $|T(E)|^2$ becomes

$$\begin{aligned} |T(E)|^2 &= \frac{\pi^3}{s^2} M^2(q_0) \left| sN(w) \sin[\theta(q_0) - \phi(w)] M(E) e^{-i\theta(E)} \right. \\ &\quad \left. + N(w) \sin[\theta(q_0) - \phi(w)] N(E) e^{-i\phi(E)} \right|^2 \end{aligned}$$

with the definitions

$$\beta = N(E)M(w)/sM(E)N(w) ,$$

$$\Delta = \phi(E) - \theta(E) ,$$

$$\delta = \phi(w) - \theta(w) ,$$

$$x = 2\theta(q_0) - \phi(w) - \theta(w) ,$$

and

$$x_{\pm} = (x \pm \delta)/2 .$$

$$|T(E)|^2 = \frac{\pi^3}{s^2} M^2(q_0) M^2(E) N^2(w) G^2(E)$$

where

$$G^2(E) = \beta^2 \sin^2(x_+) + \sin^2 x_- + 2\beta \sin x_+ \sin x_- \cos \Delta .$$

APPENDIX B
SURFACE-DUCT PROGRAM LISTING

The following is a FORTRAN listing of the virtual mode surface program and stand-alone driver.

IF SO, ALL MUSCULAR PAINS CONSIDERED WITH NO ARP

RESULTS OF DISTINCT SENSE RECEIVED NEPTUS (MAX 4) AND OF RAISE POLYNS SINU CALCULATION (MAX 50)

CUMLAIDH SABHALAN CHUAICH ACHADH
SABHALAN CHUAICH ACHADH CUMLAIDH

כ'..... יונתן אמר ליה ר' יהונתן

• **DE** → **DEUTSCHE PFERD**, **DEUTSCHE PFERD**
• **DE** → **DEUTSCHE PFERD**, **DEUTSCHE PFERD**

8.9.15 IN CHARGE OF THE DRAKE 1 FT TO THE RE 1 YD.

PRIVACY AND INFORMATION SECURITY IN THE FINANCIAL SERVICES INDUSTRY

ପାତାମେଲେ କେବଳ ଏହି ଦିନ

.....

मात्रा विद्या के अनुसार इन शब्दों का अर्थ है-

መ/ቤትና ማረጋገጫ በት/ሮ/የግብር/ንግድ/ንግድ

مودودی، احمد (۱۹۳۰-۲۰۰۷) مذکور در اینجا مذکور نشده است.

AND IN HAVING THEREFORE CHARGE DILECTIONS OF FOLIATION ARRAYS
IF INFLUENT VARIATIONS OCCUR.

卷之三

STRUCTURE: **STRUCTURE** IS THE WAY A SYSTEM ALLOWS CAPABILITY FOR VIRTUAL MODE CONTROL SURROUNDED -STRUCT-

LA JUNIOR, C.A.
SOCIETE AMERICANA, INC.
ACCIDENT INSURANCE
COMPANY

STAIID-ALUMNE DATAVEA PUA SIUFACE DUCET MODEL

ପ୍ରକାଶକ ପତ୍ର ଏବଂ ମାନ୍ୟମାନ ପତ୍ର ପରିଚୟ

כדו רשות כרכורית, ורשות מילואים, ורשות מילואים, ורשות מילואים.

ב-3 כוונתנו היא:

ה-1. רשות מילואים מילאנית, מילאנית, מילאנית.

ה-2. רשות מילואים מילאנית, מילאנית, מילאנית.

ה-3. רשות מילואים מילאנית, מילאנית, מילאנית.

ה-4. רשות מילואים מילאנית, מילאנית, מילאנית.

ה-5. רשות מילואים מילאנית, מילאנית, מילאנית.

ה-6. רשות מילואים מילאנית, מילאנית, מילאנית.

ה-7. רשות מילואים מילאנית, מילאנית, מילאנית.

ה-8. רשות מילואים מילאנית, מילאנית, מילאנית.

ה-9. רשות מילואים מילאנית, מילאנית, מילאנית.

ה-10. רשות מילואים מילאנית, מילאנית, מילאנית.

ה-11. רשות מילואים מילאנית, מילאנית, מילאנית.

ה-12. רשות מילואים מילאנית, מילאנית, מילאנית.

ה-13. רשות מילואים מילאנית, מילאנית, מילאנית.

ה-14. רשות מילואים מילאנית, מילאנית, מילאנית.

ה-15. רשות מילואים מילאנית, מילאנית, מילאנית.

ה-16. רשות מילואים מילאנית, מילאנית, מילאנית.

ה-17. רשות מילואים מילאנית, מילאנית, מילאנית.

ה-18. רשות מילואים מילאנית, מילאנית, מילאנית.

ה-19. רשות מילואים מילאנית, מילאנית, מילאנית.

ה-20. רשות מילואים מילאנית, מילאנית, מילאנית.

CONVERSATION - 1
PARTICIPANTS : A, B, C, D, E, F, G, H, I, J, K, L, M, N, O, P, Q, R, S, T, U, V, W, X, Y, Z.

THE CONVERSATION IS AS FOLLOWS :-
A : Hello, how are you?
B : I'm fine, thanks. How about you?

C : I'm also fine, thank you.
D : And I'm good too.

E : I'm great, thanks.
F : I'm also great.

G : I'm also great.
H : I'm also great.

I : I'm also great.
J : I'm also great.

K : I'm also great.
L : I'm also great.

M : I'm also great.
N : I'm also great.

O : I'm also great.
P : I'm also great.

Q : I'm also great.
R : I'm also great.

S : I'm also great.
T : I'm also great.

U : I'm also great.
V : I'm also great.

W : I'm also great.
X : I'm also great.

Y : I'm also great.
Z : I'm also great.

A : It's been a long time since we last met.
B : Yes, it has.

C : We haven't seen each other for quite some time now.
D : That's true.

E : It's been a while since we last spoke.
F : I agree.

G : We haven't communicated much recently.
H : True.

I : It's been a while since we last exchanged messages.
J : I know.

K : We haven't spoken in a while.
L : Right.

M : It's been a long time since we last spoke.
N : I know.

O : We haven't communicated much lately.
P : True.

Q : It's been a while since we last spoke.
R : I know.

S : We haven't communicated much lately.
T : True.

U : It's been a while since we last spoke.
V : I know.

W : We haven't communicated much lately.
X : True.

Y : It's been a while since we last spoke.
Z : I know.

A : It's been a long time since we last met.
B : Yes, it has.

C : We haven't seen each other for quite some time now.
D : That's true.

E : It's been a while since we last spoke.
F : I agree.

G : We haven't communicated much recently.
H : True.

I : It's been a while since we last exchanged messages.
J : I know.

K : We haven't spoken in a while.
L : Right.

M : It's been a long time since we last spoke.
N : I know.

O : We haven't communicated much lately.
P : True.

Q : It's been a while since we last spoke.
R : I know.

S : We haven't communicated much lately.
T : True.

U : It's been a while since we last spoke.
V : I know.

W : We haven't communicated much lately.
X : True.

Y : It's been a while since we last spoke.
Z : I know.

COMPOSITIONS AND PARAPHRASES

1. 1. 1.

2. 2. 2.

3. 3. 3.

4. 4. 4.

5. 5. 5.

ANSWER TO EXERCISE

1. 1. 1.

2. 2. 2.

3. 3. 3.

4. 4. 4.

5. 5. 5.

ANSWER TO EXERCISE

1. 1. 1.

2. 2. 2.

3. 3. 3.

4. 4. 4.

5. 5. 5.

ANSWER TO EXERCISE

1. 1. 1.

2. 2. 2.

3. 3. 3.

4. 4. 4.

5. 5. 5.

2161 1 100000 2161
2162 1 100000 2162
2163 1 100000 2163
2164 1 100000 2164
2165 1 100000 2165
2166 1 100000 2166
2167 1 100000 2167
2168 1 100000 2168
2169 1 100000 2169
2170 1 100000 2170
2171 1 100000 2171
2172 1 100000 2172
2173 1 100000 2173
2174 1 100000 2174
2175 1 100000 2175
2176 1 100000 2176
2177 1 100000 2177
2178 1 100000 2178
2179 1 100000 2179
2180 1 100000 2180
2181 1 100000 2181
2182 1 100000 2182
2183 1 100000 2183
2184 1 100000 2184
2185 1 100000 2185
2186 1 100000 2186
2187 1 100000 2187
2188 1 100000 2188
2189 1 100000 2189
2190 1 100000 2190
2191 1 100000 2191
2192 1 100000 2192
2193 1 100000 2193
2194 1 100000 2194
2195 1 100000 2195
2196 1 100000 2196
2197 1 100000 2197
2198 1 100000 2198
2199 1 100000 2199
2200 1 100000 2200

REF ID: A3A6021 / #1 2-00CT-40 PAGE 103

REF ID: A3A6021 / #1 2-00CT-40 PAGE 103

00051 POINT SOURCE AT 1 METER.
 00052 IN MULTIPLE WILES. INENSITY COMPUTED RELATIVE
 00053 TO POINT SOURCE AT 1 METER.
 00054 IN POINT SOURCE AT 1 METER.
 00055 RANGES
 00056 COMPUTED RELATIVE TO
 00057 INFLUENCES. ININSTA COMPUTED RELATIVE TO
 00058 INFLUENCES. ININSTA COMPUTED RELATIVE TO

00059 POINTS IN PFTS, SOUND SPEEDS IN PFTS, RANGES
 00060 IN MULTIPLE WILES. INENSITY COMPUTED RELATIVE
 00061 POINT SOURCE AT 1 METER.
 00062 INFLUENCES. ININSTA COMPUTED RELATIVE TO

***** WRITE: INPUT UNIT 3 *****

***** WRITE: INPUT UNIT 1 *****

***** WRITE: INPUT UNIT 2 *****

***** WRITE: INPUT UNIT 4 *****

***** WRITE: INPUT UNIT 5 *****

***** WRITE: INPUT UNIT 6 *****

***** WRITE: INPUT UNIT 7 *****

***** WRITE: INPUT UNIT 8 *****

***** WRITE: INPUT UNIT 9 *****

***** WRITE: INPUT UNIT 10 *****

***** WRITE: INPUT UNIT 11 *****

***** WRITE: INPUT UNIT 12 *****

***** WRITE: INPUT UNIT 13 *****

***** WRITE: INPUT UNIT 14 *****

***** WRITE: INPUT UNIT 15 *****

***** WRITE: INPUT UNIT 16 *****

***** WRITE: INPUT UNIT 17 *****

***** WRITE: INPUT UNIT 18 *****

***** WRITE: INPUT UNIT 19 *****

***** WRITE: INPUT UNIT 20 *****

***** WRITE: INPUT UNIT 21 *****

***** WRITE: INPUT UNIT 22 *****

***** WRITE: INPUT UNIT 23 *****

***** WRITE: INPUT UNIT 24 *****

***** WRITE: INPUT UNIT 25 *****

***** WRITE: INPUT UNIT 26 *****

***** WRITE: INPUT UNIT 27 *****

***** WRITE: INPUT UNIT 28 *****

***** WRITE: INPUT UNIT 29 *****

***** WRITE: INPUT UNIT 30 *****

***** WRITE: INPUT UNIT 31 *****

SOLICIT

PROPOSAL NO. 5216311 / XI 22-SPR-00 PAGE 1-3

STRUCTURAL MORTAR V-SAR6211 10043 22-SEPT-90 PAGE 1-3

Ламуда $\left(\text{Ламуда} \right)$ — это языковая единица, состоящая из двух или более слов, соединенных между собой предлогом, союзом, наречием и т. д. Ламуда может быть выражена в виде отдельного слова, а также в виде фразы, предложения и т. д.

COUNTE RIV-PANTELINAT APRCL (RMTAIS) AT SURFACE

[JOURNAL] DANIEL

THE JOURNAL OF CLIMATE

IP(0.007.45.7011) PQR(0)=Pw/607h,12

TELEVISIONSISTEMERAKENNAU

THE JOURNAL OF LITERATURE

MURVAT. RAVI SINGH & TILAK DAS PERIODICALS

Digitized by srujanika@gmail.com

ANSWER IS CORRECT IF PUPILS SAY: "NO"; OR IF PUPILS SAY: "YES" AND EXPLAIN HOW THEY GOT THE ANSWER.

APPLIED CONTINUALLY PER RAY-CYCLE DISTANCE D_n . THE RUGH SURFACE DEFLECTION COEFFICIENT IS COMPUTED IN SUBROUTINE **SURFSSI**.

הנִזְקָנָה וְהַנִּזְקָנָה הַמִּזְרָחִית

```

ALPHA=ALPHAS-ALPHAS
DOLPHIN=0.6500000000000000
RCAV=EXP(-NFLTARE(ALPHAS))
WIP(UNL)=WIPAV
IOP(DPFLIC)=WIPTRC(10(1),7,40)
FORMAT(ST,5T,5T,WIPARE(LNSTC,0,0))
1,ALPHA,IUCAV,SIMPLRS(2,-,E13.6)
PS10=-1.
RP(IN(2)-LP,0),CN PN 255

```

(((2)(0)(1)'81'94'00m)2005-05-00

SOURCE 242 MIRROR(10(2)), 242 (M0UP
 00226 00227 00228 00229 00230 00231 00232 00233 00234 00235 00236 00237 00238 00239 00240 00241 00242 00243 00244 00245 00246 00247 00248 00249 00250 00251 00252 00253 00254 00255 00256 00257 00258 00259 00260 00261 00262 00263 00264 00265 00266 00267 00268 00269 00270 00271 00272 00273 00274 00275 00276 00277 00278 00279 00280

U=7.2. H=2.7.
 U=-20 / H
 U=250 11 X=1.50
 U=100 A=100
 U=250 X=1.50
 U=250 10 X=1,50
 NOV 10244 10245 10246 10247 10248 10249 10250 10251 10252 10253 10254 10255 10256 10257 10258 10259 10260 10261 10262 10263 10264 10265 10266 10267 10268 10269 10270 10271 10272 10273 10274 10275 10276 10277 10278 10279 10280

NOV 10143 10144 22-238-80
 10145 10146 22-238-91
 SOURCE 242 MIRROR(10(2)), 242 (M0UP
 00226 00227 00228 00229 00230 00231 00232 00233 00234 00235 00236 00237 00238 00239 00240 00241 00242 00243 00244 00245 00246 00247 00248 00249 00250 00251 00252 00253 00254 00255 00256 00257 00258 00259 00260 00261 00262 00263 00264 00265 00266 00267 00268 00269 00270 00271 00272 00273 00274 00275 00276 00277 00278 00279 00280

U=7.2. H=2.7.
 U=-20 / H
 U=250 11 X=1.50
 U=100 A=100
 U=250 X=1.50
 U=250 10 X=1,50
 NOV 10244 10245 10246 10247 10248 10249 10250 10251 10252 10253 10254 10255 10256 10257 10258 10259 10260 10261 10262 10263 10264 10265 10266 10267 10268 10269 10270 10271 10272 10273 10274 10275 10276 10277 10278 10279 10280

NOV 10143 10144 22-238-80
 10145 10146 22-238-91

S0NCP C IN ERRORS DETECTED 3

• 10016 2203 • 00000 2204 • 00001 2205

TESTRESULTS 3

SCALAR AND ARRAYS + WORD AND EXPLICIT INITIALIZATION - NOT PREFERENCE 1

TESTRESULTS	1	2	3	4	5	6	7	8	9	10	11	12	13	14	15	16	17	18	19	20	21	22	23	24	25	26	27	28	29	30	31	32	33	34	35	36	37	38	39	40	41	42	43	44	45	46	47	48	49	50	51	52	53	54	55	56	57	58	59	60	61	62	63	64	65	66	67	68	69	70	71	72	73	74	75	76	77	78	79	80	81	82	83	84	85	86	87	88	89	90	91	92	93	94	95	96	97	98	99	100	101	102	103	104	105	106	107	108	109	110	111	112	113	114	115	116	117	118	119	120	121	122	123	124	125	126	127	128	129	130	131	132	133	134	135	136	137	138	139	140	141	142	143	144	145	146	147	148	149	150	151	152	153	154	155	156	157	158	159	160	161	162	163	164	165	166	167	168	169	170	171	172	173	174	175	176	177	178	179	180	181	182	183	184	185	186	187	188	189	190	191	192	193	194	195	196	197	198	199	200	201	202	203	204	205	206	207	208	209	210	211	212	213	214	215	216	217	218	219	220	221	222	223	224	225	226	227	228	229	230	231	232	233	234	235	236	237	238	239	240	241	242	243	244	245	246	247	248	249	250	251	252	253	254	255	256	257	258	259	260	261	262	263	264	265	266	267	268	269	270	271	272	273	274	275	276	277	278	279	280	281	282	283	284	285	286	287	288	289	290	291	292	293	294	295	296	297	298	299	300	301	302	303	304	305	306	307	308	309	310	311	312	313	314	315	316	317	318	319	320	321	322	323	324	325	326	327	328	329	330	331	332	333	334	335	336	337	338	339	340	341	342	343	344	345	346	347	348	349	350	351	352	353	354	355	356	357	358	359	360	361	362	363	364	365	366	367	368	369	370	371	372	373	374	375	376	377	378	379	380	381	382	383	384	385	386	387	388	389	390	391	392	393	394	395	396	397	398	399	400	401	402	403	404	405	406	407	408	409	410	411	412	413	414	415	416	417	418	419	420	421	422	423	424	425	426	427	428	429	430	431	432	433	434	435	436	437	438	439	440	441	442	443	444	445	446	447	448	449	450	451	452	453	454	455	456	457	458	459	460	461	462	463	464	465	466	467	468	469	470	471	472	473	474	475	476	477	478	479	480	481	482	483	484	485	486	487	488	489	490	491	492	493	494	495	496	497	498	499	500	501	502	503	504	505	506	507	508	509	510	511	512	513	514	515	516	517	518	519	520	521	522	523	524	525	526	527	528	529	530	531	532	533	534	535	536	537	538	539	540	541	542	543	544	545	546	547	548	549	550	551	552	553	554	555	556	557	558	559	560	561	562	563	564	565	566	567	568	569	570	571	572	573	574	575	576	577	578	579	580	581	582	583	584	585	586	587	588	589	590	591	592	593	594	595	596	597	598	599	600	601	602	603	604	605	606	607	608	609	610	611	612	613	614	615	616	617	618	619	620	621	622	623	624	625	626	627	628	629	630	631	632	633	634	635	636	637	638	639	640	641	642	643	644	645	646	647	648	649	650	651	652	653	654	655	656	657	658	659	660	661	662	663	664	665	666	667	668	669	670	671	672	673	674	675	676	677	678	679	680	681	682	683	684	685	686	687	688	689	690	691	692	693	694	695	696	697	698	699	700	701	702	703	704	705	706	707	708	709	710	711	712	713	714	715	716	717	718	719	720	721	722	723	724	725	726	727	728	729	730	731	732	733	734	735	736	737	738	739	740	741	742	743	744	745	746	747	748	749	750	751	752	753	754	755	756	757	758	759	760	761	762	763	764	765	766	767	768	769	770	771	772	773	774	775	776	777	778	779	780	781	782	783	784	785	786	787	788	789	790	791	792	793	794	795	796	797	798	799	800	801	802	803	804	805	806	807	808	809	810	811	812	813	814	815	816	817	818	819	820	821	822	823	824	825	826	827	828	829	830	831	832	833	834	835	836	837	838	839	840	841	842	843	844	845	846	847	848	849	850	851	852	853	854	855	856	857	858	859	860	861	862	863	864	865	866	867	868	869	870	871	872	873	874	875	876	877	878	879	880	881	882	883	884	885	886	887	888	889	890	891	892	893	894	895	896	897	898	899	900	901	902	903	904	905	906	907	908	909	910	911	912	913	914	915	916	917	918	919	920	921	922	923	924	925	926	927	928	929	930	931	932	933	934	935	936	937	938	939	940	941	942	943	944	945	946	947	948	949	950	951	952	953	954	955	956	957	958	959	960	961	962	963	964	965	966	967	968	969	970	971	972	973	974	975	976	977	978	979	980	981	982	983	984	985	986	987	988	989	990	991	992	993	994	995	996	997	998	999	1000
-------------	---	---	---	---	---	---	---	---	---	----	----	----	----	----	----	----	----	----	----	----	----	----	----	----	----	----	----	----	----	----	----	----	----	----	----	----	----	----	----	----	----	----	----	----	----	----	----	----	----	----	----	----	----	----	----	----	----	----	----	----	----	----	----	----	----	----	----	----	----	----	----	----	----	----	----	----	----	----	----	----	----	----	----	----	----	----	----	----	----	----	----	----	----	----	----	----	----	----	----	-----	-----	-----	-----	-----	-----	-----	-----	-----	-----	-----	-----	-----	-----	-----	-----	-----	-----	-----	-----	-----	-----	-----	-----	-----	-----	-----	-----	-----	-----	-----	-----	-----	-----	-----	-----	-----	-----	-----	-----	-----	-----	-----	-----	-----	-----	-----	-----	-----	-----	-----	-----	-----	-----	-----	-----	-----	-----	-----	-----	-----	-----	-----	-----	-----	-----	-----	-----	-----	-----	-----	-----	-----	-----	-----	-----	-----	-----	-----	-----	-----	-----	-----	-----	-----	-----	-----	-----	-----	-----	-----	-----	-----	-----	-----	-----	-----	-----	-----	-----	-----	-----	-----	-----	-----	-----	-----	-----	-----	-----	-----	-----	-----	-----	-----	-----	-----	-----	-----	-----	-----	-----	-----	-----	-----	-----	-----	-----	-----	-----	-----	-----	-----	-----	-----	-----	-----	-----	-----	-----	-----	-----	-----	-----	-----	-----	-----	-----	-----	-----	-----	-----	-----	-----	-----	-----	-----	-----	-----	-----	-----	-----	-----	-----	-----	-----	-----	-----	-----	-----	-----	-----	-----	-----	-----	-----	-----	-----	-----	-----	-----	-----	-----	-----	-----	-----	-----	-----	-----	-----	-----	-----	-----	-----	-----	-----	-----	-----	-----	-----	-----	-----	-----	-----	-----	-----	-----	-----	-----	-----	-----	-----	-----	-----	-----	-----	-----	-----	-----	-----	-----	-----	-----	-----	-----	-----	-----	-----	-----	-----	-----	-----	-----	-----	-----	-----	-----	-----	-----	-----	-----	-----	-----	-----	-----	-----	-----	-----	-----	-----	-----	-----	-----	-----	-----	-----	-----	-----	-----	-----	-----	-----	-----	-----	-----	-----	-----	-----	-----	-----	-----	-----	-----	-----	-----	-----	-----	-----	-----	-----	-----	-----	-----	-----	-----	-----	-----	-----	-----	-----	-----	-----	-----	-----	-----	-----	-----	-----	-----	-----	-----	-----	-----	-----	-----	-----	-----	-----	-----	-----	-----	-----	-----	-----	-----	-----	-----	-----	-----	-----	-----	-----	-----	-----	-----	-----	-----	-----	-----	-----	-----	-----	-----	-----	-----	-----	-----	-----	-----	-----	-----	-----	-----	-----	-----	-----	-----	-----	-----	-----	-----	-----	-----	-----	-----	-----	-----	-----	-----	-----	-----	-----	-----	-----	-----	-----	-----	-----	-----	-----	-----	-----	-----	-----	-----	-----	-----	-----	-----	-----	-----	-----	-----	-----	-----	-----	-----	-----	-----	-----	-----	-----	-----	-----	-----	-----	-----	-----	-----	-----	-----	-----	-----	-----	-----	-----	-----	-----	-----	-----	-----	-----	-----	-----	-----	-----	-----	-----	-----	-----	-----	-----	-----	-----	-----	-----	-----	-----	-----	-----	-----	-----	-----	-----	-----	-----	-----	-----	-----	-----	-----	-----	-----	-----	-----	-----	-----	-----	-----	-----	-----	-----	-----	-----	-----	-----	-----	-----	-----	-----	-----	-----	-----	-----	-----	-----	-----	-----	-----	-----	-----	-----	-----	-----	-----	-----	-----	-----	-----	-----	-----	-----	-----	-----	-----	-----	-----	-----	-----	-----	-----	-----	-----	-----	-----	-----	-----	-----	-----	-----	-----	-----	-----	-----	-----	-----	-----	-----	-----	-----	-----	-----	-----	-----	-----	-----	-----	-----	-----	-----	-----	-----	-----	-----	-----	-----	-----	-----	-----	-----	-----	-----	-----	-----	-----	-----	-----	-----	-----	-----	-----	-----	-----	-----	-----	-----	-----	-----	-----	-----	-----	-----	-----	-----	-----	-----	-----	-----	-----	-----	-----	-----	-----	-----	-----	-----	-----	-----	-----	-----	-----	-----	-----	-----	-----	-----	-----	-----	-----	-----	-----	-----	-----	-----	-----	-----	-----	-----	-----	-----	-----	-----	-----	-----	-----	-----	-----	-----	-----	-----	-----	-----	-----	-----	-----	-----	-----	-----	-----	-----	-----	-----	-----	-----	-----	-----	-----	-----	-----	-----	-----	-----	-----	-----	-----	-----	-----	-----	-----	-----	-----	-----	-----	-----	-----	-----	-----	-----	-----	-----	-----	-----	-----	-----	-----	-----	-----	-----	-----	-----	-----	-----	-----	-----	-----	-----	-----	-----	-----	-----	-----	-----	-----	-----	-----	-----	-----	-----	-----	-----	-----	-----	-----	-----	-----	-----	-----	-----	-----	-----	-----	-----	-----	-----	-----	-----	-----	-----	-----	-----	-----	-----	-----	-----	-----	-----	-----	-----	-----	-----	-----	-----	-----	-----	-----	-----	-----	-----	-----	-----	-----	-----	-----	-----	-----	-----	-----	-----	-----	-----	-----	-----	-----	-----	-----	-----	-----	-----	-----	-----	-----	-----	-----	-----	-----	-----	-----	-----	-----	-----	-----	-----	-----	-----	-----	-----	-----	-----	-----	-----	-----	-----	-----	-----	-----	-----	-----	-----	-----	-----	-----	-----	-----	-----	-----	-----	-----	-----	-----	-----	-----	-----	-----	-----	-----	-----	-----	-----	-----	-----	-----	-----	-----	-----	-----	-----	-----	-----	-----	-----	-----	-----	-----	-----	-----	-----	-----	-----	-----	-----	-----	-----	-----	-----	-----	-----	-----	-----	-----	-----	-----	-----	-----	-----	-----	-----	-----	-----	-----	-----	-----	-----	-----	-----	-----	-----	-----	-----	-----	-----	-----	-----	-----	-----	-----	-----	-----	-----	-----	-----	-----	-----	-----	-----	-----	-----	-----	-----	-----	-----	-----	-----	-----	-----	-----	-----	-----	-----	-----	-----	-----	-----	-----	-----	-----	-----	-----	-----	-----	-----	-----	-----	-----	-----	-----	-----	-----	-----	-----	-----	-----	-----	-----	-----	-----	-----	-----	-----	-----	-----	-----	-----	-----	-----	-----	-----	-----	-----	-----	-----	------

COMMON NAMES

JULY/10/121

JULY/00/111

ALPHABET

00/00/00

C7LNG

B-14

REPRODUCED BY UN authorized DRAFTSMAN 3

• 00001 116 • 00000 117 • 00001 120 • 00002 121

REPRODUCED BY UN

SCALAR AND VECTOR ELEMENTS OF THE ROTICIT REPRESENTATION - WITH DIFFERENTIATION
OF VECTORS. SCALAR. SPHERICAL. CYLINDRICAL. AIRY. ANG.

SUMMATION RULES

	4	OVERLAP	3	C2	C1	2	C2	C1	3	OVERLAP	4
SCALAR	0	0	0	0	0	0	0	0	0	0	0
VECTOR	1	1	1	1	1	1	1	1	1	1	1
ANG.	0	0	0	0	0	0	0	0	0	0	0
SPHERICAL	1	1	1	1	1	1	1	1	1	1	1
CYLINDRICAL	1	1	1	1	1	1	1	1	1	1	1
AIRY	1	1	1	1	1	1	1	1	1	1	1
OVERLAP	1	1	1	1	1	1	1	1	1	1	1

REPRODUCED BY UN AUTHORIZED DRAFTSMAN 711 15126 15126 15126

```

00001 C SUBROUTINE LEAKY(MODE, IO1, REALM)
00002 C COMPUTES PARAMETERS ASSOCIATED WITH LEAKY MODES.
00003 C ENERGY - EM-. DECAY COEFFICIENT -ALPHAH-. AND
00004 C RAY EQUIVALENT PERIOD -RH-.
00005 C *****
00006 C
00007 C *****
00008 C
00009 C DIMENSION REALM( 1 )
00010 C INTEGER ERROR
00011 C COMPLEX EM,Z,J6Z,A,A2,Z2,DE,U02,DZETA,DQ,ZETA0,E0,R0,V,DRDE
00012 C REAL KO,KOI,MM
00013 C LOGICAL DEBUG
00014 C COMMON/DUCT/S,S2,S3,KOH,S3D,D,CPLUS,CHINUS,H,K0
00015 C COMMON/MODES/NVM,ALPHA0,EM,DQ,MM,PSI0,U05Q
00016 C COMMON/CONST/P1,TWOP1,C1,C2,OVRFL0,SORT3,SORTP1
00017 C DATA R0/(-.36450537..6313421668)/
00018 C
00019 C
00020 C DEBUG=. FALSE.
00021 C IF( IO1.GT.0 ) DEBUG=. TRUE.
00022 C DQ=( 1 .. 1. )
00023 C SD=S*D
00024 C IP(S3D.LT.1.E-2) GO TO 300
00025 C
00026 C SIGNIFICANT DUCT IS PRESENT
00027 C
00028 C
00029 C ..... DETERMINE REAL PART OF ENERGY EIGENVALUE -EM-.
00030 C FOUND BY SATISFYING PHASE INTEGRAL CONDITION
00031 C
00032 C
00033 C B=SD*SORT(SD)/(PI*75)
00034 C T=(4*MODE-1)/(3.*XB)
00035 C IF(T.LE.1.) A=1.5*T-1.
00036 C IF(T.GT.1.) A=.25*(T+SORT(T*T-1.))**2
00037 C EOLD=A*S3D
00038 C
00039 C DO NEWTON/RAPHSON ITERATES TO FIND -EM-
00040 C
00041 DO 30 I=1,5
00042 AP= A-(( (A+1.)*SORT(A+1.)-A*SORT(A))/1.5-T)/(SORT(A+1.))-_
00043 C1=SORT(A)
00044 IF( ABS(AP-A).LT. ABS(A)*1.E-3) GO TO 55
00045 A=AP
00046 CONTINUE
00047 30 EM=AP*S3D
00048 IF( EM.LE.0.) RETURN
00049 C1=-5.-R*((AP+1.)*SORT(AP+1.))-AP*SORT(AP)
00050 DC1:DE=-R*(SORT(AP+1.))-SORT(AP)
00051 IF(DEBUG) WRITE(101,80) EM,FOLD,T,AP,CHI,DC1,DE
00052 FORMAT(' LEAKY ... EM,EOLD,T,AP,CHI,DC1,DE= ',0(1PE14.6))
00053 C
00054 C COMPUTE RAY-EQUIVALENT PERIOD -RM-. ASSUME RAY TURNS AT
00055 C DUCT BOTTOM, AND NORMALIZATION -NM-
00056 C

```

LEAKY FOR

FORTRAN V.5A(621) /KI 24-SEP-86

17:54 PAGE 1-1

```

00037      DM= (SQR(T(EMR+SD)) - SQR(T(EMR))) * H/SD
00038      RM= 4.*KOH*DM
00039      RH= .5*DM
00040      C..... COMPUTE AMPLITUDE DECAY TERM FOR LEAKY MODES.
00041      C..... MODEL DECAY AS REFLECTION LOSS PER RAY-EQUIVALENT
00042      C..... PERIOD APPLIED CONTINUOUSLY.
00043      C
00044      RCOEFF= REFLKT(EMR, S2, 101)
00045      IF(RCOEFF.GT. 1.) RETURN
00046      ALPHAM= -ALOG(RCOEFF)/RM
00047      ETM= -ALPHAM/(KOH*CPLUS)
00048      EM= CMPLX(EMR, EMI)
00049      IF(EMR.GT. 1.) DROF= -.5/(-EMR)**.5 + .25/EMR**2
00050      IF(EMR.LE. 1.) DROF= -(R0**2 + EMR*(.2251235 + EMR*(.16231472*RE+
00051      EM**2 + 1169137*R0**2 + .0319463474*EM))), )
00052      IF(CABS(EM).GT. 1.5*SD) GO TO 150
00053      C
00054      SMALL_ARCURENT_REGION. EXPAND IN POWER SERIES ABOUT
00055      EM=0.
00056      C
00057      C
00058      W= -EM/S2
00059      Z= W**3/6.
00060      ZFTA0= (-W+SD)**1.5/1.5 + PI/12.
00061      W02= 4.*PI*(C1*CSIN(ZETA0)*(1.+Z*(1.+Z*(ZETA0+C2*CSIN(ZETA0+PI/3.)*
00062      W*(1.+.5*Z*(1.+Z/7.)))***2)/(8*(EM+63D)**.5),
00063      C0 TO 160
00064      DZETA= (EM+SD)**1.5- (EM+SD)**1.5/(1.5*SD)
00065      U02= (CSIN(DZETA)- 5.*SD*CCOS(DZETA))/(48.*EM*(EM+SD))**.5
00066      160  CONTINUE
00067      Z= 1.+((1.+SD)*U02*DZETA
00068      NM= CADS(Z)*IV/SD
00069      IF(EMR.GT. SD) NM= DM/2.
00070      U05Q= CARS(U02)/NM
00071      IF(DEBUG) WRITE(101,200) EM, RCOEFF, RM, NM, U02, U05Q, DRDE
00072      200  FORMAT(101,200) EM, RCOEFF, RM, '4E15.7/10X,
00073      'NM, U02, U05Q, DRDE, '6(1PE14.6))
00074      GO TO 500
00075      C*****
00076      C***** WEAK DUCT CASES.
00077      C
00078      C 1) ZERO GRADIENT IN DUCT (SD=0)
00079      C 2) SMALL DUCT THICKNESS (SD SMALL)
00080      C
00081      C METHOD: USE PERTURBATION THEORY AND EXPAND AROUND SD=0 CASE.
00082      C
00083      C 300 CONTINUE
00084      C
00085      C
00086      C
00087      C FIRST FIND ASYMPTOTIC SD=0 EIGENVALUE (COMPLEX)
00088      C
00089      A= CMPLX(-.68586039, -1.1879454)
00090      A2= CMPLX(-.9408045, 1.6293299)
00091      Z= A/D
00092      Z2= A2/DRDE**2
00093
00094
00095
00096
00097
00098
00099
00100
00101
00102
00103
00104
00105
00106
00107
00108
00109
00110
00111
00112

```

```

00113      T= (2.5810567+ .27929556*(PI*FLOAT(MODE)**2)/D**3
00114      E0= (PI*FLOAT(MODE)/D)**2*(T*(1.+5.*Z)+ 7.74317/D*x*3+ 3.*Z2+
1. *Z+1.)
00115      EB=REAL(E0)
00116      EI=AIMAG(E0)
00117      IF(DEBUG) WRITE(101,320) MODE,T,Z,Z2,E0
00118      320 FORMAT('LEVEL 2 LEAKY... M:DE,T,Z,Z2,E0= ',14.6E14,7)
00119      IF(S.LT.1.E-6) GO TO 400
00120
00121      C
00122      C GRADIENT IS NON-ZERO. FUT EFFECTIVE THICKNESS OF DUCT IS SMALL.
00123      C COMPUTE FIRST ORDER PERTURBATION TO S=0 ENERGY.
00124      C
00125      Z= CSQRT(E0)*D
00126      J0Z= CSIN(Z)/Z
00127      DE= (S3D*D/4.)*(J0Z*J0Z-1.)
00128      EM= E0+DE
00129      IF(DEBUG) WRITE(101,340) Z,J0Z,DE
00130      340 FORMAT(' LEVEL 2 LEAKY... Z,J0Z,DE= ',6E15,7)
00131      C
00132      C COMPUTE RAY-EQUIVALENT PERIOD -RM-
00133      C IF ENERGY IS POSITIVE ( ABOVE BARRIER), ASSUME RAY TURNS AT
00134      C BOTTOM OF DUCT.
00135      C
00136      400  RM=0.
00137      IF(S.EQ.0.) GO TO 500
00138      EM=REAL(EM)
00139      RM=SQRT(EM+S3D)
00140      IF(EM.GE.0.) RM=(RM-SQRT(EM))*4.*SQRT(1.-CPLUS*H*(EM+S3D))
00141      B-17
00142      500 CONTINUE
00143      RETURN
00144      END
00145

```

COMMON BLOCKS

```

/DUCT/(+12)
S      +0      S2      +1      S3      +2      KOH      +3      S3D      +4
D      +5      CPLUS   +6      CMINUS  +7      H        +10     K0       +11
/MODES/(+11)
RM      +0      ALRMA0  +1      EM      +2      DQ      +4      M       +6
PSI0    +7      USGSQ  +10
/CONST/(+7)
PI      +0      TWOPI   +1      C1      +2      C2      +3      OVFLO  +4
SORT3  +5      SORTPI  +6

```

SUBPROGRAMS CALLED

```

REAL:   CABS,   SORT,   CTRIX,   CSORT,   ALOC.
CCOS:   FLOAT,  AIMAG,  REFLKT,  CSIN.

```

LEAKY LEAKY.FOR FORTTRAN V.5A(621) /KI 24-SEP-80 17:54 PAGE 1-3

SCALARS AND ARRAYS ["*" NO EXPLICIT DEFINITION - "X" NOT REFERENCED]

DE	1	DEBUG	3	Z	4	*SD	6	W	7
*AP	11	*T	12	DRDE	13	*EMR	15	*CHI	16
*B	17	*101	20	*REALEM		*RCOEFF	21	*ER	22
*ALPHAN	23	E0	24	A2	26	DZETA	36	*MODE	32
*DM	33	A	34	.S00000	36	ERROR	37	*EMI	40
*EOLD	41	*RM	42	J0Z	43	*I	45	Z2	46
*DCII/DR.	50	ZETAO	51	U02	53	R0	55	*EI	57

TEMPORARIES

.A0016	133	.000000	134	.000001	135	.000002	136	.000003	137	.000004	140
.Q0005	141										

LEAKY [NO ERRORS DETECTED]

١٥٧٦
مکالمہ حسنیہ
و ملکیہ علیاً

SUSPENDED CALIFN

COSU. PEARL. GART. RANS. PROG. EVP.
ALVTR. CSIN. CNS. WISQ. AVINT.

SCALAR IN ARRAYS & NEW FOR PRIORITY DEFINITION & NEW NOT REDEFINED

	0%	2	5%	3	6%	4	9	5
DRPGC	1	0%	10	0%	11	0%	12	0%
ENK	7	0%TA	16	0%TA	17	P	21	0%
OO	14	0%SQ	24	0%	25	0%	27	0%
SPRNG	31	0%	33	0%	34	ZETA0	35	0%
SPRSQ	40					ZETA0	37	

TEMPERATURE

	A0011 75	A0011 76	A0016 77	A0002 100	A0007 101	A0004 102
AU010	75	A0011 76	A0016 77	A0002 100	A0007 101	A0004 102
AU065	103	A0006 104	A0007 105	A0000 106	A0001 107	A0002 110
700003	111	00004 112				

SOUND & NEW ERRORS DETERMINED

Statement If ALPHY(X,ALPH,ALPH,ALPH,ALPH)

PURPOSE: COMPUTES ALPHY FUNCTIONS AND DERIVATIVES FOR REAL ARGUMENTS.

PERMITS A COMBINATION OF CONVERGENT POWER SERIES FOR SMALL ARGUMENTS, WITH ASYMPTOTIC EXPANSIONS FOR LARGE POSITIVE AND NEGATIVE ARGUMENTS.
REFS APPENDIX AND STEGUM, HANDBOOK OF MATHEMATICAL FUNCTIONS.

AUTHOR: F. J. HAYAN
ICFAA' ACOUSTICS DIV.
SCIENCE APPLICATIONS, INC.
LA JOLLA, CA

SUBPROGRAMS CALLED: NONE

ARGUMENTS:

X.....ARGUMENT OF ALPHY FUNCTION
ALPH.....ALPHY FUNCTION INPUT
ALP, RPI.....ALPHY FUNCTION COMPUTED
PARMS.....
.....#1 ONLY ALPH COMPUTED
.....#2 ONLY ALPH, RPI COMPUTED
.....#3 ALPH, ALP, RPI COMPUTED

B-22

DATA C1,C2,S1,W1,T1,R1,U1,V1,W2,R2,U2,V2,
DATA C1,C2,S1,W1,T1,R1,U1,V1,W2,R2,U2,V2,
DATA R1,INVFLN/S,1.015926, #0.//

F.....LITTLE FUNCTIONS

F1(X)= (1.0+X)*C1 + 34.506*(1.0+221.0*(1.0+109.25*X))//
1 1.772*54651
F2(X)= (1.0+7.0*X)*(1.0+32.506*(1.0+209.0*(1.0+106.25*X)))//
1 1.772*54651
F3(X)= (1.0+4.0*X)*(1.0+15.567)/1.772*54651
F4(X)= (1.0-7.0*X)*(1.0+432.544)/1.772*54651
T(X)=1.7-2.0*UP(X,X,2.0) GN TH 50

POWER SERIES REGION:

78 1003/0
TF1,...,FC1,F3,?1 GN TH 30
C.....ALPH COMPUTATION
F2 (1.0+7.0*2*7*(1.0+(2/12)*(1.0+(7/22)*(1.0+(2/26)*(1.0+0.025*X))))*C1
F3=(1.0+7.0*2*7*(1.0+(2/12)*(1.0+(2/15)*(1.0+(2/26)*(1.0+0.025*X))))*C2
A1= F= 1.
112 SUMP (1.0+ C)
112 SUMT (1.0+ C)
50 TF1,FC1,F3,?1 FFT1,N
F2=(1.0+2*7*(1.0+125.0*(1.0+(7/16.5)*(1.0+2/26)))*(1.0+0.0567*(1.0+7/32.5)))*C1
C1'= (1.0+2*7*(1.0+25.0*(1.0+(7/16.5)*(1.0+2/26)))*(1.0+0.0567*(1.0+7/32.5)))*C2
ALPH F1=F3

卷之三

BRIEF REPORTS

SIN. 14

SCALARS AND ARRAYS. (See NOT EXPLICIT DEFINITION - "Z" NOT REFERENCED)

*CIP	1	*F0001	2	*T	1	*F0003	4	*F0002	5
*F0001	6	*F0000	7	*TWTYA	10	N	11	*START	12
*ETA	13	*I	14	*AI	15	*WIP	16	*FP	17
N	20	*E	21	*M000F	22	*VRFLO	23	*AIP	24
*C2	25	*X	26	*SAHTZ	27	*PMI	30	*F	31
*C1	32	*U	33						

TERMINATORS

*ENDFILE
*EOT
*EOF

AIRY 1 AIRY 1 AIRY 1 AIRY 1

STRUCTURE AND USES

SQRT.
ASIN.
ATAN
COS.

SCALARS AND ARRAYS & HOW TO EXPLICIT DEFINITION & HOW NOT REFERENCED

DEFUNC	1	DEFUN	?
OF	7	OF	10
CAT	14	CAT	15
AIN	21	AIN	22
CCL	30	CCL	31

FUNCTIONS

AUD10	56	AUD11	57	AUD12	60
AUD1K	54	AUD02	65	AUD01	66
AUD007	72	AUD000	73	AUD001	74

PRFLKT & HOW GROUPS DEFEND

DEFUN	4
OF	11
CAT	16
AIN	23
CCL	32

DEFUN	5
OF	12
CAT	17
AIN	25
CCL	31

DEFUN	6
OF	13
CAT	20
AIN	27
CCL	37

SUPERIOR'S CALLETS

B-27

Curing times		Temperature °C					
		11	12	13	14	15	16
65 min	10	9	8	7	6	5	4
65 min	17	16	15	14	13	12	11

SCALLOPED EDGE AWLING A 1000°K FOLIATE SPECIMENS - 100°K REFERENCE 1
B-27. SCALLOPED EDGE AWLING A 1000°K FOLIATE SPECIMENS - 100°K REFERENCE 1
B-27. SCALLOPED EDGE AWLING A 1000°K FOLIATE SPECIMENS - 100°K REFERENCE 1

SUPERIOR'S CALLETS

Curing times		Temperature °C					
		11	12	13	14	15	16
65 min	10	9	8	7	6	5	4
65 min	17	16	15	14	13	12	11
65 min	11	10	9	8	7	6	5
65 min	12	11	10	9	8	7	6
65 min	13	12	11	10	9	8	7
65 min	14	13	12	11	10	9	8
65 min	15	14	13	12	11	10	9
65 min	16	15	14	13	12	11	10
65 min	17	16	15	14	13	12	11
65 min	18	17	16	15	14	13	12
65 min	19	18	17	16	15	14	13
65 min	20	19	18	17	16	15	14
65 min	21	20	19	18	17	16	15
65 min	22	21	20	19	18	17	16
65 min	23	22	21	20	19	18	17
65 min	24	23	22	21	20	19	18
65 min	25	24	23	22	21	20	19
65 min	26	25	24	23	22	21	20
65 min	27	26	25	24	23	22	21
65 min	28	27	26	25	24	23	22
65 min	29	28	27	26	25	24	23
65 min	30	29	28	27	26	25	24
65 min	31	30	29	28	27	26	25
65 min	32	31	30	29	28	27	26
65 min	33	32	31	30	29	28	27
65 min	34	33	32	31	30	29	28
65 min	35	34	33	32	31	30	29
65 min	36	35	34	33	32	31	30
65 min	37	36	35	34	33	32	31
65 min	38	37	36	35	34	33	32
65 min	39	38	37	36	35	34	33
65 min	40	39	38	37	36	35	34
65 min	41	40	39	38	37	36	35
65 min	42	41	40	39	38	37	36
65 min	43	42	41	40	39	38	37
65 min	44	43	42	41	40	39	38
65 min	45	44	43	42	41	40	39
65 min	46	45	44	43	42	41	40
65 min	47	46	45	44	43	42	41
65 min	48	47	46	45	44	43	42
65 min	49	48	47	46	45	44	43
65 min	50	49	48	47	46	45	44
65 min	51	50	49	48	47	46	45
65 min	52	51	50	49	48	47	46
65 min	53	52	51	50	49	48	47
65 min	54	53	52	51	50	49	48
65 min	55	54	53	52	51	50	49
65 min	56	55	54	53	52	51	50
65 min	57	56	55	54	53	52	51
65 min	58	57	56	55	54	53	52
65 min	59	58	57	56	55	54	53
65 min	60	59	58	57	56	55	54
65 min	61	60	59	58	57	56	55
65 min	62	61	60	59	58	57	56
65 min	63	62	61	60	59	58	57
65 min	64	63	62	61	60	59	58
65 min	65	64	63	62	61	60	59
65 min	66	65	64	63	62	61	60
65 min	67	66	65	64	63	62	61
65 min	68	67	66	65	64	63	62
65 min	69	68	67	66	65	64	63
65 min	70	69	68	67	66	65	64
65 min	71	70	69	68	67	66	65
65 min	72	71	70	69	68	67	66
65 min	73	72	71	70	69	68	67
65 min	74	73	72	71	70	69	68
65 min	75	74	73	72	71	70	69
65 min	76	75	74	73	72	71	70
65 min	77	76	75	74	73	72	71
65 min	78	77	76	75	74	73	72
65 min	79	78	77	76	75	74	73
65 min	80	79	78	77	76	75	74
65 min	81	80	79	78	77	76	75
65 min	82	81	80	79	78	77	76
65 min	83	82	81	80	79	78	77
65 min	84	83	82	81	80	79	78
65 min	85	84	83	82	81	80	79
65 min	86	85	84	83	82	81	80
65 min	87	86	85	84	83	82	81
65 min	88	87	86	85	84	83	82
65 min	89	88	87	86	85	84	83
65 min	90	89	88	87	86	85	84
65 min	91	90	89	88	87	86	85
65 min	92	91	90	89	88	87	86
65 min	93	92	91	90	89	88	87
65 min	94	93	92	91	90	89	88
65 min	95	94	93	92	91	90	89
65 min	96	95	94	93	92	91	90

Transcript

.A0016 21 .A0002 22 .A0001 23 .A0004 24 .A0005 25 .A0000 26
.20001 27

MIC 0 & NO RECORDS RECEIVED 1

APPENDIX C

SAMPLE EXECUTION

The following is transmission-loss (TL) output for the test case considered in Section 3. The values have been scaled by a factor of 10 and volume attenuation [$\alpha = .125 (f/1000)^2$ dB/nm] subtracted.*

* The virtual-mode model does not include volume loss. However, the PE runs used in section 3 did, so I added volume loss to the values shown in the following paper to get the results plotted in section 3. The TL values in this appendix have been converted to dB re \equiv .

	75 (ft)	750	250	750	250	500	500	500	500	750	750	750	1000	1000	1250	1250	1500	1500	1500	
H	61.6	64.7	65.0	64.9	67.4	71.3	71.2	71.4	62.6	63.5	68.7	68.2	64.6	64.1	59.1	60.0	55.9	54.0	51.6	
	2.00	66.0	64.0	71.9	71.4	71.6	71.1	71.4	62.6	63.5	68.7	68.2	64.6	64.1	59.1	59.5	54.6	54.6	50.5	
	3.00	66.4	64.4	71.4	71.0	69.3	69.2	71.1	62.6	63.5	68.7	68.2	64.6	64.1	59.1	59.5	54.6	54.6	50.5	
	4.00	69.1	71.1	75.5	72.4	81.8	85.4	72.9	73.0	77.4	70.9	80.2	71.0	75.7	71.6	67.5	67.4	66.8	3.00	
	5.00	69.1	72.3	76.4	71.5	87.7	89.7	74.1	75.4	80.6	83.1	83.9	74.5	70.5	81.9	82.4	77.9	74.7	4.00	
	6.00	69.0	71.2	77.4	65.1	90.5	90.6	75.1	76.6	82.7	95.6	95.6	75.7	71.6	94.6	95.5	95.5	95.6	6.00	
	7.00	70.6	71.0	79.7	87.2	90.9	62.7	76.0	77.7	94.4	87.5	89.7	75.8	77.5	96.7	87.8	85.9	86.4	1.00	
	8.00	71.2	74.6	78.3	81.7	91.5	91.6	71.1	76.7	97.5	90.1	90.3	77.7	84.9	88.2	95.5	93.4	93.9	8.00	
	9.00	71.7	76.1	80.2	81.1	92.9	94.1	77.4	77.4	97.0	90.4	91.7	79.4	86.0	92.5	90.8	90.4	91.4	9.00	
	10.00	72.2	75.6	81.9	81.6	91.7	95.7	78.0	69.0	91.5	92.0	92.0	79.2	97.0	90.5	91.0	92.2	95.0	9.00	
	11.00	72.6	74.6	81.5	81.2	94.4	95.0	74.5	80.7	94.0	92.5	93.0	79.4	91.4	92.9	93.8	96.7	99.6	10.00	
	12.00	72.0	72.0	76.5	32.1	91.1	95.5	79.6	70.0	90.6	97.2	94.7	90.5	94.5	92.2	91.7	90.4	10.23	10.13	
	13.00	73.4	74.9	82.6	85.5	97.7	97.7	79.5	81.0	90.3	94.0	95.5	81.6	92.2	92.9	94.4	95.3	10.95	13.00	
	14.00	73.7	77.3	93.1	90.7	96.2	97.0	79.0	92.4	90.0	94.7	95.2	91.6	97.6	97.6	95.1	97.2	10.20	10.39	
	15.00	74.0	77.6	93.6	92.8	96.7	98.1	90.3	93.0	91.5	95.1	96.9	92.2	90.4	95.7	98.1	10.16	10.30	15.00	
	16.00	74.1	77.0	94.0	91.2	97.3	94.8	90.6	97.5	97.0	95.8	97.4	82.7	90.9	94.7	96.2	94.8	10.24	10.38	
	17.00	74.6	74.2	94.4	91.8	97.8	95.0	91.0	97.0	92.5	96.3	97.0	91.5	95.2	96.7	90.5	10.31	10.46	17.00	
	18.00	74.9	74.0	94.4	91.1	94.2	95.9	91.3	94.4	91.0	96.8	99.4	81.7	97.0	95.7	10.00	10.37	10.52	18.00	
	19.00	75.1	76.5	95.3	91.7	96.7	10.07	91.6	94.1	91.5	97.5	97.0	94.2	97.4	96.2	97.8	10.06	10.43	19.00	
	20.00	75.0	70.0	95.6	95.7	96.7	96.1	10.07	91.0	95.3	94.0	97.9	99.4	94.6	97.0	99.2	10.11	10.59	20.00	
	21.00	75.6	70.2	96.0	94.6	96.2	96.2	91.7	92.2	95.7	94.4	98.7	99.8	95.1	97.4	97.1	10.16	10.53	21.00	
	22.00	76.9	70.5	96.4	96.0	10.00	10.14	92.5	96.1	94.8	98.7	10.02	95.5	99.1	97.6	99.1	10.20	10.59	22.00	
	23.00	76.0	70.7	96.7	96.4	10.94	10.26	92.9	96.5	95.3	99.1	10.07	95.9	94.2	99.0	99.6	10.63	10.79	23.00	
	24.00	76.7	70.2	96.9	97.1	96.6	10.84	10.29	93.0	96.0	95.7	99.8	10.11	96.4	94.7	99.4	10.00	10.43	24.00	
	25.00	76.4	80.1	97.4	97.4	97.7	10.12	10.26	93.9	97.7	96.1	10.00	10.15	96.9	95.1	99.0	10.04	10.46	25.00	
	26.00	76.5	80.3	97.7	97.6	97.6	10.15	10.37	93.5	97.7	96.5	10.04	10.10	97.2	95.5	99.3	10.09	10.49	26.00	
	27.00	76.7	80.5	97.0	97.0	97.9	10.50	10.37	93.7	97.9	96.9	10.08	10.23	97.6	95.0	99.7	10.12	10.42	27.00	
	28.00	76.0	80.0	97.3	97.3	97.3	10.74	10.40	93.0	99.4	97.3	10.11	10.27	99.0	96.3	10.01	10.16	10.45	28.00	
	29.00	76.6	80.0	97.6	97.6	97.6	10.74	10.40	93.0	99.4	97.3	10.11	10.27	99.0	96.3	10.01	10.16	10.45	29.00	
	30.00	76.0	80.0	97.9	97.9	97.9	10.74	10.47	94.1	97.7	10.15	10.31	98.4	96.7	10.20	10.40	10.67	10.74	30.00	
	31.00	77.1	91.2	96.4	96.4	96.4	10.87	10.47	94.7	97.7	96.0	10.19	10.35	98.7	97.1	10.04	10.24	10.65	31.00	
	32.00	77.5	91.1	96.4	97.7	97.7	10.74	10.51	94.7	97.7	96.4	10.22	10.38	99.1	97.4	10.12	10.29	10.64	32.00	
	33.00	77.6	91.5	96.7	96.7	96.7	10.61	10.57	94.0	96.1	96.1	10.10	10.46	99.0	98.2	10.20	10.55	10.71	33.00	
	34.00	74.0	80.0	77.0	80.9	94.3	94.3	94.1	97.7	10.77	10.47	96.1	99.5	10.34	90.2	99.6	10.23	10.30	10.66	34.00
	35.00	74.0	80.0	77.0	81.1	96.6	96.6	96.1	97.7	10.77	95.0	99.1	10.15	96.7	99.0	10.23	10.41	10.57	35.00	
	36.00	75.0	80.6	77.6	81.1	96.6	96.6	96.4	97.7	10.77	95.2	99.3	10.15	96.8	99.3	10.23	10.41	10.60	36.00	
	37.00	76.0	80.0	77.0	80.1	96.1	96.1	96.4	97.7	10.77	95.0	99.1	10.15	96.6	99.1	10.23	10.41	10.59	37.00	
	38.00	76.4	80.0	77.6	81.1	96.6	96.6	96.4	97.7	10.77	95.2	99.3	10.15	96.8	99.3	10.23	10.41	10.60	38.00	
	39.00	76.4	80.0	77.6	81.1	96.6	96.6	96.4	97.7	10.77	95.0	99.1	10.15	96.6	99.1	10.23	10.41	10.59	39.00	
	40.00	75.5	80.0	77.6	81.1	96.6	96.6	96.4	97.7	10.77	95.2	99.3	10.15	96.8	99.3	10.23	10.41	10.60	40.00	
	41.00	76.6	82.5	92.5	92.5	96.1	96.1	96.4	97.7	10.77	95.0	99.1	10.15	96.6	99.1	10.23	10.41	10.59	41.00	
	42.00	76.7	82.6	92.6	92.6	96.7	96.7	96.5	97.0	10.56	96.3	99.3	92.7	10.21	10.61	97.7	10.62	10.77	42.00	
	43.00	76.0	82.0	92.4	92.4	96.4	96.4	96.4	97.0	10.56	96.4	99.4	92.0	10.25	10.64	97.1	10.65	10.81	43.00	
	44.00	75.0	82.4	92.4	92.4	96.4	96.4	96.4	97.0	10.56	96.5	99.5	92.2	10.28	10.65	97.2	10.66	10.80	44.00	
	45.00	76.0	82.5	92.4	92.4	96.4	96.4	96.7	97.0	10.56	96.7	99.5	92.1	10.31	10.64	97.4	10.67	10.81	45.00	
	46.00	76.1	82.1	91.1	92.4	96.1	96.1	96.4	97.0	10.56	96.1	99.4	92.7	10.27	10.64	97.5	10.68	10.80	46.00	
	47.00	76.0	82.0	92.2	92.2	96.2	96.2	96.4	97.0	10.56	96.0	99.4	92.0	10.27	10.63	97.6	10.67	10.81	47.00	
	48.00	76.0	81.9	91.2	92.7	92.7	92.7	96.7	97.0	10.56	97.0	99.5	92.7	10.27	10.64	97.7	10.68	10.80	48.00	
	49.00	76.4	81.4	92.9	92.9	94.5	94.5	96.0	97.0	10.56	97.1	99.5	92.6	10.27	10.64	97.8	10.68	10.81	49.00	
	50.00	76.5	83.5	93.1	93.1	96.6	96.6	96.6	97.0	10.56	97.3	99.6	92.7	10.27	10.64	97.9	10.68	10.81	50.00	

75 (FT)	250	250	250	250	250	500	500	500	500	500	750	750	1000	1000	1250	1250	1500	1500
ft (m)	2.00	7.00	12.00	17.00	22.00	2.00	7.00	12.00	17.00	22.00	7.00	12.00	1000	1000	1250	1250	1500	1500
1.00	672	673	674	677	677	624	675	675	675	675	674	674	640	641	601	607	621	620
2.00	675	674	721	715	749	747	671	703	725	726	670	684	710	657	675	676	692	2.00
3.00	674	704	740	701	877	877	671	751	778	791	605	714	764	707	729	717	749	3.00
4.00	677	714	766	818	856	856	694	820	825	825	913	913	913	914	910	947	777	796
5.00	704	724	774	879	903	904	706	761	761	759	777	777	777	777	905	905	905	4.00
6.00	715	717	794	911	942	947	715	771	832	874	884	884	877	877	911	916	941	5.00
7.00	771	743	795	935	974	991	722	781	847	847	903	905	746	851	905	829	867	6.00
8.00	777	730	902	856	856	1009	728	790	960	960	920	920	753	864	914	925	935	7.00
9.00	772	765	907	664	1016	1027	734	795	972	972	920	933	759	975	927	940	956	8.00
10.00	777	912	676	1025	1047	718	901	942	931	944	975	975	969	969	979	922	933	9.00
11.00	761	764	817	971	1079	1056	747	907	907	941	955	970	961	946	960	903	926	10.00
12.00	745	921	927	1045	1056	747	912	900	951	964	975	957	905	949	961	993	1005	11.00
13.00	780	771	925	1052	1051	1066	751	917	969	950	973	973	975	974	969	1005	1016	12.00
14.00	752	774	920	992	1056	1071	754	821	916	967	991	774	976	964	970	973	986	13.00
15.00	785	912	1011	1051	1051	1074	754	925	923	975	994	994	988	912	969	939	945	14.00
16.00	789	780	975	1056	1056	1056	761	919	919	947	946	970	970	961	966	995	1004	15.00
17.00	781	783	933	1005	1049	1095	763	931	931	986	986	1003	976	971	974	993	1005	16.00
18.00	783	786	941	1011	1073	1066	766	917	942	995	1010	979	975	982	994	990	1016	17.00
19.00	786	786	944	1017	1077	1057	766	914	949	1001	1016	902	970	946	1002	1024	1074	18.00
20.00	786	786	945	1016	1080	1076	771	951	1007	1022	906	971	990	977	995	1071	1094	19.00
21.00	789	791	911	1021	1064	1064	773	949	949	971	1017	1027	906	977	994	1003	1054	20.00
22.00	772	785	951	1077	1067	1102	776	951	963	1017	1032	912	970	997	1001	1043	1054	21.00
23.00	774	907	953	1010	1000	1106	779	954	957	1022	1037	615	944	1001	1014	1052	1055	22.00
24.00	776	909	956	1031	1062	1106	780	957	972	1027	1041	917	947	1004	1020	1060	1074	23.00
25.00	774	901	959	1071	1075	1111	782	960	976	1031	1046	920	950	1004	1023	1027	1076	24.00
26.00	761	911	950	1019	1064	1111	784	951	951	1035	1050	923	944	1011	1026	1034	1064	25.00
27.00	772	785	951	1077	1067	1102	786	956	956	1036	1054	925	957	1014	1029	1040	1064	26.00
28.00	774	907	953	1010	1000	1106	787	959	969	1047	1058	929	950	1017	1032	1047	1104	27.00
29.00	765	906	956	1031	1062	1106	790	971	990	1046	1061	930	963	1020	1036	1053	1104	28.00
30.00	760	900	957	1071	1075	1117	790	971	971	1063	1078	941	977	1034	1050	1074	1121	29.00
31.00	761	901	958	1071	1075	1117	791	971	974	1050	1065	941	977	1023	1038	1058	1124	30.00
32.00	762	902	959	1071	1075	1117	792	976	977	1053	1068	945	980	1017	1036	1053	1124	31.00
33.00	763	903	960	1071	1075	1117	793	976	977	1054	1069	946	980	1026	1041	1063	1125	32.00
34.00	761	907	960	1071	1075	1117	794	976	977	1055	1070	947	981	1027	1042	1064	1126	33.00
35.00	760	909	961	1071	1075	1117	795	976	977	1056	1075	948	981	1028	1043	1065	1127	34.00
36.00	761	910	962	1071	1075	1117	796	976	977	1057	1076	949	982	1029	1044	1066	1128	35.00
37.00	762	911	963	1071	1075	1117	797	976	977	1058	1077	949	983	1030	1045	1067	1129	36.00
38.00	763	912	964	1071	1075	1117	798	976	977	1059	1078	950	983	1031	1046	1068	1130	37.00
39.00	764	913	965	1071	1075	1117	799	976	977	1060	1079	951	984	1032	1047	1069	1131	38.00
40.00	765	914	966	1071	1075	1117	800	976	977	1061	1080	952	984	1033	1048	1070	1132	39.00
41.00	767	915	967	1071	1075	1117	801	976	977	1062	1081	953	985	1034	1049	1071	1133	40.00
42.00	762	912	965	1071	1075	1117	802	976	977	1063	1082	954	985	1035	1050	1072	1134	41.00
43.00	901	961	971	1071	1075	1117	803	976	977	1064	1083	955	985	1036	1051	1073	1135	42.00
44.00	902	962	972	1071	1075	1117	804	976	977	1065	1084	956	986	1037	1052	1074	1136	43.00
45.00	903	963	973	1071	1075	1117	805	976	977	1066	1085	957	986	1038	1053	1075	1137	44.00
46.00	904	964	974	1071	1075	1117	806	976	977	1067	1086	958	987	1039	1054	1076	1138	45.00
47.00	905	965	975	1071	1075	1117	807	976	977	1068	1087	959	988	1040	1055	1077	1139	46.00
48.00	906	966	976	1071	1075	1117	808	976	977	1069	1088	960	989	1041	1056	1078	1140	47.00
49.00	907	967	977	1071	1075	1117	809	976	977	1070	1089	961	990	1042	1057	1079	1141	48.00
50.00	908	968	978	1071	1075	1117	810	976	977	1071	1090	962	991	1043	1058	1080	1142	49.00
51.00	909	969	979	1071	1075	1117	811	976	977	1072	1091	963	992	1044	1059	1081	1143	50.00

CONTRACTS WITH THE STATE OF CALIFORNIA

R (cm)		250	260	270	280	290	300	310	320	330	340	350	360	370	380	390	400	410	420	430	440	450	460	470	480	490	500	510	520	530	540	550	560	570	580	590	600	610	620	630	640	650	660	670	680	690	700	710	720	730	740	750	760	770	780	790	800	810	820	830	840	850	860	870	880	890	900	910	920	930	940	950	960	970	980	990	1000	1010	1020	1030	1040	1050	1060	1070	1080	1090	1100	1110	1120	1130	1140	1150	1160	1170	1180	1190	1200	1210	1220	1230	1240	1250	1260	1270	1280	1290	1300	1310	1320	1330	1340	1350	1360	1370	1380	1390	1400	1410	1420	1430	1440	1450	1460	1470	1480	1490	1500	1510	1520	1530	1540	1550	1560	1570	1580	1590	1600	1610	1620	1630	1640	1650	1660	1670	1680	1690	1700	1710	1720	1730	1740	1750	1760	1770	1780	1790	1800	1810	1820	1830	1840	1850	1860	1870	1880	1890	1900	1910	1920	1930	1940	1950	1960	1970	1980	1990	2000	2010	2020	2030	2040	2050	2060	2070	2080	2090	2100	2110	2120	2130	2140	2150	2160	2170	2180	2190	2200	2210	2220	2230	2240	2250	2260	2270	2280	2290	2300	2310	2320	2330	2340	2350	2360	2370	2380	2390	2400	2410	2420	2430	2440	2450	2460	2470	2480	2490	2500	2510	2520	2530	2540	2550	2560	2570	2580	2590	2600	2610	2620	2630	2640	2650	2660	2670	2680	2690	2700	2710	2720	2730	2740	2750	2760	2770	2780	2790	2800	2810	2820	2830	2840	2850	2860	2870	2880	2890	2900	2910	2920	2930	2940	2950	2960	2970	2980	2990	3000	3010	3020	3030	3040	3050	3060	3070	3080	3090	3100	3110	3120	3130	3140	3150	3160	3170	3180	3190	3200	3210	3220	3230	3240	3250	3260	3270	3280	3290	3300	3310	3320	3330	3340	3350	3360	3370	3380	3390	3400	3410	3420	3430	3440	3450	3460	3470	3480	3490	3500	3510	3520	3530	3540	3550	3560	3570	3580	3590	3600	3610	3620	3630	3640	3650	3660	3670	3680	3690	3700	3710	3720	3730	3740	3750	3760	3770	3780	3790	3800	3810	3820	3830	3840	3850	3860	3870	3880	3890	3900	3910	3920	3930	3940	3950	3960	3970	3980	3990	4000	4010	4020	4030	4040	4050	4060	4070	4080	4090	4100	4110	4120	4130	4140	4150	4160	4170	4180	4190	4200	4210	4220	4230	4240	4250	4260	4270	4280	4290	4300	4310	4320	4330	4340	4350	4360	4370	4380	4390	4400	4410	4420	4430	4440	4450	4460	4470	4480	4490	4500	4510	4520	4530	4540	4550	4560	4570	4580	4590	4600	4610	4620	4630	4640	4650	4660	4670	4680	4690	4700	4710	4720	4730	4740	4750	4760	4770	4780	4790	4800	4810	4820	4830	4840	4850	4860	4870	4880	4890	4900	4910	4920	4930	4940	4950	4960	4970	4980	4990	5000
R (cm)		1.00	1.12	1.24	1.36	1.48	1.60	1.72	1.84	1.96	2.08	2.20	2.32	2.44	2.56	2.68	2.80	2.92	3.04	3.16	3.28	3.40	3.52	3.64	3.76	3.88	3.90	4.02	4.14	4.26	4.38	4.50	4.62	4.74	4.86	4.98	5.10	5.22	5.34	5.46	5.58	5.70	5.82	5.94	6.06	6.18	6.30	6.42	6.54	6.66	6.78	6.90	7.02	7.14	7.26	7.38	7.50	7.62	7.74	7.86	7.98	8.10	8.22	8.34	8.46	8.58	8.70	8.82	8.94	9.06	9.18	9.30	9.42	9.54	9.66	9.78	9.90	10.02	10.14	10.26	10.38	10.50	10.62	10.74	10.86	10.98	11.10	11.22	11.34	11.46	11.58	11.70	11.82	11.94	12.06	12.18	12.30	12.42	12.54	12.66	12.78	12.90	13.02	13.14	13.26	13.38	13.50	13.62	13.74	13.86	13.98	14.10	14.22	14.34	14.46	14.58	14.70	14.82	14.94	15.06	15.18	15.30	15.42	15.54	15.66	15.78	15.90	16.02	16.14	16.26	16.38	16.50	16.62	16.74	16.86	16.98	17.10	17.22	17.34	17.46	17.58	17.70	17.82	17.94	18.06	18.18	18.30	18.42	18.54	18.66	18.78	18.90	19.02	19.14	19.26	19.38	19.50	19.62	19.74	19.86	19.98	20.10	20.22	20.34	20.46	20.58	20.70	20.82	20.94	21.06	21.18	21.30	21.42	21.54	21.66	21.78	21.90	22.02	22.14	22.26	22.38	22.50	22.62	22.74	22.86	22.98	23.10	23.22	23.34	23.46	23.58	23.70	23.82	23.94	24.06	24.18	24.30	24.42	24.54	24.66	24.78	24.90	25.02	25.14	25.26	25.38	25.50	25.62	25.74	25.86	25.98	26.10	26.22	26.34	26.46	26.58	26.70	26.82	26.94	27.06	27.18	27.30	27.42	27.54	27.66	27.78	27.90	28.02	28.14	28.26	28.38	28.50	28.62	28.74	28.86	28.98	29.10	29.22	29.34	29.46	29.58	29.70	29.82	29.94	30.06	30.18	30.30	30.42	30.54	30.66	30.78	30.90	31.02	31.14	31.26	31.38	31.50	31.62	31.74	31.86	31.98	32.10	32.22	32.34	32.46	32.58	32.70	32.82	32.94	33.06	33.18	33.30	33.42	33.54	33.66	33.78	33.90	34.02	34.14	34.26	34.38	34.50	34.62	34.74	34.86	34.98	35.10	35.22	35.34	35.46	35.58	35.70	35.82	35.94	36.06	36.18	36.30	36.42	36.54	36.66	36.78	36.90	37.02	37.14	37.26	37.38	37.50	37.62	37.74	37.86	37.98	38.10	38.22	38.34	38.46	38.58	38.70	38.82	38.94	39.06	39.18	39.30	39.42	39.54	39.66	39.78	39.90	40.02	40.14	40.26	40.38	40.50	40.62	40.74	40.86	40.98	41.10	41.22	41.34	41.46	41.58	41.70	41.82	41.94	42.06	42.18	42.30	42.42	42.54	42.66	42.78	42.90	43.02	43.14	43.26	43.38	43.50	43.62	43.74	43.86	43.98	44.10	44.22	44.34	44.46	44.58	44.70	44.82	44.94	45.06	45.18	45.30	45.42	45.54	45.66	45.78	45.90	46.02	46.14	46.26																																																																																																	

REFERENCES

1. C. W. Spofford, "The FACT Model, Volume 1," Maury Center Report 109, (November 1974).
2. C. S. Clay, "Sound Propagation in a Half Channel and Surface Duct," Technical Notes on Sound Propagation in the Sea II, Meteorology International, Inc., Monterey, CA, (1968).
3. F. M. Labianca, "Critique of C. S. Clay's 'Sound Transmission in a Half Channel and Surface Duct'," Reference 8 in Continuation of LRAPP, February 1972, Bell Laboratories.
4. H. E. Morris, "Comparison of Propagation Prediction Models with SUDS I Acoustic Data," NUC-TP-377, (April 1974).
5. H. W. Marsh and M. Schulkin, Report on the Status of Project AMOS, U. S. Naval Underwater Sound Laboratory, New London, Conn., May 1977.
6. H. P. Bucker, "Sound Propagation in a Channel with Lossy Boundaries," J. Acoust. Soc. Am., Vol. 48, 1187-1194, (1970). This is an extension, to include rough surface effects, of the normal mode code of Pedersen and Gordon, Reference 12.
7. F. M. Labianca, "Normal Modes, Virtual Modes, and Alternative Representations in the Theory of Surface-Duct Sound Propagation," J. Acoust. Soc. Am., Vol. 53, 1137-1147, (1973).
8. C. W. Spofford, "Improved Surface Duct Model for FACT," Science Applications, Inc. Report No. SAI-78-687-WA, (1977).
9. W. H. Furry, "The Bi-linear Modified-Index Profile," in Propagation of Short Radio Waves, edited by D. E. Kerr, McGraw-Hill, (1951).
10. H. W. Marsh, "Theory of Anomalous Propagation of Acoustic Waves in the Ocean," U. S. Naval Underwater Sound Laboratory Report No. 111, (1950).
11. M. Hall, "Mode Theory of Wave Propagation in a Bilinear Medium: the WKB Approximation," J. Acoust. Soc. Am., Vol. 60, 810-814, (1976).
12. M. A. Pedersen and D. F. Gordon, "Normal-Mode Theory Applied to Short-Range Propagation in an Underwater Acoustic Surface Duct," J. Acoust. Soc. Am., Vol. 37, 105-118, (1965); M. A. Pedersen and D. F. Gordon, "Theoretical Investigation of a Double Family of Normal Modes in an Underwater Acoustic Surface Duct," ibid, Vol. 47, 304-326, (1970).

13. The form of Eq. (2.6) is equivalent to Labianca's Eq. (23.a) (Ref. 7) if the following identifications between Labianca's notation and the present are made

$$k^2 \lambda = \kappa^2 = (E + s^3 D)/H^2$$

$$\phi(Z, \lambda) = \psi(x, E)$$

$$A(\lambda) \pm iB(\lambda) = T_{\pm}(E) .$$

The factor of H arises from use of the dimension-less variable x instead of Z in the delta-function source term.

14. The intensity is normalized against a value of $4\pi r_0^2$ at unit distance r_0 (i.e., one foot or one meter).
15. M. Abramowitz and I. A. Stegun, Handbook of Mathematical Functions, Chapter 10, Dover Publications, (1965).
16. H. K. Brock, "The AESD PARABOLIC Equation Model," NORDA Tech Note 12, (1978).
17. R. E. Keenan and C. W. Spofford, "Rough Surface Loss for FACT," SAI Report No. SAI-78-688-WA, (November 1977).